FLEXURAL MODELING OF THE HIMALAYAN FORELAND BASIN:
IMPLICATIONS FOR THE PRESENCE OF A FOREBULGE AND FORMATION OF BASEMENT RIDGES

An Abstract of a Thesis

Presented to

the Faculty of the Department of Earth and Atmospheric Sciences

University of Houston

In Partial Fulfillment

of the Requirements for the Degree

Master of Science

By

Nicole F. Arres

August 2013

FLEXURAL MODELING OF THE HIMALAYAN FORELAND BASIN:

IMPLICATIONS FOR THE PRESENCE OF A FOREBULGE AND FORMATION OF BASEMENT RIDGES

_____

Nicole F. Arres

APPROVED:

_____

Dr. Jolante van Wijk, Advisor

_____

Dr. Michael Murphy

_____

Dr. Peter Copeland

_____

Dr. An Yin
University of California at Los Angeles

_____

Dean, College of Natural Sciences and Mathematics

FLEXURAL MODELING OF THE HIMALAYAN FORELAND BASIN:
IMPLICATIONS FOR THE PRESENCE OF A FOREBULGE AND FORMATION OF BASEMENT RIDGES

_____

An Abstract of a Thesis

Presented to

the Faculty of the Department of Earth and Atmospheric Sciences

University of Houston

_____

In Partial Fulfillment

of the Requirements for the Degree

Master of Science

_____

By

Nicole F. Arres

August 2013

Abstract

The purpose of this study is to evaluate the formation and shape of the Himalayan Foreland Basin system as it responds to lithospheric thrusting and loading. The study area is an elongate trough with an arcuate shape that mimics the shape of the Himalayan arc. The Eocene Himalayan Foreland Basin formed on the Indian Plate following subduction and continent-continent collision between the Indian and Eurasian Plates. The deepest part of the foreland basin adjacent to the Himalayan Main Frontal Thrust is covered with about 6 km of sediments.

The basement is characterized by several basement ridges; elongated structures oriented perpendicular to the plate boundary. The origin of these basement ridges is unknown. In a foreland basin system, a forebulge is expected to form when a plate has strength. There are some indications that a forebulge may have developed in the Himalayan Foreland Basin, but its exact location and amplitude are debated.

Three-dimensional flexural models were produced to determine the effective elastic thickness and flexural strength of the Indian Plate. Preferred models using realistic parameters predict that a low, broad forebulge has developed on the Indian Plate. The forebulge has an amplitude of about 30-50 m, and the lack of forebulge observed in the field and in stratigraphic columns is probably a result of the small amplitude of the forebulge.

The formation of the basement ridges was addressed by along-strike variations in the load with 3D flexural models, and by modeling compression of an

elastic plate using Abaqus. Lateral variations in the load did produce basement ridges, but did not produce realistic basin depths. In the compression model, forces were applied to the sides of the Indian Plate to simulate compression as the Plate continues to be subducted beneath the Eurasian Plate. The model produced basement ridges using realistic values of plate rigidity. It is proposed that the basement ridges observed in the Himalayan Foreland Basin are the result of compression of the Indian Plate, and lateral variation of load is the result of non-uniform basin depths and subsequent sediment in-fill.

TABLE OF CONTENTS

LIST OF FIGURES

LIST OF TABLES

1. INTRODUCTION

The Himalayan Foreland Basin is a flexural basin that formed between the Himalaya orogenic belt and the stable Indian craton (Figure 1). The northern boundary of the basin is defined by the Main Frontal Thrust (MFT), while the southern boundary is more diffuse. In a foreland basin system a forebulge is expected to form when a plate has strength. Gravity studies suggest that a forebulge has formed on the Indian Plate; however, the location and amplitude have not been identified in the field. The basement of the Himalayan Foreland Basin is characterized by several basement ridges. The origin of these ridges is unknown and may be a result of along-strike variations of the emplaced load or by compression of the Indian Plate during subduction beneath Eurasia.

Figure 1: Regional map showing foreland basin in northern India (modified after http://www.geosci.usyd.edu/au/users/prey/Teaching/Geol-3101/Mountain02/structuregeocollision.htm).

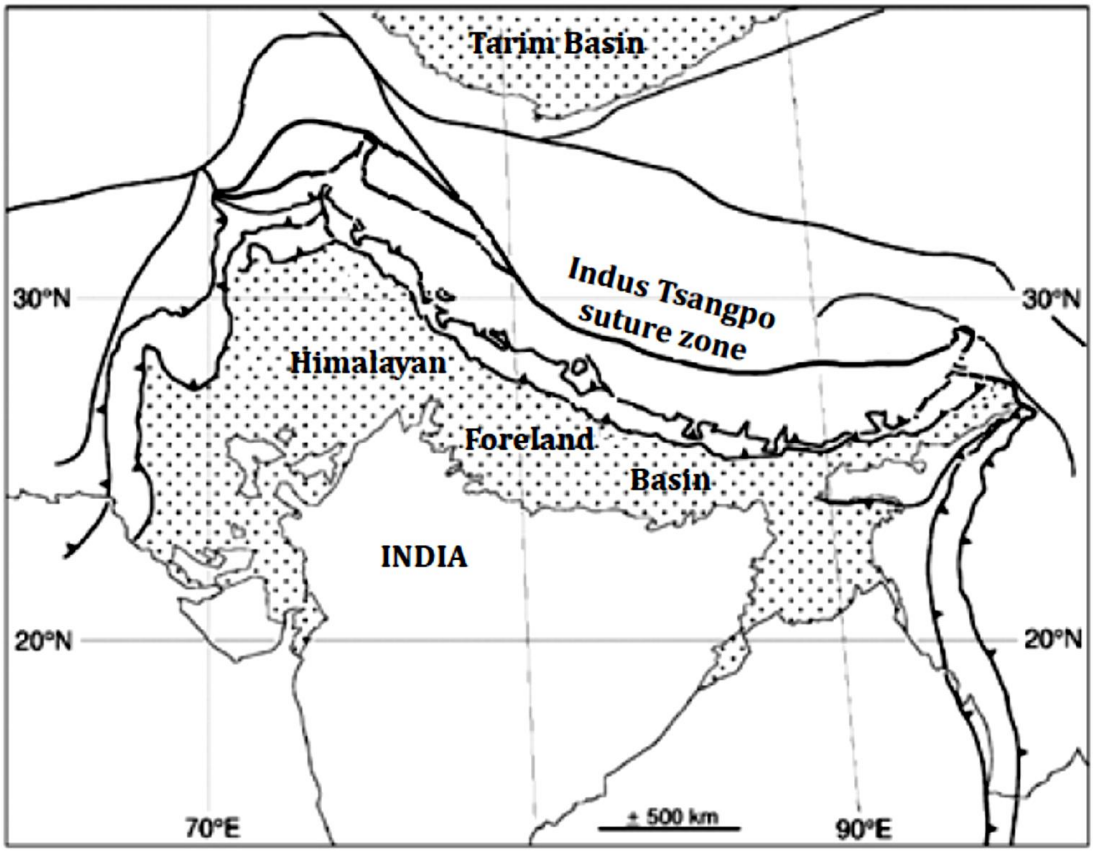

A foreland basin is an asymmetrical, elongate, flexural depression that forms parallel and adjacent to a mountain belt. There are two types of foreland basins; peripheral and retroarc (DeCelles and Gilles, 1996). The Himalayan Foreland Basin is a peripheral foreland basin, formed along the outer arc of the Himalayan orogen, on the subducting Indian Plate as a result of collision with the Eurasian Plate (Figure 2). A retroarc foreland basin forms on-top of the plate that over-rides the subducting slab during convergence. Most retroarc foreland basins are associated with convergence of oceanic lithosphere and continental lithosphere rather than continental-continental lithosphere collision (DeCelles and Gilles, 1996).

Figure 2: The peripheral Himalayan Foreland Basin formed on the subducting Indian Plate (modified after DeCelles and Giles, 1996).

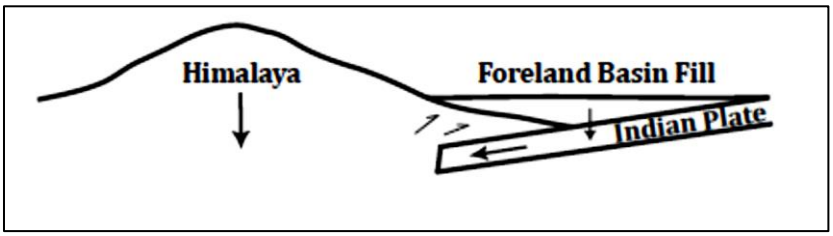

Foreland basins form as an over-riding plate is up-thrusted during the subduction of a denser slab creating shortening and crustal thickening, resulting in the creation of a mountain belt, and bending of the lithosphere. The bending of the lithosphere is known as lithospheric flexure. The dimensions and shape of the foreland basin are determined by the flexural rigidity of the subducted lithosphere and by the dimensions of the topographic load, the mountain belt (DeCelles and Gilles, 1996). As a result of elastic deformation of the lithosphere, the lithosphere compensates for the topographic load emplaced by bulging on the peripheral of the foreland basin; this is called the forebulge (Figure 3).

DeCelles and Giles (1996) describe a foreland basin system as being composed of three characteristic properties: an elongate region of potential sediment accommodation forming between the orogenic belt and the adjacent craton, four depositional zones (depo-zones): wedge-top, foredeep, forebulge, and

back-bulge basin; and the longitudinal dimension of the foreland basin system which is approximately equal to the length of the fold-thrust belt (Figure 4).

Figure 3: Diagram depicting typical formation of a foreland basin (modified from DeCelles and Giles, 1996). Upper panel: map view of typical basin structure, Lower panel: transect showing tectonic features based on foreland basin development.

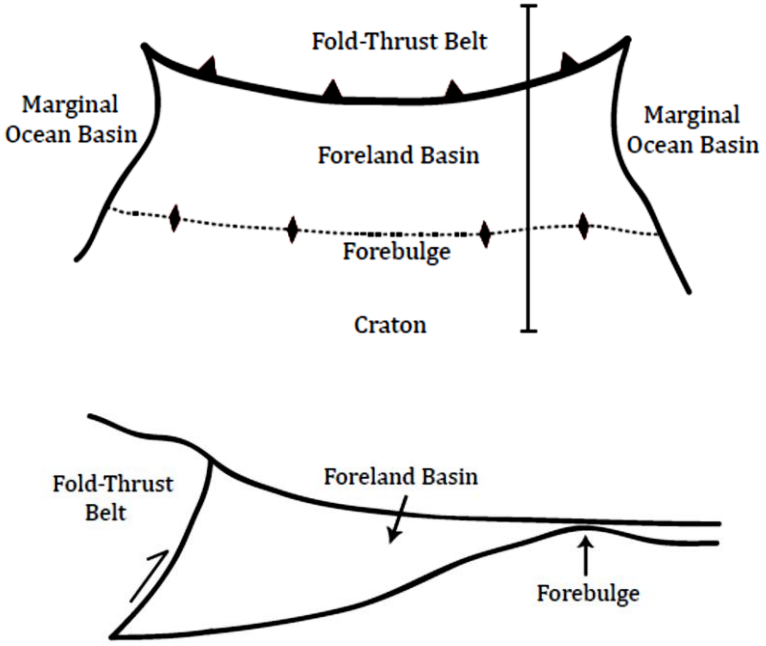

Figure 4: Diagram of foreland basin system (modified after DeCelles and Giles, 1996).

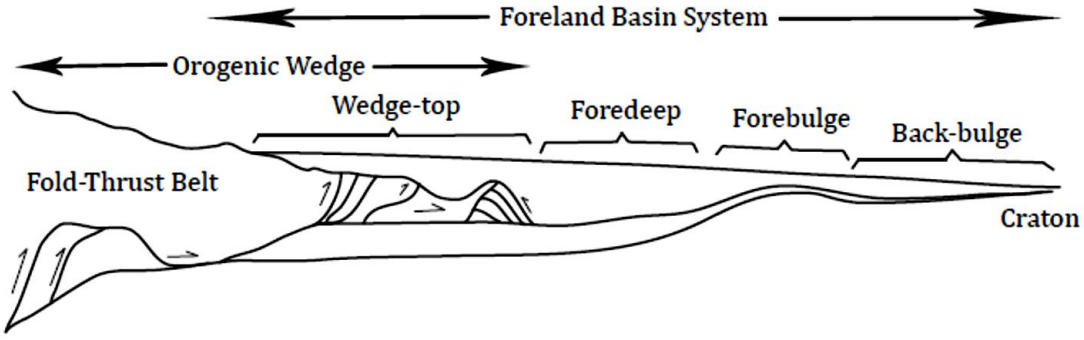

The wedge-top depo-zone is situated on-top of the migrating thrust sheets and contains the sediment from the active tectonic thrust wedge. The foredeep forms the deepest sediment basin, and is wedge-shaped, thickening at the orogen and thinning toward the distal reaches of the basin, typically on-lapping the forebulge. The forebulge is created in elastic response of the lithosphere as a result of loading; it is the thinnest and one of the most distal zones, and not always present. If the forebulge is not present, there will not be a back-bulge. The forebulge and back-bulge are usually defined by regional unconformities (Clift and VanLaningham, 2010).

The fold-thrust belt is mobile; change in or migration of the topographic load on the lithosphere results in deformation and/or migration of the foreland basin. The motion of the migration has been described in the literature as a wave-like motion that propagates from the emplaced load through the foreland basin system (Bilham, 2004 and Catuneanu, 2004). As the load increases, decreases, or migrates, the foreland basin flexes in response, changing the dimensions and locations of the features within the foreland basin system such as the forebulge and back-bulge (Figure 5). There is discussion on whether a forebulge has developed adjacent to the Himalayan Foreland Basin.

The development of the forebulge has important implications for the strength of the Indian Plate as well as correctly interpreting the relationship between the development of the foreland basin and the evolution of the fold-thrust belt. The identification of depo-zones that characterize the foreland basin system is crucial to this interpretation. The depo-zones typically contain evidence of the beginning stages of foreland basin evolution (DeCelles et al., 1998).
Gravity data (Duroy et al., 1989; Mishra et al., 2004) suggests that a forebulge has been produced (Yin, 2006). Yin (2006) suggests that the topographic expression of the forebulge may be significantly smaller than that of the basement ridges. The basement ridges are elongated structures that are oriented perpendicular to the Plate boundary. The formation of the basement ridges is unknown; but may be a result of lateral variations in the load. When a non-uniform load is emplaced on a

plate, the plate will respond locally to the load; this response may produce the structural highs and lows observed with basement ridge formation.

Figure 5: Diagram depicting change in foreland basin as change in the topographic load occurs (modified after Jordan and Watts, 2005 and Catuneanu, 2004).

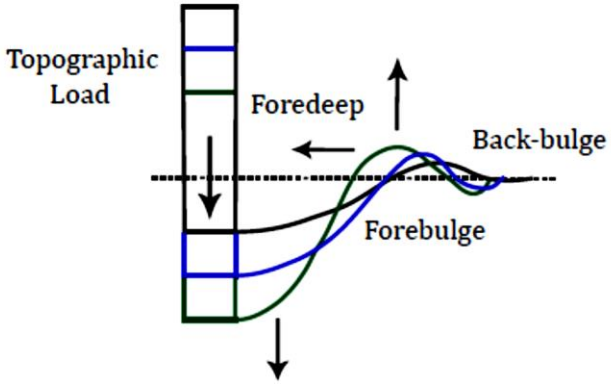

This paper aims to address the lack of forebulge observed in the field and the origin of the basement ridges. The lack of forebulge will be addressed by mapping the basement depth, and by developing flexural (3D) models to determine the effective elastic thickness of a subducting plate, whether a forebulge is predicted, and its location and amplitude. The origin of the basement ridges as a result of along-strike variations of the load will be addressed by developing flexural (3D) models and laterally varying the mountain load. To investigate the origin of basement ridges by compression, thin plate compression models will be generated. The models produced are constrained by stratigraphic and load data for the Himalayan mountain range and the sediment infill of the Himalayan Foreland Basin, and slab tomography and geophysical data for structure of the basin and underlying crust.

2. GEOLOGIC BACKGROUND

2.1 REGIONAL: HIMALAYAN OROGENY

The Himalayan Foreland Basin (also known as the Indo-Gangetic depression, Indo-Gangetic foreland basin, Ganga or Gangetic basin, and Sub-Himalaya) is an elongate trough (Figure 1) that originated as a result of the north-south shortening and crustal thickening that occurred during the continent-continent collision between the Eurasian Plate and Indian Plate (Paracha, 2004). Under-thrusting of the Indian Plate aids in the uplift of the Himalayan mountain belt and loading of the lithosphere, resulting in flexural subsidence and the formation of the Eocene Himalayan Foreland Basin.

The collision began ~50 Ma when the Indian Plate under-thrust the southern margin of Eurasia (Brookfield, 1998). Paleomagnetic evidence suggests that during the Cenozoic, India indented Eurasia by as much as ~2,000 km. During this process, the crust thickened to ~70 km below the Tibetan plateau and deformation occurred across a 1,500 km wide region to the north of the Indian Plate (Windley, 1988; Jordan and Watts, 2005). The Himalayan arc is approximately 2,500 km long and is convex toward central India (Gahalaut and Kundu, 2012).

Four main stages in the collision of the Eurasian Plate with the Indian Plate have been identified (Brookfield, 1998). The first stage occurred from 80 to 50 Ma, and included the closure of the Tethys ocean as the Indian craton moved toward the Eurasian Plate. The second stage occurred from approximately 50 to 25 Ma and is characterized by the collision of India with Eurasia, indention of Eurasia causing lithospheric shortening and uplift of the Himalayan mountain range, and subduction of the Indian Plate. During this stage the Himalayan Foreland Basin formed in response to the uplifting Himalayan mountain range. During the third stage, occurring approximately 25 to 5 Ma, lithospheric shortening, faulting, and deformation continued to occur as India and Eurasia continued to converge.

The fourth stage, occurred between 5 Ma and present, and is characterized by the gravitation spreading of the Himalayan mountain range and continual subsidence throughout the Himalayan Foreland Basin (Royer and Sandwell, 1989;

Brookfield, 1998). Gravitation spreading occurs in zones of thickened crust; at a critical threshold, the thickened crust can no longer support its structure and will begin to extend through a series of normal faults. As a result of extension, the Himalayan thrust wedge migrates toward the foreland basin. The additional load aids in the deflection of the Indian Plate.

The Himalayas consist of a series of three tectonic slices bounded by north-dipping Late Cenozoic fault systems: The Main Boundary Thrust (MBT), the Main Central Thrust (MCT), and the South Tibetan Detachment System (STDS), also known in the literature as the South Tibetan Detachment Zone (STDZ) (Yin and Harrison, 2000) (Figure 6). The Greater (or High) Himalaya is crystalline in structure with steep gradients characterized by gorges where fluvial incision and channelized erosion have been significant. The Lesser Himalaya is characterized by low gradients, with river knick-points that establish the erosion-deposition boundary of the fluvial system. The Sub-Himalayas and Lower Himalayas rise to approximately 3 km at the boundary between the Lower and Higher Himalayas (Seeber and Gornitz, 1983).

The Sub-Himalayas are characterized as an alluvial plain where fluvial systems begin to meander, cut-off other fluvial systems, coalesce, and deposit their loads. The diversion of river courses in the Sub-Himalayas is a result of aggradation near the erosion-deposition boundary, upstream of uplifts and the Sub-Himalayas (Seeber and Gornitz, 1983).

The deposition of sediments from the Higher and Lesser Himalayas occurring in the Sub-Himalayas accounts for a portion of the basin fill observed in the Himalayan Foreland Basin. These sediments act as an additional load that is emplaced on the lithosphere in addition to the thrust load, which causes flexure and subsidence of the basin. Because the trajectory of the major rivers in the region is very dynamic, deposition within the basin has not been laterally uniform (Seeber and Gornitz, 1983) (Figure 7).

Figure 6a: Tectonic map and interpretation of the Himalayan orogen (modified after Zhou et al., 2004). Upper panel (a): tectonic map of Tibet-Himalaya collision zone, Lower panel (b): cross-section (A-A') showing tectonic interpretation of underthrusting lithosphere and thrust faulting in the Himalayan fold-thrust belt. AKMS, Ayimaqin-Kunlun Mutztagh suture; BNS, Bangong-Nujiang suture; IYS, Indus-Yalu Suture; JS, Jinsha suture; MFT, Main Frontal Thrust; MBT, Main Boundary thrust; MCT, Main Central thrust; STD, South Tibet detachment; GCT, Great Counter thrust; ATF, Altyn Tagh fault; LM, lithospheric mantle.

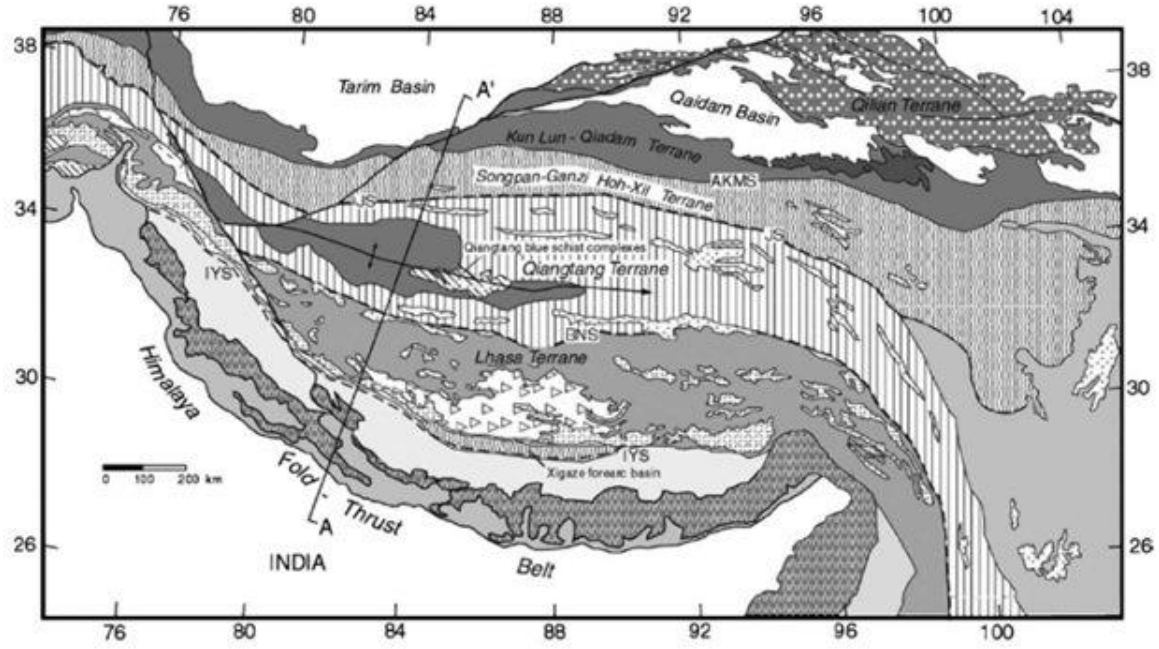

Figure 6b: Cross-section (A-A') showing tectonic interpretation of underthrusting lithosphere and thrust faulting in the Himalayan fold-thrust belt (modified after Zhou et al., 2004).

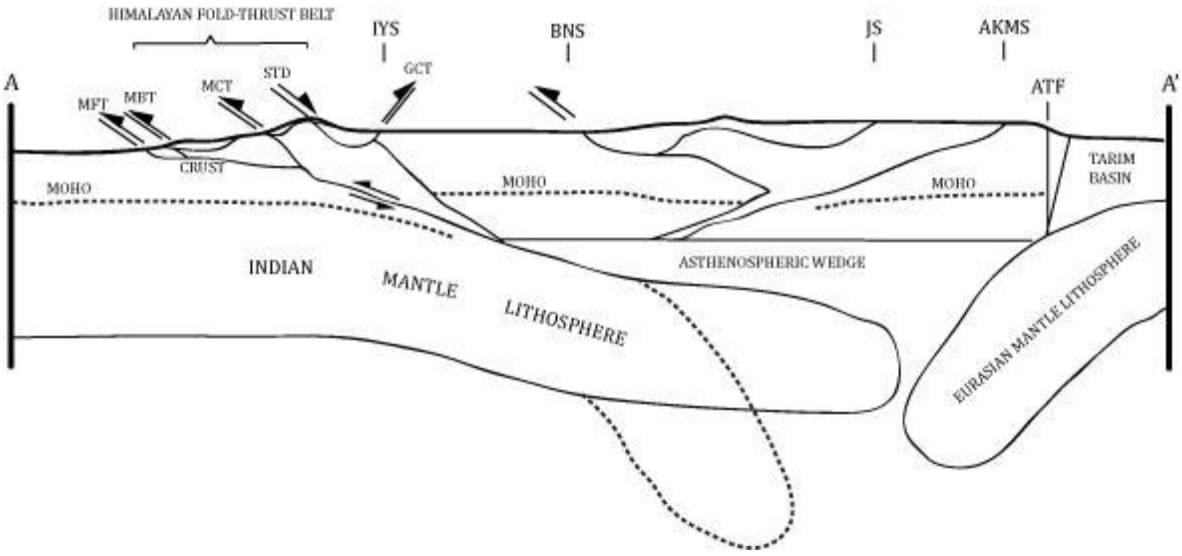

Figure 7: Paleogeographic sketch maps of India-Eurasia collision zone and fluvial flow reversal during Early Miocene and Middle Miocene time as the Himalayan Foreland Basin system developed (modified after DeCelles et al., 1998).

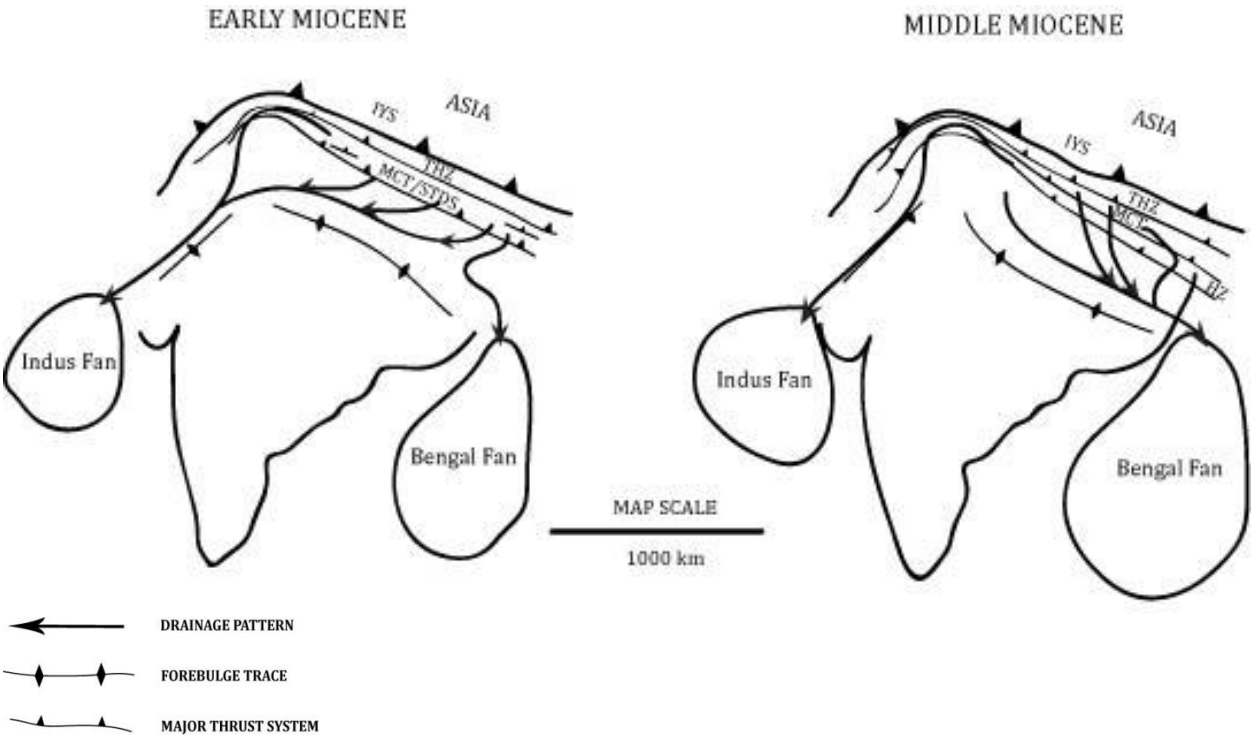

2.2 STUDY AREA: HIMALAYAN FORELAND BASIN

The Himalayan Foreland Basin is a flexural basin that formed between the Himalaya orogenic belt and the stable Indian craton. It is bounded by the Himalayan orogenic belt, Lesser and Greater/High Himalaya, and the Main Frontal Thrust (MFT) to the north and by the Peninsula Highlands of the Indian craton to the south. The southern boundary can best be described as diffuse, the presence of prominent fluvial systems has aided in the dynamic morphology of the southern portion of the basin, specifically near the Bengal Basin (Yin, 2006). For the purpose of this study, the study area has been confined to the central portion of the foreland basin (Figure 8).

The width and depth of the flexure of the Indian Plate as a result of loading and basin infill are a reflection of the load emplaced and are dependent on the

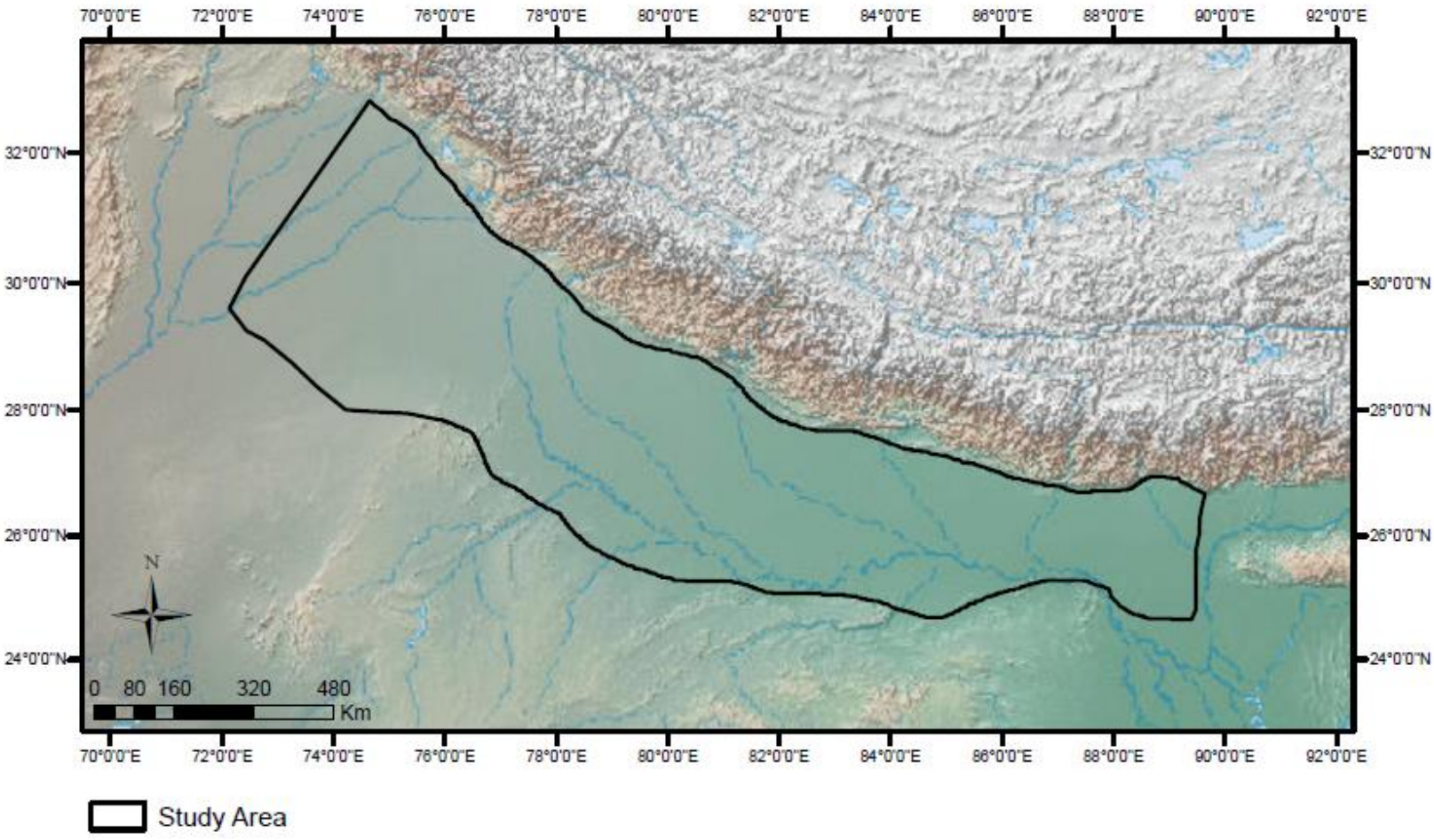

Figure 8: Study Area. Elevation legend is on Figure 15.

rigidity of the flexed crust and on the location of the emplaced load in relation to the edge of the underthrust plate (Burbank et. al., 1996). The lithospheric flexure creates accommodation space that is then infilled with sediments. Studies have shown that the foreland basin is a high effective elastic thickness (T_e) region. Hetenyi et al. (2006) produce a T_e of 60-80 km with a northward decreasing trend to approximately 20-30 km, Jordan and Watts (2005) describe the central portion of the basin as a 'rigid block' and estimate $40<T_e<100$, and Cattin et al. (2001) suggests that T_e varies between 40-50 km.

The Himalayan Foreland Basin is also characterized by a deficit of mass; it is an under-filled basin. A deficit of mass is associated with rapid thrusting resulting in a narrow under-filled basin (Flemings and Jordan, 1989). Flemings and Jordan (1989) describe an under-filled basin as a basin with a forebulge that remains a topographic high and is separated from the thrust belt by a central depositional axis. Most foreland basins begin as an under-filled basin. The Himalayan Foreland Basin continues to be under-filled basin; however, the topographic high associated with the forebulge is not readily identifiable in the field and stratigraphic columns.

Subsidence is at a greater rate near the orogen (Seeber and Gornitz, 1983). The basement of the basin dips at approximately 2-3° towards the Himalayan orogen, and the thickness of basin fill increases progressively to approximately 4-5 km against the Himalayan front (Yin, 2006). Jordan and Watts (2005) derive a collision rate of 10 to 15mm/a using basal sediments as a marker and determining their distance from the MFT, they were able to then divide the distance by the corresponding age of the sediments.

The basin is comprised of four sub-basins; from west to east these are the Indus Basin, Ganga Basin, Brahmaputra Basin and the Bengal Basin. These sub-basins are separated by structural highs that form drainage divides, and the sub-basins correspond to the drainage areas of the respective Indus, Ganges, Brahmaputra, and joined Brahmaputra-Ganges rivers (Yin, 2006) (Figure 9). In addition to the structural highs that create drainage divides, there are also

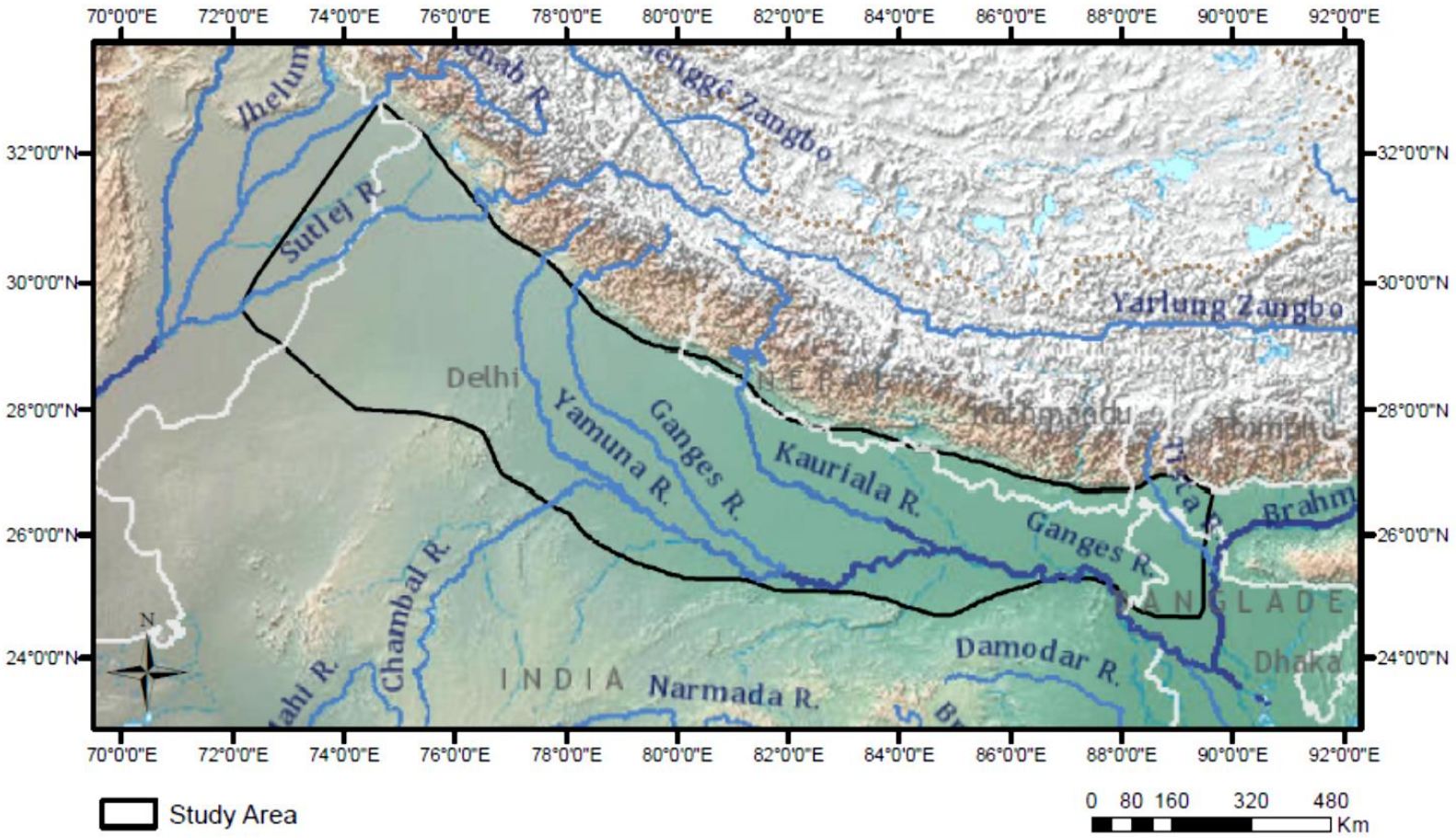

Figure 9: Drainage within study area. Elevation legend is on Figure 15.

basement structural highs that have been mapped from magnetic, seismic, gravity, and aeromagnetic studies (Gahalaut and Kundu, 2012).

The basement structural highs have been referred to as basement ridges. Yin (2006) suggests that the ridges are either Precambrian in age or were developed in the Cenozoic. This suggestion is based upon work by Rao (1973), Duroy et al. (1989), and Raiverman (2000). The interpretation of basement ridges being formed during the Cenozoic is based on observations of Cenozoic sedimentation being controlled by the ridges (Yin, 2006). Kumar et al. (2013) suggest that basement ridge formation is the result of lithospheric flexure.

There have been five ridges identified in the Himalayan Foreland Basin. Three of the five ridges are located within the study area; from west to east they are the Delhi-Hardwar Ridge, Faizabad Ridge, and the Monghyr (or Munger) Saharsa Ridge (Figure 10). The geometry of the Himalayan Foreland Basin mimics the arcuate shape of the Himalaya. Some researchers believe that the basement ridges affect the geometry of the Himalayan arc and subsequently the Himalayan Foreland Basin. Vogt (1973) and Gahalaut and Kundu (2012) suggest that the arcuate shape of the Himalayan arc may have been produced by the interaction of basement ridges with the subduction arc at the MFT during subduction of the Indian Plate. As convergence of the Indian and Eurasian Plates continues, the Himalayan Foreland Basin continues to migrate toward the Indian craton.

Yin (2006), Bilham (2004), and Zhou et al. (2004) have suggested that the subduction of the Indian Plate is not occurring uniformly. In Yin (2006), the total amount of crustal shortening in the eastern Himalaya is occurring faster than in the western Himalaya due to a non-uniform convergence rate between India and Eurasia. As a result, the northeastern corner of the Indian craton begins to tilt northeastward while the remaining portion of northern India continues a northwestward tilt. Bilham (2004) discusses the rotation and translation of the Indian Plate and agrees with Sella et al. (2002) that India is slowly rotating counterclockwise. Zhou et al. (2004) describes the subduction of India as "subhorizontal".

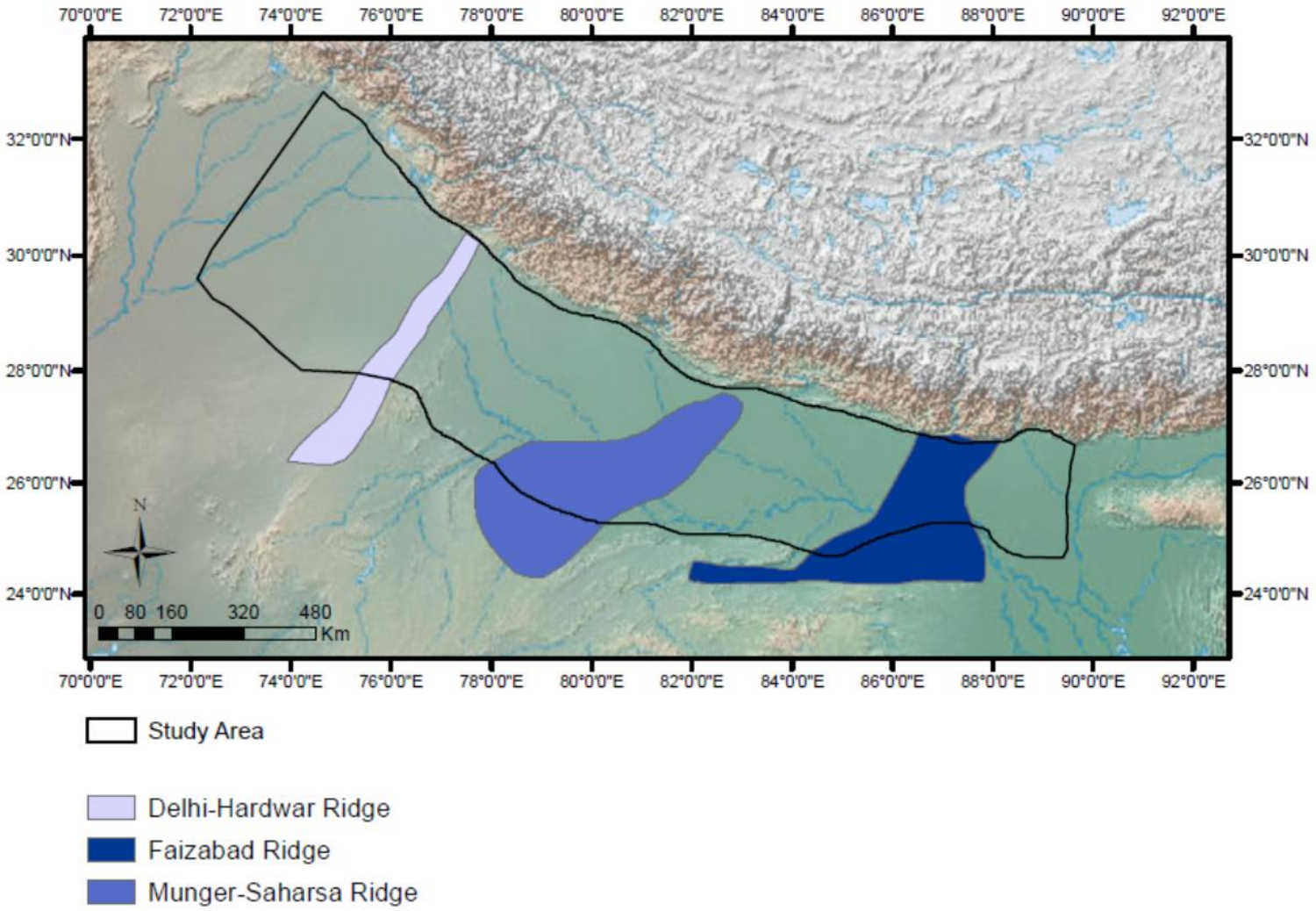

Figure 10: Topographic map of the Himalayan orogen with basement ridges. Elevation legend is on Figure 15.

Although the Indian Plate has a high T_e, $40<T_e<100$ (Jordan and Watts, 2005), 40-50 km (Cattin et al., 2001), and 60-80 km (Hetenyi et al., 2006), the load of the High Himalaya is too great to be solely supported by the elastic stress in the Indian Plate. Flexural modeling studies (Lyon-Caen and Molnar, 1983 and 1985), using a thin elastic plate overlying an inviscid fluid, find that the contribution of an additional force is required to support the high topography of the Himalaya. Gravity studies across the Himalaya suggest that the Himalaya is supported by the strength of the underthrusting Indian Plate (Cattin et al., 2001). Lyon-Caen and Molnar (1985) and Hetenyi et al. (2006) show that in order for the present-day load compensation observed to be predicted, the crust must have separated from the mantle as it is subducted creating a buoyancy beneath the up-thrusted Himalayas.

The Himalayan Foreland Basin is comprised of all of the components expected to be found in a foreland basin system; however, there is debate on the location and amplitude of the forebulge. When a lithospheric plate has strength, a forebulge is expected to develop cratonward of the foreland basin. Modern values for the flexural rigidity of the Indian Plate are quite high, ranging from 3E23 Nm to 7E24 Nm (DeCelles et al., 1998). The rigidities were determined through modeling techniques and are dependent on the size of the orogenic load used in the models (DeCelles et. al., 1998; Jordan and Watts, 2005).

DeCelles et al. (1998) produce a southward migrating forebulge in their models and identify a regional unconformity during the Eocene-Oligocene as the forebulge migrated through the region. Clift and VanLaningham (2010) suggest that "basal 'forebulge unconformities' are well known" in foreland basins. Duroy et al. (1989) identified a forebulge on the Indian Plate that is largely buried beneath sediment.

2.2.1 FOREBULGE

The forebulge is created in elastic response to the flexure of the lithosphere as a result of loading. It is one of the most distal zones, commonly the site of stratigraphic thinning and unconformity development; and is not always present (DeCelles and Giles, 1996). When a lithospheric plate has strength, a forebulge is expected to develop cratonward of the foreland basin. Modern values of the flexural rigidity of the Indian Plate are quite high, and therefore a forebulge is expected to be produced.

In the literature, the lack of a prominent forebulge observed in the field has been associated with Himalaya-derived sediment burying the forebulge and interfering with the lithosphere's flexural response (Crampton and Allen, 1995), and lithospheric loading of the Indian craton promoting a low, wide forebulge that is not readily identified in stratigraphic columns or well logs (DeCelles and Giles, 1996). DeCelles et al. (1998) associated the Oligocene unconformity with a broad forebulge as a result of thrust loading from the Himalayan orogen (Yin, 2006).

Gravity studies completed by Duroy et al. (1989) and Yeats and Lawrence (1984) identified structures with relief as the flexural bulge or forebulge. Both studies suggest that the Delhi-Sargodha Ridge or Sargodha Ridge marks the active forebulge in the west. The Delhi-Sargodha Ridge (Sargodha Ridge) is located immediately south of the Salt Range in Pakistan (Yin, 2006). Cina et al. (2009) suggest that the Shillong Plateau, located to the east of the Himalayan Foreland Basin and north of the Bengal Basin, is the forebulge (Figure 11).

Figure 11: Shillong Plateau identified as forebulge (taken from Cina et. al., 2009).

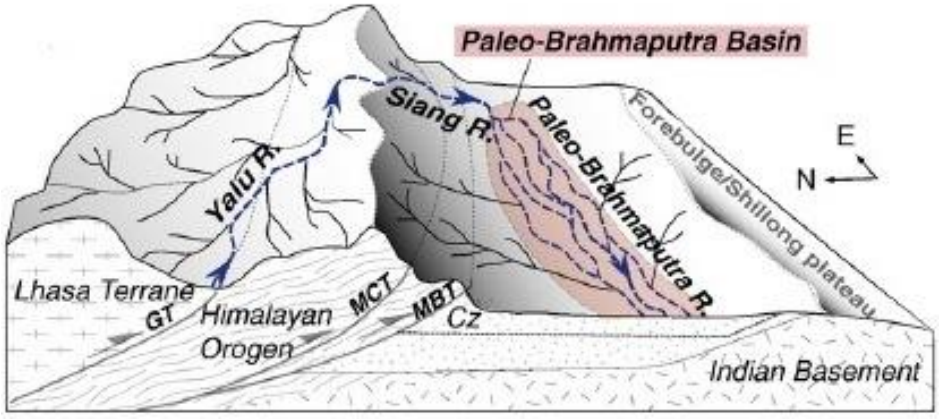

2.2.2 BASEMENT RIDGES

As a result of sediment deposition up to 6 km thick, the basement ridges of the Himalayan Foreland Basin cannot readily be observed at the surface; however, their presence has been determined by aeromagnetic, gravity, magnetic, and seismic surveys conducted by the ONGC (Oil and Natural Gas Corporation Limited)(Gahalaut and Kundu, 2012). The three ridges located within the study area, from west to east are Delhi-Hardwar Ridge, Faizabad Ridge, and the Munger (Monghyr)-Saharsa Ridge. These ridges are expected to be high relief features located on the Indian shield or basement rocks (Gahalaut and Kundu, 2012) (Figure 10 and 14).

Many authors have hypothesized the formation of the basement ridges that are located within the Himalayan Foreland Basin. Yin (2006) suggests that the ridges are an extension of the Peninsula Highlands. Much of the research conducted has been related to the seismicity of the region and the role of the basement ridges during subduction (Gahalaut and Kundu, 2012). The extent of the ridges is not known due to "lack of deep seismic data"; however, many researchers hypothesize that the ridges extend beneath the Himalayan wedge (Gahalaut and Kundu, 2012; Kumar et al., 2013).

Gahalaut and Kundu (2012) base their hypothesis upon the rupture extent and magnitude of earthquakes in the Himalaya. Kumar et al. (2013) studied the Jaisalmer-Ganganagar basement ridge located in the far west Himalayan Foreland

Basin. They originally hypothesized that the ridge was formed by a “mafic intrusive” event related to a larger thermal event in the region. However, during their research they noted that the ridges’ “subparallel nature with the geoid highs of the western fold belt clearly indicate it to be caused by the lithospheric flexure on the western side”.

2.2.3 BASIN MIGRATION

The India-Eurasia margin is an “active” margin and can be described as a continent-continent convergent boundary. During collision, if one slab is more dense the other, it is subducted, and thus “destroyed” or injected into the mantle lithosphere. The less dense lithospheric plate is typically up-thrusted onto the subducting slab. This margin can also be called a “convergent orogen”.

Convergent orogens are characterized by subduction of continental lithosphere, lithospheric delamination, refrigeration and heating of the crust, crustal melting, and development of thrust belts. These thrust belts, such as the Himalayas, have a wide variety of shortening structures including over-thrusts, imbricate thrusts, and duplexes. The thrust belts form in with a wedge-shape geometry. This means that there is a decrease in the shortening and thickening of the lithosphere as you move toward the collision zone on the thrust-wedge. Therefore, the deformation structures young in the direction of the thrust. In the case of the Himalayas, the deformation youngs toward the foreland.

The mechanics of thrust wedges include forelandward push, basal shear stress, and gravitational body force. All of these affect the morphology of the foreland basin, especially the forelandward push. There is a critical threshold for shortening and thickening of the thrust-wedge, which varies for all thrust wedges; once this threshold is reached, the thrust-wedge begins to lengthen through a series of normal faults (Figure 12).

Figure 12: Schematic crustal-scale section of the Himalayan collision zone, denoting the active foreland fold-and-thrust belt (modified after Powers et al., 1998).

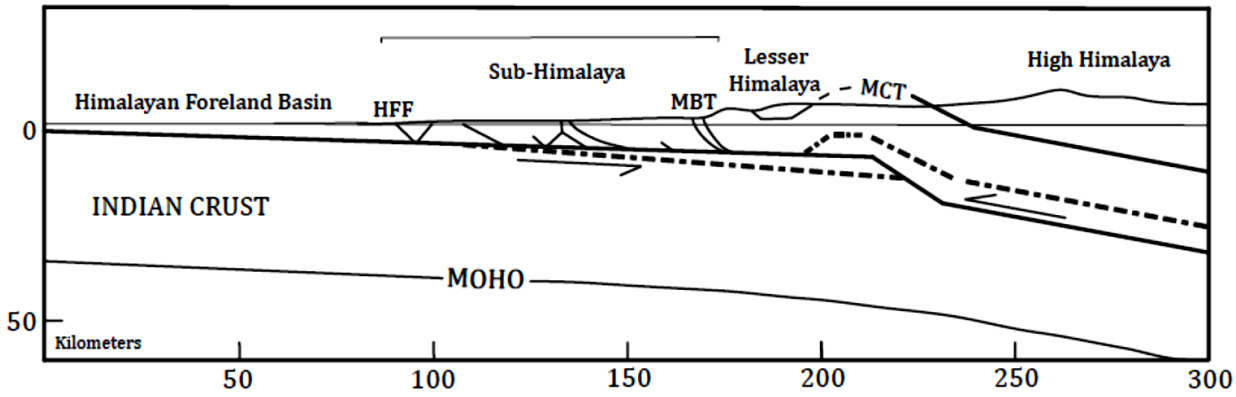

These faults bring the thrust toward the foreland. The foreland then responds by migrating basinward. This basinward migration of the foreland basin system results in the vertical stacking of the four depo-zones, producing an upward coarsening succession several kilometers thick. This sediment sequence characterizes the low initial rates of subsidence during deposition within the back-bulge depo-zone, development of a major unconformity or condensed section as the forebulge migrates through the basin, followed by rapid rates of subsidence during deposition within the foredeep, and decreased and variable rates of subsidence in the wedge-top depo-zone (DeCelles et al., 1998) (Figure 13).

Figure 13: Basinward migration of the foreland basin will vertically stack the four depo-zones (modified after DeCelles et al., 1998).

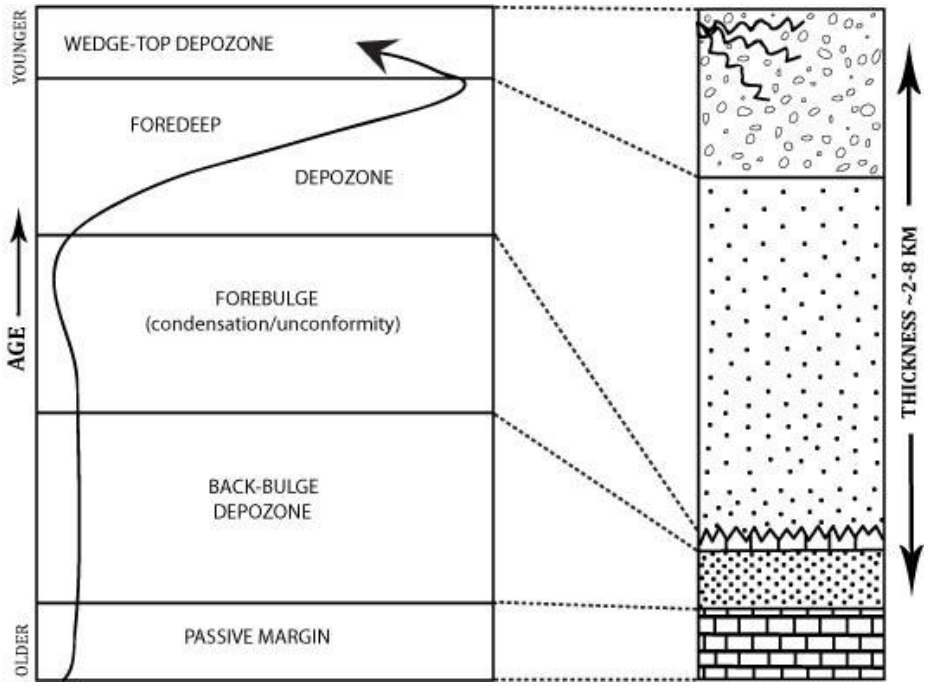

3. DEPTH OF BASEMENT OF THE HIMALAYAN FORELAND BASIN

3.1 METHODS AND DATA

ArcGIS was used to create a series of two-dimensional maps that were used to constrain the three-dimensional flexural models for this study. The completion of the maps included data and figures from previously published literature analyzed to create data points, and a basemap chosen from the ESRI ArcGIS User Community online database. The data points compiled were brought into ArcGIS as independent layers that allowed for the mapping of the study area in relation to tectonic features such as the MFT and Shillong Plateau, location and dimensions of the basement ridges within the study area, location of known depths via well log data and earthquake data studies, and fluvial system paths throughout the foreland basin.

To produce the Tectonic map, a latitude and longitude grid overlay was constructed to correctly map the locality of the MFT and Shillong Plateau. The data

points were created from previous studies (Yin, 2006; Lyon-Caen, 1980; and Lyon-Caen and Molnar, 1985). The Basement Ridge map, that identifies the basement ridges located within the study area, was also created through a latitude and longitude grid overlay that was constructed to correctly map the locality of the Delhi-Hardwar Ridge, Faizabad Ridge, and the Munger-Saharsa Ridge. The data points were chosen from Gahalaut and Kundu (2012).

Similarly to the Tectonic and Basement Ridge maps, the data points for the Well-log Data map were generated through a grid overlay placed onto a cross-section figure from Gahalaut and Kundu (2012) (Figure 14). The data points generated from the cross-section were placed at a distance of 130 km south of the MFT, in agreement with the approximate distance of 100-150 km noted in association with the cross-section of Gahalaut and Kundu (2012). Several data points, including a depth to basement, were located on a well log correlation modified after Sastri et al. (1971) found in Mallick et al. (2012).

The basemap chosen is a World Relief Map from the ESRI ArcGIS website. The shaded relief map depicts low-lying areas as well as areas of greater elevation with contrasting colors. Using a topographic or shaded relief map for a basemap allows us to see the elevation contrast on the surface of the study area and region in addition to the subsurface data overlain (Figure 15).

Figure 14: Cross-section of basement ridges within the Himalayan Foreland Basin. Cross-section is located approximately 100-150 km south of the MFT. Vertical features are Oil and Gas wells (modified after Gahalaut and Kundu, 2012).

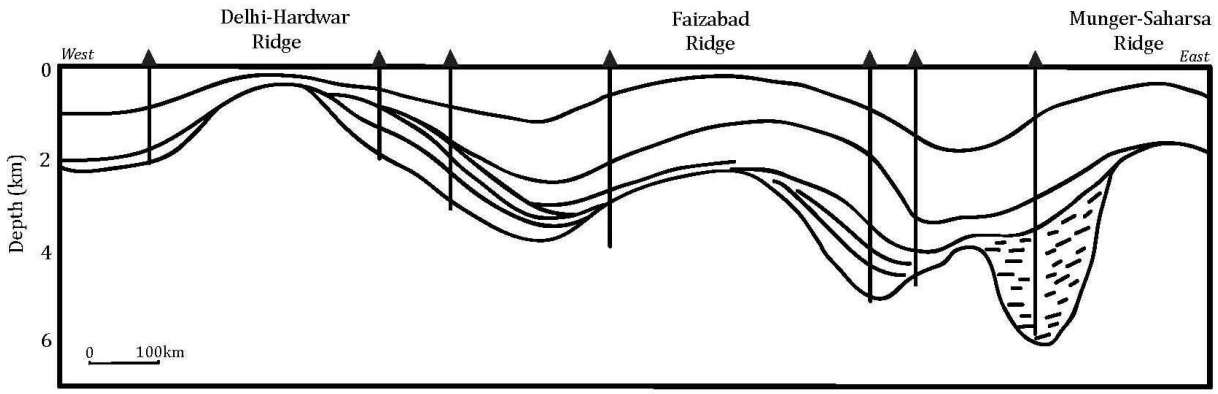

Figure 15: General topographic basemap general legend of color contrast by elevation and region (taken from www.shadedrelief.com/world_relief/home.html). Legend used for Figures 8, 9, 10, and subsequent maps).

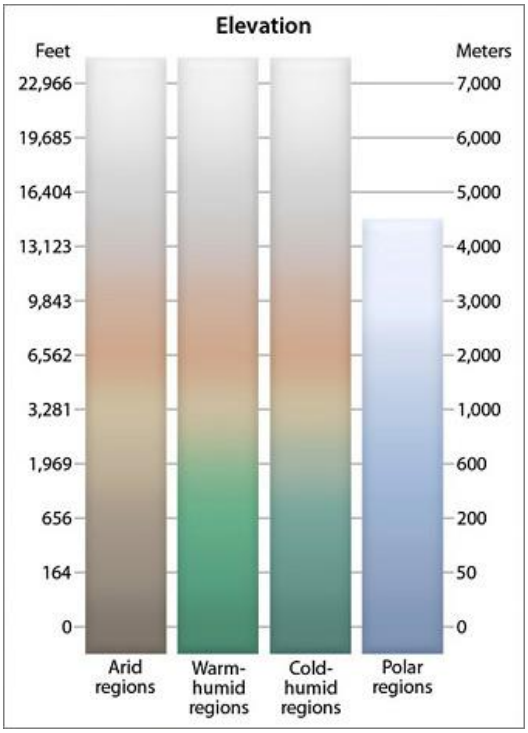

The IDW (Inverse Distance Weighted) map, created to depict the basement structure and depth contours, was produced using the Well-log Data map data and the Inverse Distance Weighted (IDW-Spatial Analyst) feature in ArcGIS. IDW-Spatial Analyst works by determining the value of cell data using a linearly weighted combination of a set of sample points. The weight assigned is a function of the inverse distance, the surface being interpolated must be that of a locationally dependent variable. The surface overlay created as a raster surface output by the IDW-Spatial Analyst feature acts to create depth contours, highlighting basement features (www.arcgis.com).

The Fluvial Systems map was created using the World Hydro Reference Overlay from ESRI ArcGIS online. The overlay maps all major and minor fluvial systems that traverse the study area. The fluvial paths are important features because they are the major cause of erosion in the Himalaya and deposition of sediment in the Himalayan Foreland Basin. A Middle Miocene reversal in drainage pattern (DeCelles et al., 1998) in the foreland basin has been related to regional tectonics (Figure 7).

3.2 RESULTS

The two-dimensional maps are used as a tool to assist in the visualization of the dynamics occurring in the study area. The Tectonic map identifies the major tectonic features in the Himalaya region in relation to the study area (Figure 16), the Basement Ridge map shows the placement of the ridges formed on the Indian Plate (Figure 9), the IDW map creates contours that allow for better understanding of the depth to basement (Figure 17), and the Fluvial Systems map shows the fluvial paths that traverse the foreland basin (Figure 9).

The IDW raster surface does not cover the entire study area on the IDW map. This is the result of the limited range of the data used for the interpolation. The best results are observed from IDW when the sampling, or data points, are dense. In this study, there are limited data points which affected the size of the covered area (Watson and Philip, 1985). However, the depth contours are visible and the basement structures can be observed in the contours that are mapped because the depth "extremes" have been sampled (Watson and Philip, 1985).

It is interesting to note that, in the Fluvial Systems map, the Yamuna river changes its course from southerly to south-eastern where it coalesces with the Ganges river. The Ganges river continues the south-eastern path, with rivers such as the Gomati, Ghaghara, and Kosi merging into the Ganges river, before the Ganges and the Brahmaputra rivers coalesce on their path toward the Bengal Basin. The change in direction and flow path of the Ganges river has important implications for the location of the forebulge. The flow path of the river may be diverted in response to the presence of an uplifted structure, the forebulge, which may be creating a structural high that is acting as a levee to obstruct the otherwise southerly flow of the Yamuna and Ganges rivers.

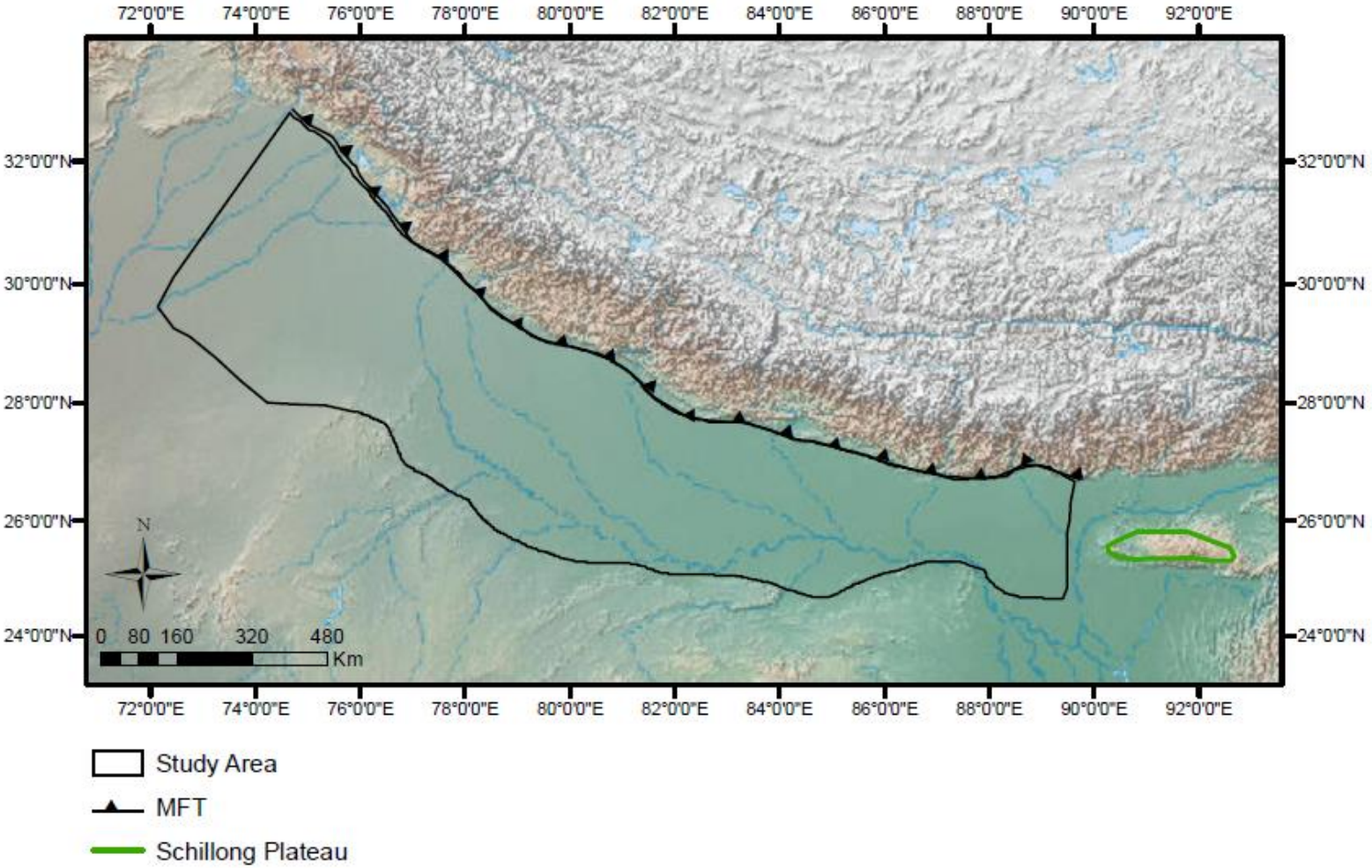

Figure 16: Tectonic map identifying the MFT and Shillong Plateau in relation to the study area. Elevation legend is on Figure 15.

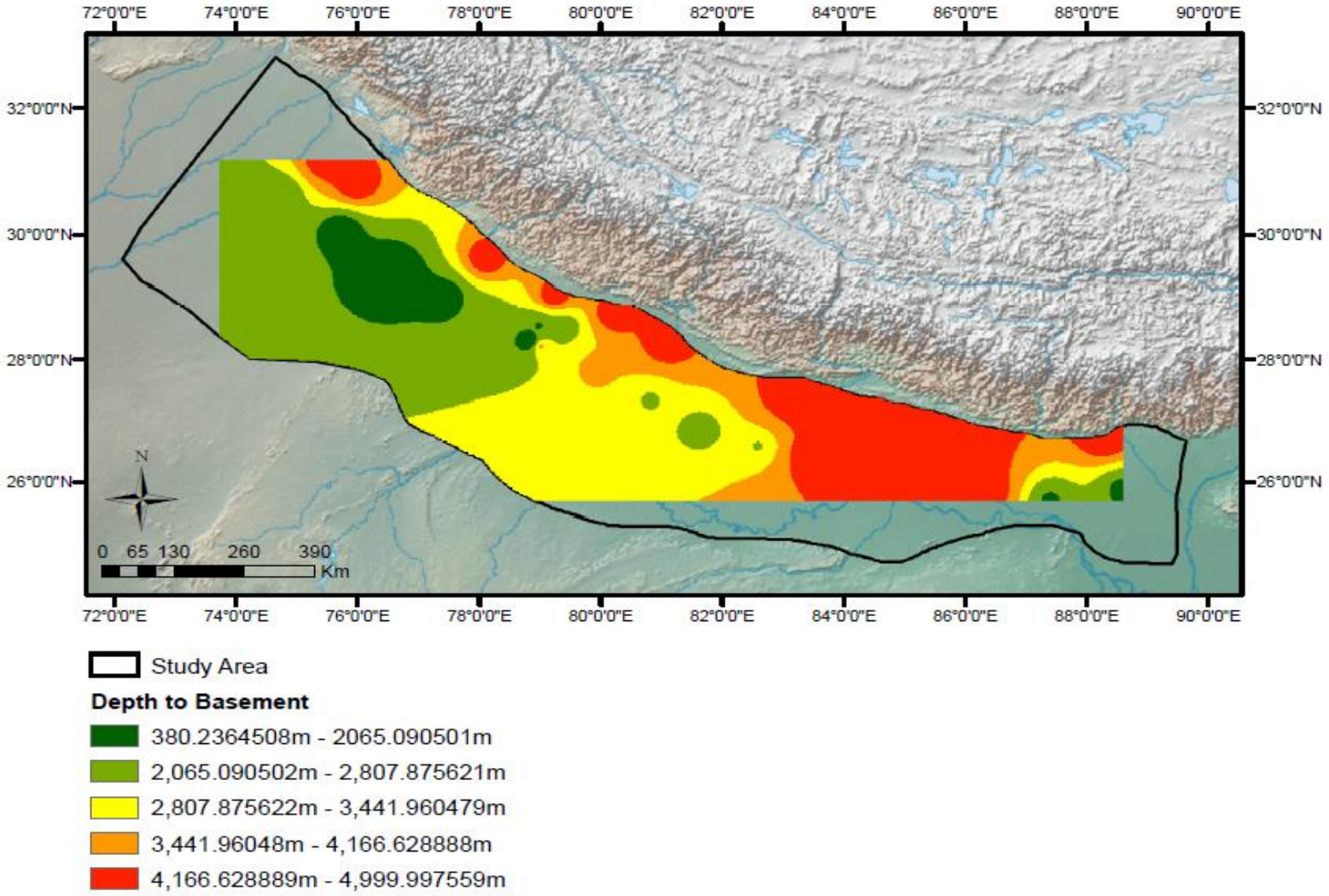

Figure 17: IDW map depicting the contours created with ESRI ArcGIS spatial analysis techniques.

4. MODELS OF COMPRESSION OF AN ELASTIC PLATE

The origin of the ridges located on the basement of the Himalayan Foreland Basin is unknown. There are two hypotheses for the formation of the basement ridges: lateral variation of the loading of the Indian Plate and compression of the Indian Plate as it converges with and is subducted by the Eurasian Plate. We test here whether the side-ward compression, simulating an east-west compression, of the elastic Indian Plate could result in the formation of basement ridges.

4.1 METHODS AND DATA

The general purpose finite element software package Abaqus (http://www.simulia.com), is used to analyze the deformation of an elastic plate under compression. For the purpose of this study, Abaqus was used to create finite element elastic models through the manipulation of a beam model. The beam model tests the linear elasticity of an object.

The linear elasticity of an object defines the behavior of a solid object during deformation using Young's modulus, a constant given to quantify the stiffness of an elastic material; and Poisson's ratio, a measure of the Poisson effect which occurs when a material responds to compression by expanding perpendicular to the applied force; the dimensions of the object, and the effective elastic thickness of the plate (T_e).

For both models, the dimensions for the "beam" are 2000 km long and 1000 km wide; this simulates the size of the study area, the subducting Indian Plate. A Young's modulus of 70 Ga and Poisson's ratio of 0.25 were used. In Model 1 an effective elastic thickness (T_e) of 50 km was used, and a T_e of 70 km for Model 2. The T_e values chosen were based off of previous studies, T_e of 60-80 km with a northward decreasing trend to approximately 20-30 km (Hetenyi et al., 2006), $40<T_e<100$ (Jordan and Watts, 2005), and T_e variation between 40-50 km (Cattin et al., 2001).

The model domain consists of the Indian Plate. The plate is constrained on the northern and western boundary so that the force imposed from the east onto the beam is acting to compress the beam. Once the values and constraints are included in the model, a

deformable planar shell is created in Abaqus. Abaqus then computes the linear perturbation and the buckling of the beam.

4.2 RESULTS

Basement ridges were produced in both models (T_e of 50 km and 70 km). In both models, the force was applied to the right side of the model domain; producing higher ridges closest to the applied force and ridges of smaller amplitude further from the applied force. Depressions are formed in between the ridges.

Figure 18 shows the results of Abaqus Model 1 which has a T_e of 50 km. Four distinct ridges are formed which are elongate and formed with almost equal spacing; this is similar to what is observed in the Himalayan Foreland Basin.

Figure 19 shows the results of Abaqus Model 2 which has a T_e of 70 km. Here, five distinct ridges are formed; the three ridges located in the center and on the left side of the model domain are elongate and formed with almost equal spacing. The two ridges located on the right side of the model domain appear to pinch out. The ridges exhibit higher amplitudes the closer they are located to the applied force.

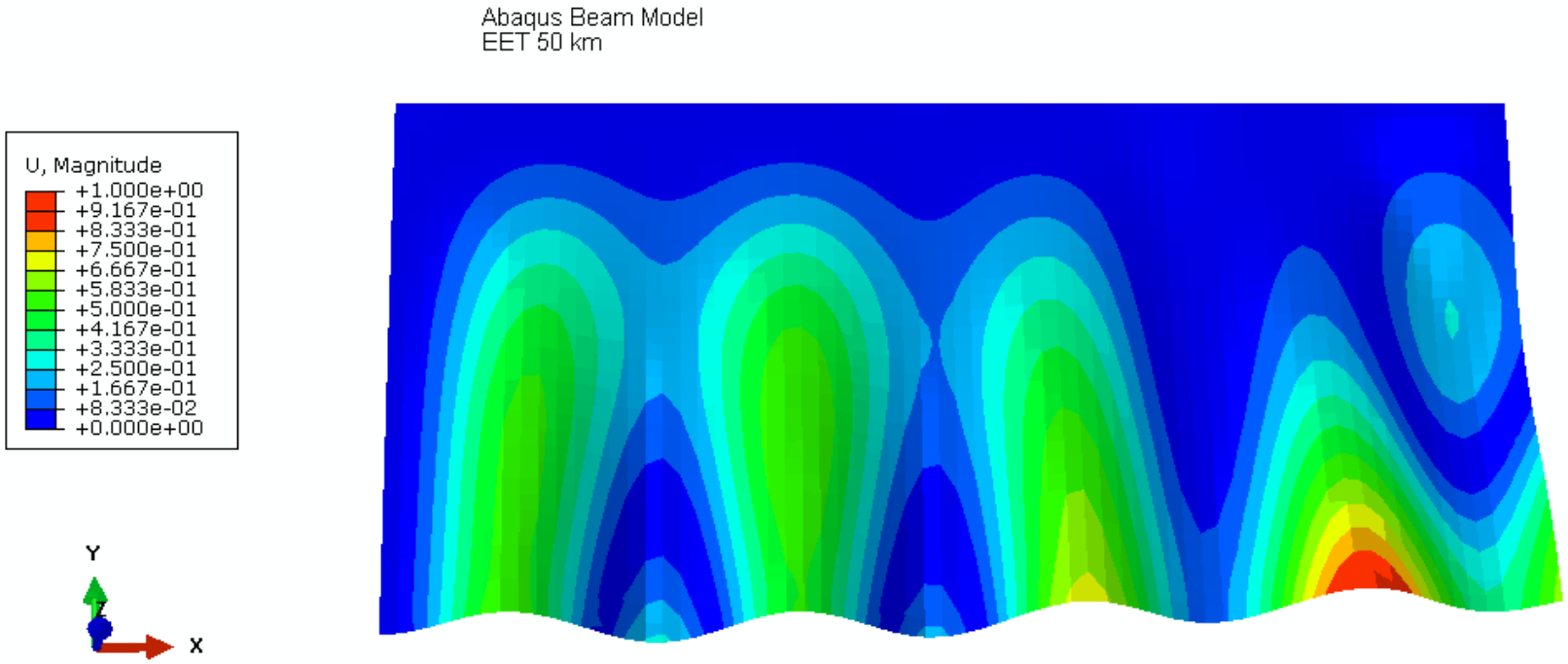

Figure 18: Abaqus model results of Model 1, with T_e of 50 km. Three distinct ridges are formed, three elongate ridges with almost equal spacing; similar to what is observed in the Himalayan Foreland Basin. Model created by Rediet Abera. Green and yellow colors denote ridges, blue colors denote depressions. Color scale is dimensionless. A compressional force was applied on the right side of the model domain in the –x direction.

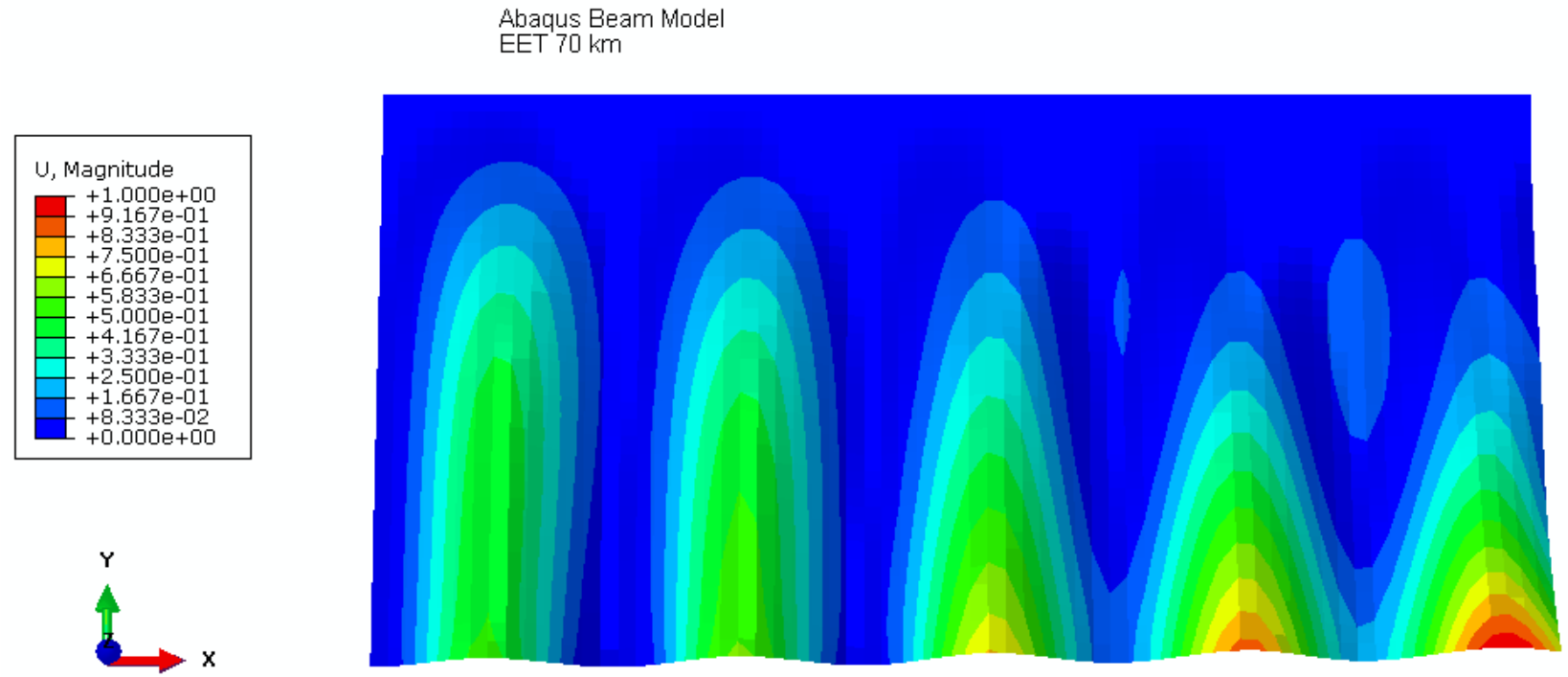

Figure 19: Abaqus model results for Model 2, with T_e of 70 km. Three- to four distinct ridges are formed, they are elongate ridges with almost equal spacing. Model created by Rediet Abera. Green and yellow colors denote ridges, blue colors indicate depressions. Color scale is dimensionless. A compressional force was applied on the right side of the model domain in the –x direction.

5. FLEXURAL MODELS OF THE HIMALAYAN FORELAND BASIN

5.1 METHODS AND DATA

The flexural code developed by Li et al. (2004) was used in this study to create three-dimensional models of the Indian craton following the emplacement of the Himalaya mountain range and subsequent foreland basin formation and sediment infill. In this study, we assume that the (elastic) lithosphere acts as an elastic plate.

The flexural model was chosen for this study because it helps to define the dimensions and shape of smaller-scale features, such as the forebulge. The flexural model uses the flexural equation to compute the deflection of the lithosphere: $D*(d^4w(x)/dx^4) = -(p_m-p_{fill})*gw(x) + q(x)$, where $D = Eh^3/12(1-v^2)$. The variables in this equation are defined as: "D" = the flexural rigidity or the resistance to deflection, "E" = Young's modulus, "*v*" = Poisson's ratio, "q(x)" = the load (downward force per unit area), "h" = the thickness of the elastic plate, "p_m" = mantle density, "p_{fill}" = density of deflection fill (basin fill), "w(x)" = the deflection of the plate, and "g"= gravitational acceleration (Li et al., 2004).

The model parameters used to produce the three-dimensional models include gravity, the flexural rigidity of the continental lithosphere, the mantle density, the density of the load and its dimensions, and the density of the infill load. The main load, "load", is the thrust load, defined as the Himalayan mountain chain; both the Higher Himalayas and the Lesser Himalayas. The secondary load, "infill", is the sediment infill load, defined as the sediment infill in the accommodation space created as the load deflected the Indian Plate. The subducting Indian slab is assumed to be buoyant, so its density is not included in the load.

The gravity and density data used are the same values used in previous studies completed by Lyon-Caen and Molnar (1985) and Jordan and Watts (2005) (Tables 1 and 2). Both Lyon-Caen and Molnar (1985) and Jordan and Watts (2005) created two-dimensional flexural models of the Himalaya foreland basin in their studies wherein they discussed the T_e of the Indian craton. Lyon-Caen and Molnar (1985) found the T_e of the Indian Plate to be between 40 and 100 km, and suggest a flexural rigidity of 1E24 Nm and 7E24 Nm. They infer significant variation of the flexural rigidity of the Indian Plate

along the northern margin. Jordan and Watts (2005) found a T_e of 70 km for the central region of the foreland basin and a decrease to 30-50 km in the east and west portions of the basin. They suggest an overall T_e of $40< T_e<100$ km and describe the basin as a rigid block with well-defined edges suggested by the localization of faulting and deformation along the northern margin.

The flexural rigidity of the lithosphere tells us about the strength of the Indian Plate during the convergence with the Eurasian plate. The T_e of the plate(s) is proportional to the strength and therefore related to the rigidity of the lithosphere. A plate with a small flexural rigidity will behave more weak and elastic than a plate with a larger flexural rigidity and T_e. This will in turn affect the dimensions of the foreland basin produced in response to the loading of the lithosphere and could have implications for the presence or absence of the forebulge.

Table 1: Model parameters from previous flexural study (modified after Lyon-Caen and Molnar, 1985).

	Mean Densities (g/cm^3)	**Width** (km)
Foreland Basin		200-250
Sediments (Infill)	2.4	
Load	2.7	
Mantle	3.35	
Crust	2.8	

Table 2: Model parameters from previous flexural study (modified after Jordan and Watts, 2005).

	Mean Densities (kg/m^3)	**Model Dimensions** (km)
Foreland Basin		2000 x 200 x 5
Infill	2650	
Load	2650	
Mantle	3330	
Crust	2800	

5.1.1 UNIFORM LOAD

For this study, 17 uniform load models were generated. All parameters remained constant in the models with the exception of the flexural rigidity, load density, and infill density (Table 3). The load in these models has a length of 2000 km, width of 200 km, and a height of 5 km. This load acts like a block creating a downward force on the edge of the planar surface (plate) in the model (Figure 20). The flexure produced resembles the dimensions of the load. The magnitude of the deflection and forebulge are dependent on the flexural rigidity and load densities.

Through the use of uniform values, we are able to determine whether features, such as the forebulge, can be produced with realistic parameters in a constrained model. Variance, such as change in the load or T_e, becomes important when features other than those that are expected to be observed in a typical foreland basin system have formed.

Table 3: Uniform load models produced with their parameters.

Model	Flexural Rigidity (Nm)	Load (kg/m^3)	Infill Load (kg/m^3)	Mantle (kg/m^3)	Load Dimensions (km)	Basin Depth (m)	Forebulge (Y/N)
D1	8.00E+25	2650	2650	3330	2000 x 200 x 5	-2400	N
D2	8.00E+24	2650	2650	3330	2000 x 200 x 5	-6000	Y
D3	7.00E+24	2650	2650	3330	2000 x 200 x 5	-6500	Y
D4	9.00E+24	2650	2650	3330	2000 x 200 x 5	-6000	Y
D5	1.00E+25	2650	2650	3330	2000 x 200 x 5	-5500	N
D6	2.00E+25	2650	2650	3330	2000 x 200 x 5	-4000	N
D7	9.00E+23	2650	2650	3330	2000 x 200 x 5	-12000	Y
D8	8.00E+25	3000	2650	3330	2000 x 200 x 5	-3800	N
D9	8.00E+24	2700	2400	3330	2000 x 200 x 5	-6000	Y
D10	8.00E+24	2670	2400	3330	2000 x 200 x 5	-5000	Y
D11	8.00E+24	3500	2650	3330	2000 x 200 x 5	-8000	Y
D12	1.00E+25	3000	2650	3330	2000 x 200 x 5	-6500	N
D13	1.00E+25	3500	2650	3330	2000 x 200 x 5	-7500	N
D14	1.00E+24	2650	2650	3330	2000 x 200 x 5	-12000	Y
D15	5.00E+24	2650	2650	3330	2000 x 200 x 5	-7500	Y
D16	1.00E+25	2670	2400	3330	2000 x 200 x 5	-4500	Y
D17	1.00E+25	2700	2400	3330	2000 x 200 x 5	-4500	Y

Figure 20: Uniform load model showing placement of load on plate.

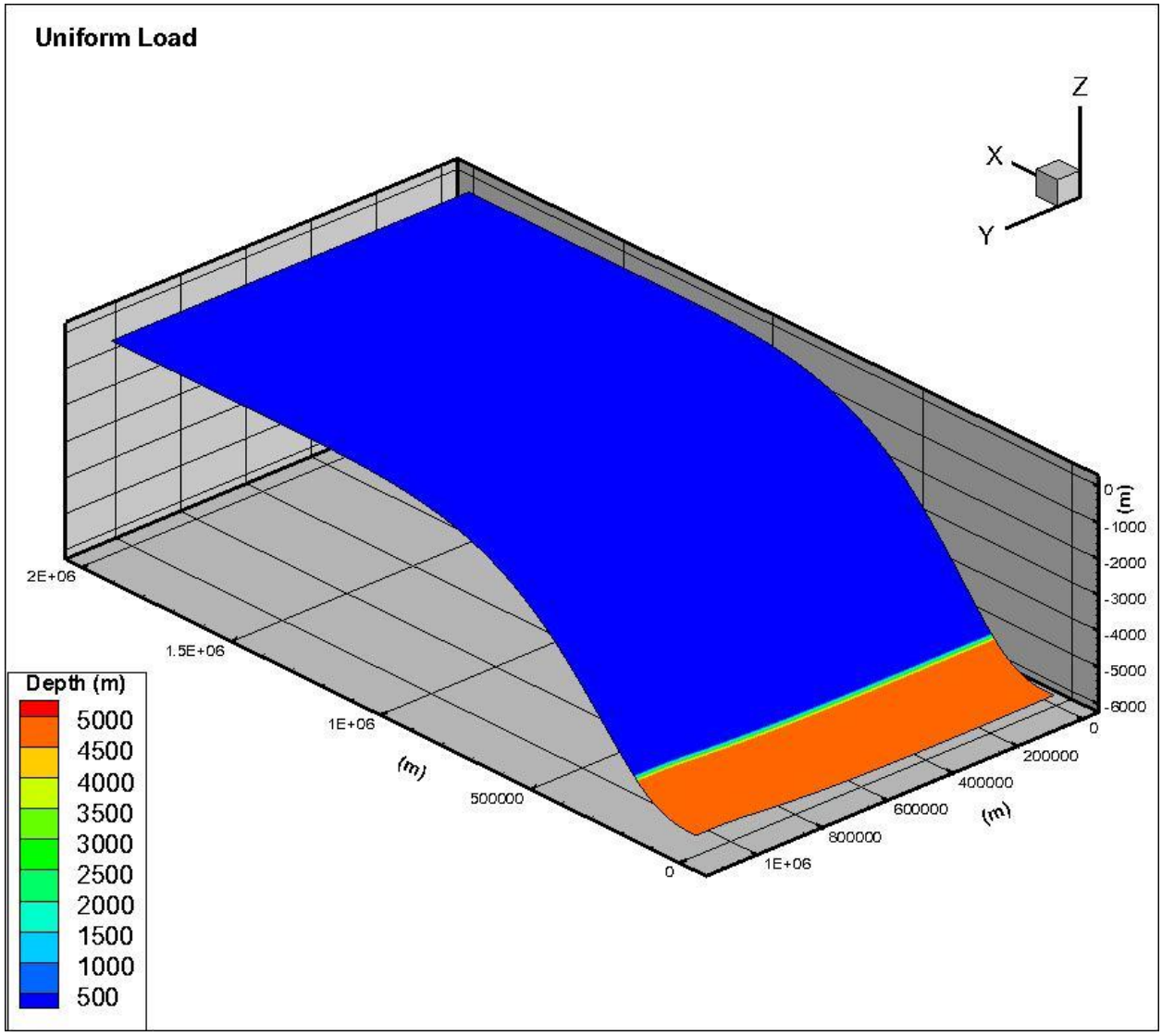

5.1.2 LATERALLY VARYING LOAD

For this study, 17 laterally varying load models were generated. The load height was varied to simulate the dynamics of the Himalayas. The load height chosen for each model is based on the average height of the Himalayan mountain range. The load acts like a block creating a downward force on the plate, the flexure produced resembles the dimensions of the load.

Models DLV1-DLV11 have two different loads emplaced that cover the entire model domain (Figure 21), one load varied from 4000 m to 5000 m while the remaining load was held constant at 7000 m. Models DLVR1-DLVR3 have two loads with a height of 5000 m emplaced on the edges of the model domain (Figure 22). Models DLVR4-DLVR6 have three loads of 5000 m emplaced on the edges and center of the model domain (Figure 23).

For models DLV1-DLV8, all parameters remained constant with the exception of the flexural rigidity and the load height. For models DLV9-DLV11, all parameters remained constant with the exception of the flexural rigidity, load height, and load density. Models DLVR1-DLVR6 have varying flexural rigidities and load height; all remaining parameters were held constant (Tables 4a, b, c).

The non-uniformity of the load should create a greater deflection of the plate in the portion of the model where the load is greater. A load was emplaced on the edges of the plate in models DLVR1-DLVR3 to simulate lateral variations in the load in an effort to produce one ridge. The load emplaced on the center and edges of the plate in models DLVR4-DLVR6 also simulate lateral variations in the load in an effort to produce two ridges. In addition to the basement ridges, a forebulge is expected to form on the plate in response to loading.

Table 4a: Models with varying flexural rigidity (8E24 Nm, 9E24 Nm, 1E 25 Nm) and laterally varying load and their respective parameters.

Model	Flexural Rigidity (Nm)	Load/Infill Density (kg/m^3)		Mantle (kg/m^3)	Laterally Varying Load (m)		Laterally Varying Max. Depth (m)		Forebulge (Y/N)
DLV1	1.00E+25	2650	2650	3330	4000	7000	-900	-1400	Y
DLV2	1.00E+25	2650	2650	3330	4000	7000	-900	-1500	Y
DLV3	8.00E+24	2650	2650	3330	4000	7000	-1000	-1600	Y
DLV4	8.00E+24	2650	2650	3330	4000	7000	-1300	-1600	Y
DLV5	1.00E+25	2650	2650	3330	5000	7000	-1100	-1500	Y
DLV6	8.00E+24	2650	2650	3330	5000	7000	-1200	-1600	Y
DLV7	9.00E+24	2650	2650	3330	4000	7000	-1100	-1600	Y
DLV8	9.00E+24	2650	2650	3330	5000	7000	-1100	-1500	Y
DLV9	1.00E+25	3000	2650	3330	3500	7000	-1200	-1600	Y
DLV10	8.00E+24	3000	2650	3330	3500	7000	-1300	-1700	Y
DLV11	9.00E+24	3000	2650	3330	3500	7000	-1100	-1700	Y

Table 4b: Models with varying flexural rigidity (8E24 Nm, 9E24 Nm, and 1E 25 Nm) and load varied on edges of model and their respective parameters; in attempt to produce one ridge.

Model	Flexural Rigidity (Nm)	Load/Infill Density (kg/m^3)		Mantle (kg/m^3)	Laterally Varying Load (m)			Max. Depth (m)	Forebulge (Y/N)
DLVR1	8.00E+24	2650	2650	3330	5000	0	5000	-7500	Y
DLVR2	9.00E+24	2650	2650	3330	5000	0	5000	-7000	Y
DLVR3	1.00E+25	2650	2650	3330	5000	0	5000	-7000	N

Table 4c: Models with varying flexural rigidity (8E24 Nm, 9E24 Nm, and 1E 25 Nm) and load varied on center and edges of model and their respective parameters; in attempt to produce two ridges.

Model	Flexural Rigidity (Nm)	Load/Infill Density (kg/m^3)		Mantle (kg/m^3)	Laterally Varying Load (m)					Max. Depth (m)	Forebulge (Y/N)
DLVR4	8.00E+24	2650	2650	3330	5000	0	5000	0	5000	-3800	Y
DLVR5	9.00E+24	2650	2650	3330	5000	0	5000	0	5000	-3600	Y
DLVR6	1.00E+25	2650	2650	3330	5000	0	5000	0	5000	-3500	N

Figure 21: Laterally Varying Load Placement Model.

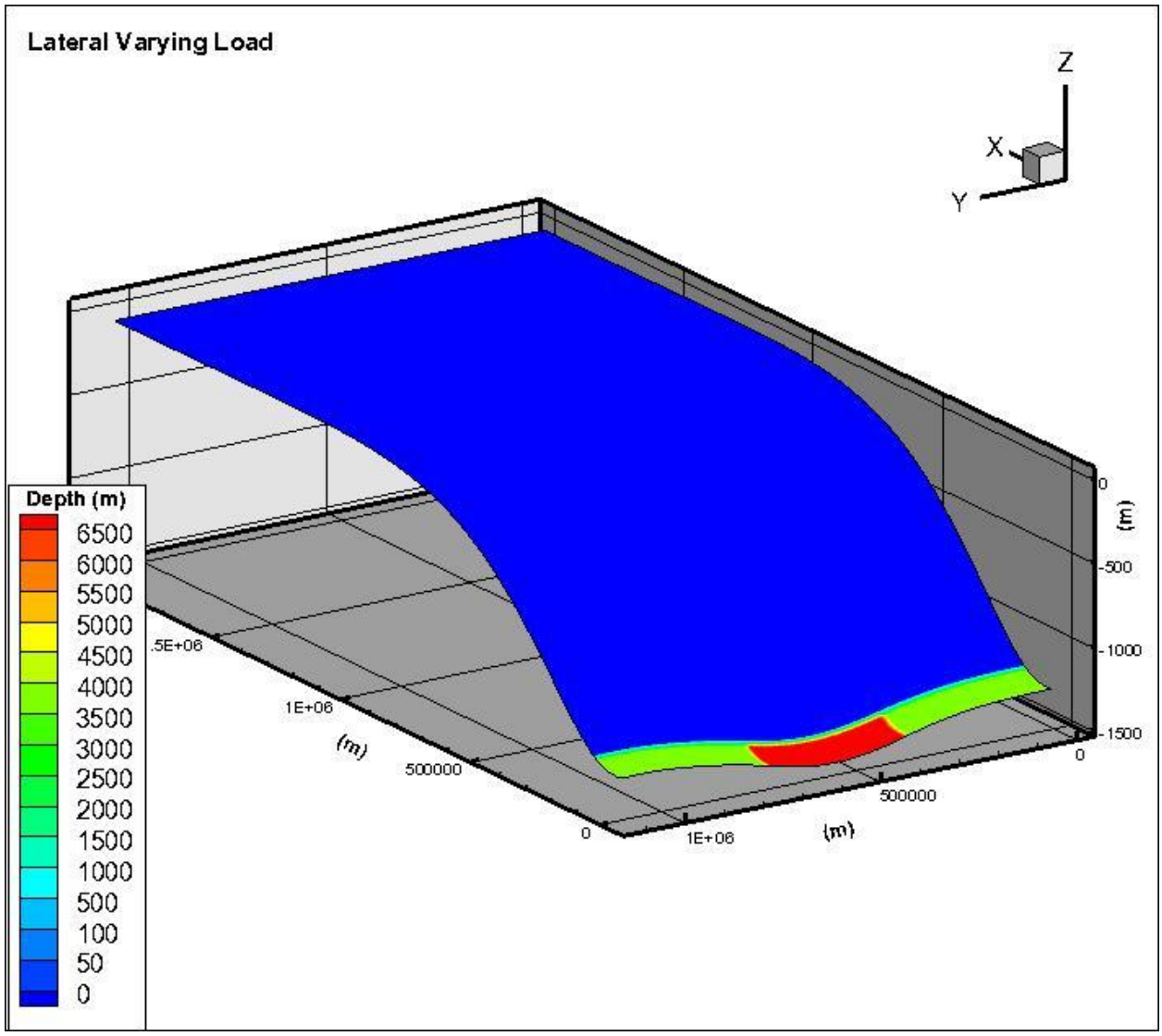

Figure 22: Laterally Varying Load Placement Model, loading on edges of plate in attempt to produce one basement ridge.

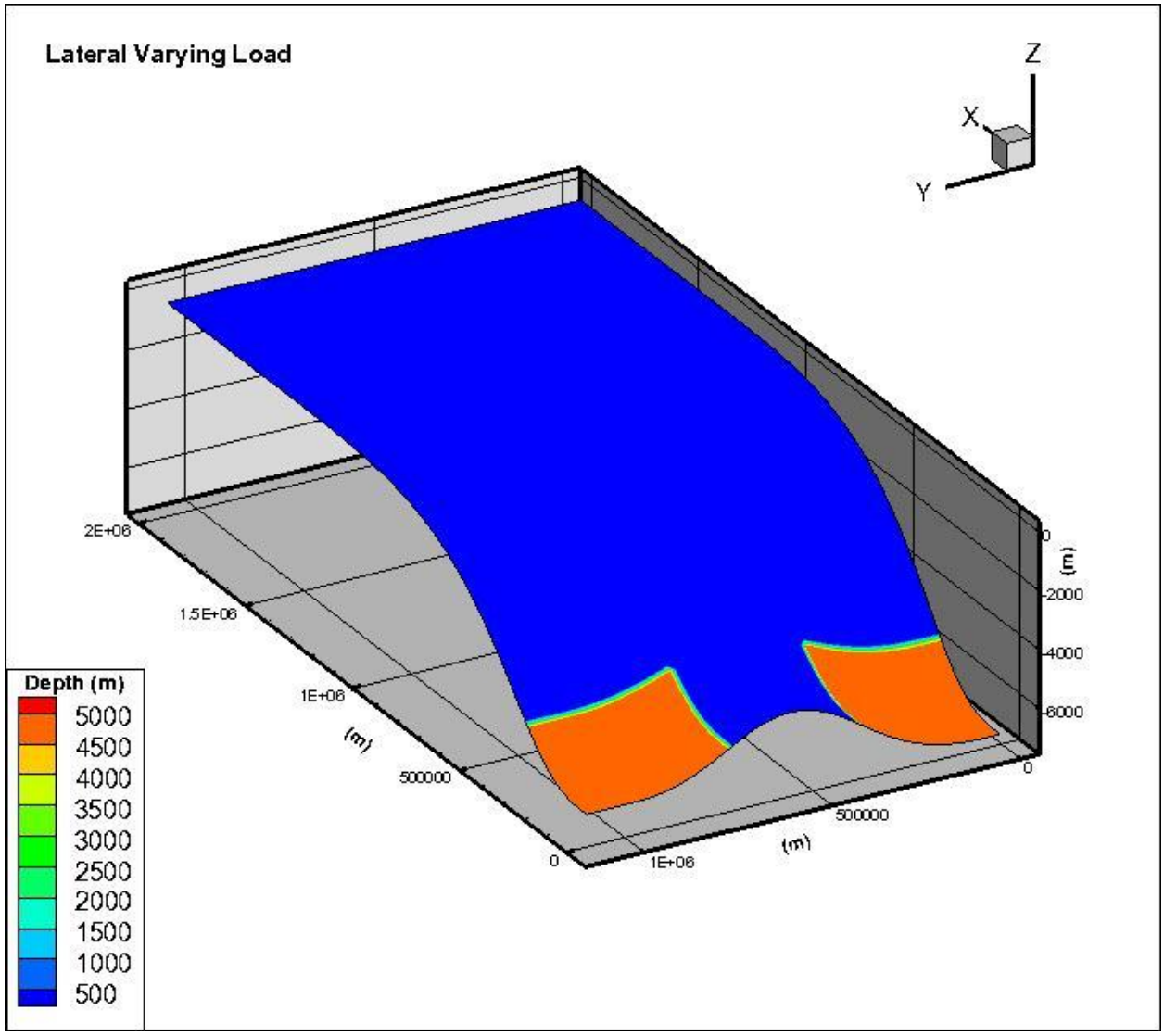

Figure 23: Laterally Varying Load Placement, in attempt to produce two ridges.

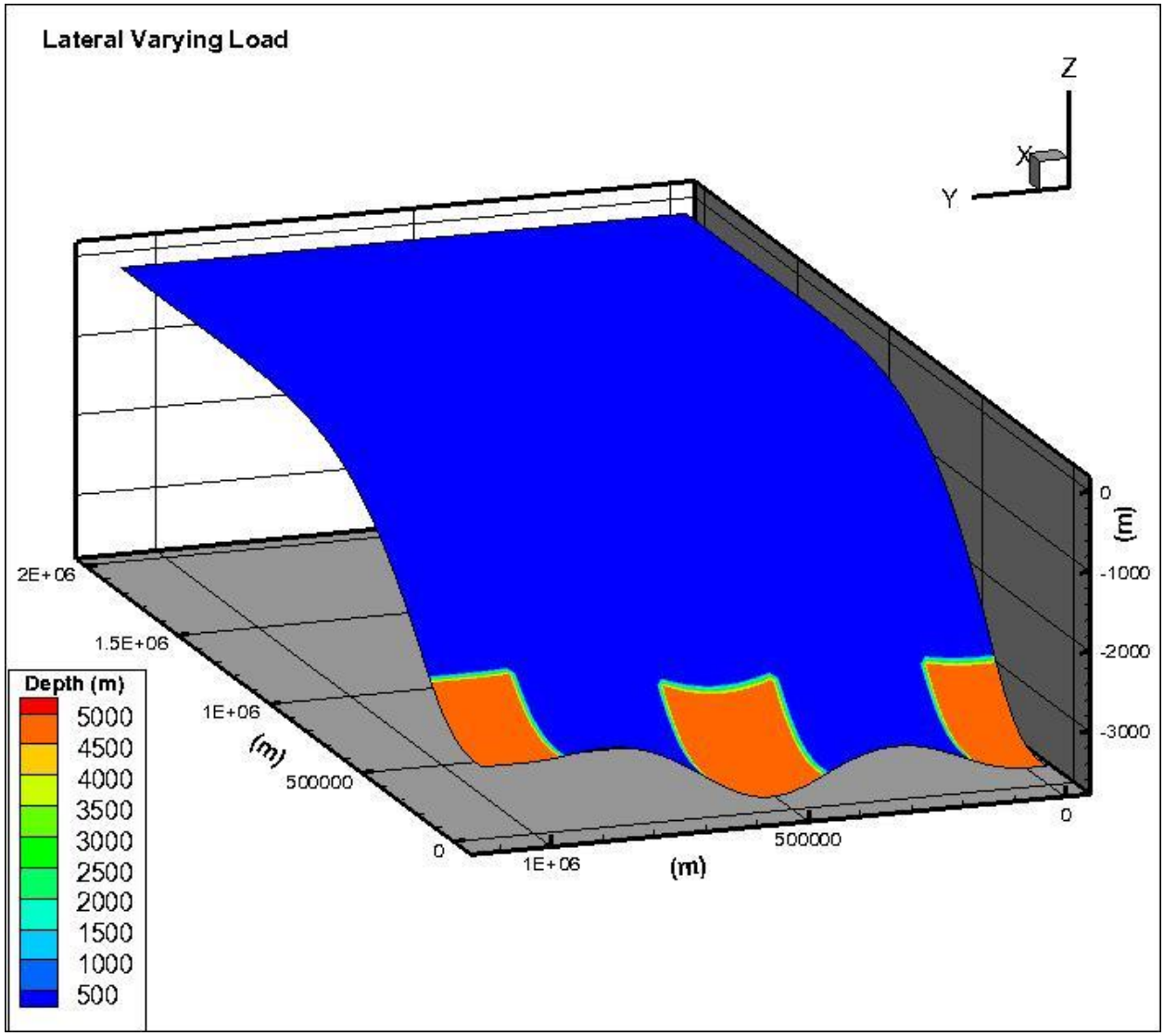

5.2 RESULTS

5.2.1 UNIFORM LOAD

Of the 17 models that were generated (Appendix A), there are four models that have depths that resemble what studies have estimated to be the maximum depth of the basin at the MFT (Table 3). These models are: D2, D4, D5, and D9. Models D2, D4, and D5 have the same load values (load = 2650 kg/m^3, infill = 2650 kg/m^3) with varying flexural rigidities. Model D9 and Model D2 have the same flexural rigidity (8E24 Nm), however, the load and infill load differ with D9 having load values of 2700 kg/m^3 and 2400 kg/m^3, respectively. Model D4 has a flexural rigidity of 9E24 Nm and D5 has a flexural rigidity of 1E25 Nm.

All of these models also have a low, broad forebulge produced, except for Model D5 which continues to increase in height across the model domain. Model D2, D4, and D9 have a deflection of 6000 m with a forebulge amplitude of <50 m (Figures 25, 26, 29). Model D5 has a deflection of 5500 m with no apparent forebulge produced (Figure 27).

Models D2, D9, D10, and D11 have a flexural rigidity of 8E24 Nm (Table 5). Model D10 has a load of 2650 kg/m^3 and an infill load of 2400 kg/m^3, with a deflection of 5000 m; with a forebulge amplitude of <50 m (Figure 29). Model D11 has a load of 3500 kg/m^3 and an infill load of 2650 kg/m^3, with a deflection of 8000 m; forebulge with an amplitude of <50 m produced (Figure 30).

Table 5: Models produced with flexural rigidity of 8E24Nm.

Model	Flexural Rigidity (Nm)	Load (kg/m^3)	Infill Load (kg/m^3)	Mantle (kg/m^3)	Load Dimensions (km)	Model Depth (m)	Forebulge (Y/N)
D2	8.00E+24	2650	2650	3330	2000 x 200 x 5	-6000	Y
D9	8.00E+24	2700	2400	3330	2000 x 200 x 5	-6000	Y
D10	8.00E+24	2670	2400	3330	2000 x 200 x 5	-5000	Y
D11	8.00E+24	3500	2650	3330	2000 x 200 x 5	-8000	Y

Models D5, D12, D13, D16, and D17 have a flexural rigidity of 1E25 Nm (Table 6). Model D12 has a load of 3000 kg/m^3 and an infill load of 2650 kg/m^3, with a deflection of 6500 m; no forebulge is produced (Figure 31). Model D13 has a load of 3500 kg/m^3 and an infill load of 2650 kg/m^3, with a deflection of 7500 m; forebulge with an amplitude of <50 m produced (Figure 32). Model D16 has a load of 2650 kg/m^3 and an infill load of 2400 kg/m^3, with a deflection of 4500 m; with a forebulge amplitude of <50 m (Figure 33). Model D17 has a load of 2700 kg/m^3 and an infill load of 2400 kg/m^3, with a deflection of 4500 m; forebulge with an amplitude of <50 m produced (Figure 34).

Table 6: Models produced with flexural rigidity of 1E25 Nm.

Model	Flexural Rigidity (Nm)	Load (kg/m^3)	Infill Load (kg/m^3)	Mantle (kg/m^3)	Load Dimensions (km)	Model Depth (m)	Forebulge (Y/N)
D5	1.00E+25	2650	2650	3330	2000 x 200 x 5	-5500	N
D12	1.00E+25	3000	2650	3330	2000 x 200 x 5	-6500	N
D13	1.00E+25	3500	2650	3330	2000 x 200 x 5	-7500	Y
D16	1.00E+25	2670	2400	3330	2000 x 200 x 5	-4500	Y
D17	1.00E+25	2700	2400	3330	2000 x 200 x 5	-4500	Y

The remaining models, D1, D3, D4, D6, D7, D8, D14, and D15 have varying flexural rigidities and load values (Table 7). Model D1 has a flexural rigidity of 8E25 Nm, a load of 2650 kg/m^3, infill load of 2650 kg/m^3, and a deflection of 2400 m; no apparent forebulge is produced (Figure 35). Model D3 has a flexural rigidity of 7E24 Nm, a load of 2650 kg/m^3, infill load of 2650 kg/m^3, and a deflection of 6500 m; a forebulge with an amplitude of <50 m produced (Figure 36). Model D6 has a flexural rigidity of 2E25 Nm, a load of 2650 kg/m^3, infill load of 2650 kg/m^3, and a deflection of 4000 m; no apparent forebulge is produced (Figure 37).

Model D7 has a flexural rigidity of 9E23 Nm, a load of 2650 kg/m^3, infill load of 2650 kg/m^3, and a deflection of 12000 m; a more pronounced forebulge with amplitude of 0<50<100 m is produced along with a secondary structural high with an amplitude of <50 m (Figure 38). Model D8 has a flexural rigidity of 8E25 Nm, a load of 3000 kg/m^3,

infill load of 2650 kg/m^3, and a deflection of 3800 m; no apparent forebulge is produced (Figure 39). Model D14 has a flexural rigidity of 1E24 Nm, a load of 2650 kg/m^3, infill load of 2650 kg/m^3, and a deflection of 12000 m; a more pronounced forebulge with amplitude of 0<50<100 m is produced along with a secondary structural high with an amplitude of <50 m (Figure 40). Model D15 has a flexural rigidity of 5E24 Nm, a load of 2650 kg/m^3, infill load of 2650 kg/m^3, and a deflection of 7500 m; no forebulge is produced (Figure 41).

Table 7: Models with varying flexural rigidity and their respective parameters.

Model	Flexural Rigidity (Nm)	Load (kg/m^3)	Infill Load (kg/m^3)	Mantle (kg/m^3)	Load Dimensions (km)	Model Depth (m)	Forebulge (Y/N)
D1	8.00E+25	2650	2650	3330	2000 x 200 x 5	-2400	N
D3	7.00E+24	2650	2650	3330	2000 x 200 x 5	-6500	Y
D4	9.00E+24	2650	2650	3330	2000 x 200 x 5	-6000	Y
D6	2.00E+25	2650	2650	3330	2000 x 200 x 5	-4000	N
D7	9.00E+23	2650	2650	3330	2000 x 200 x 5	-12000	Y
D8	8.00E+25	3000	2650	3330	2000 x 200 x 5	-3800	N
D14	1.00E+24	2650	2650	3330	2000 x 200 x 5	-12000	Y
D15	5.00E+24	2650	2650	3330	2000 x 200 x 5	-7500	N

5.2.2 LATERALLY VARYING LOAD

Most of the 17 models generated have consistent forebulge and depth results (Appendix A). None of the models produced reached depths that resemble what studies have estimated to be the maximum depth of the basin at the MFT (Tables 8, 9, 10). All models, with the exception of DLVR3 and DLVR6, have a low broad forebulge (amplitude <50 m) (Figures 43 and 46). Although subtle, the forebulge appears to migrate basinward as the load is increased. The slope of the foreland basin steepens, in each model, as the load is increased. The models produced in an attempt to form one basement ridge have more structural highs, with significant relief in the relation to the basin depth, than the models produced in an attempt to form two basement ridges.

From model set DLV1-DLV11, models DLV10 and DLV11 have the deepest basins reaching a maximum depth of -1700 m (Table 4a). Model DLV10 has a flexural rigidity of 8E24 Nm, load density of 3000 kg/m^3, infill density of 2650 kg/m^3, laterally varying load of 3500 m and 7000 m; basin depths of -1300 m and -1700 m, respectively (Figure 51). Model DLV11 has a flexural rigidity of 9E24 Nm, load density of 3000 kg/m^3, infill density of 2650 kg/m^3, laterally varying load of 3500 m and 7000 m; basin depths of -1100 m and -1700 m, respectively (Figure 52). Model DLV1 has the shallowest basin reaching a maximum depth of -1400 m. Model DLV1 has a flexural rigidity of 8E24 Nm, load density of 2650 kg/m^3, infill density of 2650 kg/m^3, laterally varying load of 4000 m and 7000 m; basin depths of -900 m and -1400 m, respectively (Figure 42).

Model set DLVR1-DLVR3 (Figures 53-55) was produced in an attempt to produce a basement ridge. In all models, a structural high was produced in the center of the basin. The location of the structural high in the models is consistent with the lack of load placement. The height of the structural highs, from the basement, is 3500 m in Model DLVR1, 2500 m in Model DLVR2, and 2500 m in Model DLVR3. Model DLVR1 has the deepest basin with a maximum depth of -7500 m (Table 4b).

Model DLVR1 has a flexural rigidity of 8E24 Nm, load density of 2650 kg/m^3, infill density of 2650 kg/m^3, laterally varying load of 5000 m, 0 m, 5000 m; model depths of -7000 m, -4000 m, and -7500 m; respectively (Figure 53). A lack of forebulge is observed in Model DLVR3. Model DLVR3 has a flexural rigidity of 1E25 Nm, load density of 2650 kg/m^3, infill density of 2650 kg/m^3, laterally varying load of 5000 m, 0 m, 5000 m, 0 m, 5000 m; model depths of -6000 m, -4500 m, and -7000 m; respectively (Figure 55).

Model set DLVR4-DLVR6 (Figures 56-58) was produced in an attempt to produce two basement ridges. Two structural highs were produced in models DLVR4, one structural high was produced in models DLVR5 and DLVR6. Both models DLVR5 and DLVR6 have two troughs or mini-basins produced in the basin rather than three as observed in model DLVR4. The location of the structural highs in the model DLVR4 is consistent with the lack of load placement. The lack of a second structural high in models

DLVR5 and DLVR 6 may be a result of the flexural rigidity, 9E24 Nm and 1E25 Nm; respectively. The heights of the structural highs, from the basement, are 2800 m and 3200 m in Model DLVR4, 3200 m in Model DLVR5, and 3000 m in Model DLVR 6. Model DLVR4 has the deepest basin with a maximum depth of -3800 m (Table 4c).

Model DLVR4 has a maximum depth of -3800 m; flexural rigidity of 8E24 Nm, load density of 2650 kg/m^3, infill density of 2650 kg/m^3, laterally varying load of 5000 m, 0 m, 5000 m, 0 m, 5000 m; model depths of -3000 m, -2800 m, -3800 m, -3200 m, and -3800 m; respectively (Figure 56). A lack of forebulge is observed in Model DLVR6. Model DLVR6 has a flexural rigidity of 1E25 Nm, load density of 2650 kg/m^3, infill density of 2650 kg/m^3, laterally varying load of 5000 m, 0 m, 5000 m, 0 m, 5000 m; model depths of -2500 m, -2500 m, -3500 m, -3000 m, and -3500 m; respectively (Figure 58).

Table 8: Models produced with flexural rigidity of 1E25 Nm.

Model	Flexural Rigidity (Nm)	Load/Infill Density (kg/m^3)		Mantle (kg/m^3)	Laterally Varying Load (m)		Laterally Varying Max. Depth (m)		Forebulge (Y/N)
DLV1	1.00E+25	2650	2650	3330	4000	7000	-900	-1400	Y
DLV2	1.00E+25	2650	2650	3330	4000	7000	-900	-1500	Y
DLV5	1.00E+25	2650	2650	3330	5000	7000	-1100	-1500	Y
DLV9	1.00E+25	3000	2650	3330	3500	7000	-1200	-1600	Y

Table 9: Models produced with flexural rigidity of 8E24 Nm.

Model	Flexural Rigidity (Nm)	Load/Infill Density (kg/m^3)		Mantle (kg/m^3)	Laterally Varying Load (m)		Laterally Varying Max. Depth (m)		Forebulge (Y/N)
DLV3	8.00E+24	2650	2650	3330	4000	7000	-1000	-1600	Y
DLV4	8.00E+24	2650	2650	3330	4000	7000	-1300	-1600	Y
DLV6	8.00E+24	2650	2650	3330	5000	7000	-1200	-1600	Y
DLV10	8.00E+24	3000	2650	3330	3500	7000	-1300	-1700	Y

Table 10: Models produced with flexural rigidity of 9E24 Nm.

Model	Flexural Rigidity (Nm)	Load/Infill Density (kg/m^3)		Mantle (kg/m^3)	Laterally Varying Load (m)		Laterally Varying Max. Depth (m)		Forebulge (Y/N)
DLV7	9.00E+24	2650	2650	3330	4000	7000	-1100	-1600	Y
DLV8	9.00E+24	2650	2650	3330	5000	7000	-1100	-1500	Y
DLV11	9.00E+24	3000	2650	3330	3500	7000	-1100	-1700	Y

6. DISCUSSION

6.1 FLEXURAL RIGIDITY OF THE INDIAN PLATE

The flexural rigidity of the lithosphere tells us about the strength of the Indian Plate during the convergence with the Eurasian Plate. The T_e of the plate(s) is proportional to the strength and therefore related to the rigidity of the lithosphere. A plate with a small flexural rigidity will behave more weak than a plate with a larger flexural rigidity. The dimensions and shape of the foreland basin are determined by the flexural rigidity of the subducted lithosphere and by the dimensions of the topographic load, the mountain belt (DeCelles and Gilles, 1996).

The interpretation of the flexural models produced in this study finds a flexural rigidity for the Indian lithosphere ranging from 8E24 Nm – 1E25 Nm. This range for the flexural rigidity was determined by the depth of the uniform load models. The laterally varying load models did not reach realistic depths, and therefore are used as a tool for determining the formation of basement ridges rather than the flexural rigidity of the Indian Plate.

Of the 17 uniform load models produced, four models produced a realistic maximum depth of 5.5 – 6 km. The models, D2, D4, D5, and D9 have flexural rigidities ranging from 8E24 Nm – 1E 24 Nm. These results indicate that the Indian Plate has a relatively higher flexural rigidity than previously found in the flexural studies of DeCelles et al. (1998), Lyon-Caen and Molnar (1985), and Jordan and Watts (2005).

DeCelles et al., 1998 produced flexural rigidities of 3E23 Nm to 7E24 Nm in their flexural studies. These values are lower than the values found in this study; however, the orogenic load parameters used in DeCelles et al. (1998) differ from those used in this study. If the same parameters were used in the models for this study, it is likely that the results would be similar to those found by DeCelles et al. (1998).

Models D2, D4, and D5 have load and infill densities of 2650 kg/m^3 and 2650 kg/m^3, respectively; which were used in Jordan and Watts (2005) flexural studies. Jordan and Watts (2005) discuss the T_e of the Indian Plate in their study rather than the flexural rigidity. However, the T_e of the plate(s) is proportional to the strength and therefore related to the rigidity of the lithosphere. Their study found a T_e of 70 km for the central region of the foreland basin and a decrease to 30-50 km in the east and west portions of the basin. They suggest an overall T_e of $40< T_e<100$ km and describe the basin as a rigid block.

Model D9 has load and infill densities of 2700 kg/m^3 and 2400 kg/m^3, respectively; which were used in Lyon-Caen and Molnar (1985) flexural studies. Lyon-Caen and Molnar (1985) found the T_e of the Indian Plate to be between 40 and 100 km, and suggest a flexural rigidity of 1E24 Nm and 7E24 Nm. They infer significant variation of the flexural rigidity of the Indian Plate along the northern margin.

The variation in flexural rigidities is probably the result of the variation in parameters used; specifically the dimensions and placement of the load and/or infill load. Although the rigidities vary, all of the studies find that the Indian Plate has significant strength.

6.2 FOREBULGE

The forebulge is created in elastic response to the flexure of the lithosphere as a result of loading. It is one of the most distal zones, commonly the site of stratigraphic thinning and unconformity development; and is not always present (DeCelles and Giles, 1996). When a lithospheric plate has strength, a forebulge is

expected to develop cratonward of the foreland basin. This study finds that the flexural rigidity of the Indian Plate is quite high and a low, broad forebulge (amplitude <50 m) has developed approximately 400 km south of the MFT.

Of the four models interpreted to predict the flexural rigidity of the Indian Plate, three models produced a forebulge. Model D5 did not produce a forebulge. The flexural rigidity used in the model is 1E25 Nm; this is a relatively high flexural rigidity. The lack of forebulge can be explained by the size of load and infill load emplaced in the model. A plate with significant strength can accommodate a larger load. The results of Model D5 suggest that the Indian Plate with an assumed flexural rigidity of 1E25 Nm can accommodate more weight before elastically responding to the flexure of the lithosphere.

A forebulge with amplitude <50 m was produced in both uniform and laterally varying load models. Uniform load models D7 and D14 produce a forebulge with amplitude 0<50<100 km. Although a forebulge with greater amplitude was observed in models D7 and D14; the flexural rigidities of these models 9E24 Nm and 1E24 Nm, respectively; produce an unrealistic basin depth of 12,000 m at the MFT.

In the laterally varying load models, the location of the forebulge was affected by the size of the load. With a larger load emplaced, the forebulge migrated toward the basin. This migration is observed as a slight change in the location of the forebulge in the models. This has important implications for the location of the forebulge suggested in the literature. The amplitude of the forebulge was not affected by the size of the load, but rather the flexural rigidity of the plate.

The Himalayan Foreland Basin is an elongate basin that mimics the shape of the Himalayan arc. Our study area is located in the central portion of the basin and does not include the eastern and western-most portions of the basin. The forebulge location discussed in the literature describes features found in both the eastern and western portions of the Himalayan Foreland Basin. Although the features are not located within our study area, if they are a portion of the forebulge; they should be in relative alignment with the forebulge produced in this study.

The lack of prominent forebulge observed in the field and stratigraphic columns can be explained by the low, broad structure of the forebulge. This finding is in agreement with DeCelles and Giles (1996) who suggest that the lithospheric loading of the Indian craton promotes a low, wide forebulge, and Yin (2006) who suggests that the topographic expression of the forebulge may be significantly smaller than that of the basement ridges.

6.3 BASEMENT RIDGES

The basement of the Himalayan Foreland Basin is characterized by several basement ridges oriented perpendicular to the plate boundary. Three ridges have formed on the basement within our study area. The ridges, from east to west, are the Delhi-Hardwar Ridge, Faizabad Ridge, and the Munger (Monghyr)-Saharsa Ridge. These ridges are expected to be high relief features (Gahalaut and Kundu, 2012); they are not observed at the surface as a result of sediment deposition up to 6 km thick. The origin of the ridges is unknown; however, our findings suggest that the ridges observed in the Himalayan Foreland Basin are the result of both lateral variations of load and compression of the Indian Plate.

The interpretation of the six laterally varying load models (DLVR1-DLVR6) finds that basement ridges can be produced by non-uniform load placement on the edge of an elastic plate. The highest amplitude structural high was produced in model DLVR1 with a height of 3500 m (from the basement); and a maximum basin depth of -7500 m. Four of the six models, with flexural rigidities of 8E24 Nm and 9E24 Nm, produce a forebulge in addition to the ridge(s). Models DLVR3 and DLVR6, with a flexural rigidity of 1E25 Nm, did not produce a forebulge.

Model set DLVR1 – DLVR3 produce basin depths of -7000 m – -7500 m with a load height of 5000 m emplaced on the edges of the flexural model. The amplitude of the structural highs ranges from 2500 - 3500 m. Model set DLVR4-DLVR6 produce basin depths of -3500 m – - 3800 m with a load height of 5000 m emplaced on the edges and center of the flexural model. The amplitude of the structural highs ranges from 2800 m –

3400 m. The location of the structural highs formed is consistent with the lack of load placement.

Models DLVR5 and DLVR6 did not produce three depressions with two structural highs, as would be assumed. There was an overall depression, however, there were two distinctly deeper troughs or mini-basins separated by a structural high. This is probably the result of the flexural rigidity of the plate, 9E24 Nm and 1E25 Nm, respectively, and its compensation of the laterally varying load.

The interpretation of the numerical beam models finds that basement ridges can be formed by the compression of an elastic plate with a force being applied in an east-west direction. When a force is applied to one side of the model domain, plates with a T_e of 50 km and 70 km undergo perturbation and a buckle effect occurs. In both models, the ridges formed closest to the applied force have higher amplitude and appear to pinch out, while the ridges that formed furthest from the applied force have a more elongate structure and are equally spaced. The elongate structures with equal spacing closely resemble the basement ridge formation in the Himalayan Foreland Basin.

Compression of the Indian Plate, as it continues to converge with and be subducted by the Eurasian Plate, in addition to a laterally varying load emplaced on the Indian Plate, is probably the cause of the ridge formation within the Himalayan Foreland Basin. The lateral variation in the load does not create realistic depths and consistent ridge formation, and is therefore not likely the sole cause of the ridge formation.

6.4 DRAINAGE PATTERN

The drainage pattern of the fluvial systems that traverse the Himalayan Foreland Basin is probably a reflection of the loading of the Indian Plate. The deposition of sediments from the Higher and Lesser Himalayas occurring in the Sub-Himalayas accounts for a portion of the basin fill observed in the Himalayan Foreland Basin. These sediments act as an additional load that is emplaced on the lithosphere in addition to the thrust load, which causes flexure and subsidence of the basin.

It has also been documented that the total amount of crustal shortening in the eastern Himalaya is occurring faster than in the western Himalaya due to a non-uniform convergence rate been India and Asia (Yin, 2006). As a result, the northeastern corner of the Indian craton begins to tilt northeastward while the remaining portion of northern India continues a northwestward tilt. Bilham (2004), Sella et al. (2002), and Zhou et al. (2004) agree that there is rotation and translation of the Indian Plate and subduction can be described as "subhorizontal".

DeCelles et al. (1998) suggest that the major fluvial system and paleo-Ganges River experienced a drainage pattern reversal, flowing in a south-southwest direction during the Early Miocene and flowing in a south-southeast direction during the Middle Miocene. During this time, there was significant lithospheric shortening, faulting, and deformation as India continued to converge with Eurasia. As lithospheric shortening occurs, there becomes greater topographic relief and an increased load.

The models in this study have shown that laterally varying loads, as a result of non-uniform crustal thickening probably as a result of non-uniform subduction of the Indian Plate; produce varying basin depths. With greater topographic relief rivers begin to incise and their knick-points, which establish the erosion-deposition boundary, migrate. As a result, the depositional pattern of the rivers changes. Seeber and Gornitz (1983) show that the trajectory of the major rivers in the Himalayan region is very dynamic and deposition within the basin has not been laterally uniform.

The increasing load emplaced on the Indian Plate creates lithospheric flexure and greater accommodation space for sediment infill. The models in this study have shown that an elastic plate with strength will respond elastically by producing a forebulge. DeCelles et al. (1998) discuss the migration of the forebulge through the foreland basin during the Oligocene as a cause for the change in trajectory of the major fluvial system and paleo-Ganges River. Forebulge migration through the Himalayan Foreland Basin during the Oligocene probably occurred in response to the increasing load emplacement on the Indian Plate. The amplitude of the forebulge

and slab tilting in the Early and Middle Miocene are probably the mechanisms behind the flow direction of the major fluvial system and paleo-Ganges River.

6.5 EARTHQUAKES IN THE INDIAN PLATE

Although earthquakes are often associated with the deformation of the Earth's crust occurring at tectonic plate boundaries or geological fault localities, major earthquakes have been recorded in regions deep within continental interiors (Banerjee et al., 2008). These earthquakes, known as intraplate earthquakes, may reflect significant deformation or fragmentation of plate interiors. The accumulating stress in the plate interiors, causing the earthquakes, may be relatively modest and local perturbations of lithospheric stress or strength may result in the occurrence of these earthquakes (Banerjee et al. 2008).

While most of the earthquakes associated within the Indian subcontinent have been recorded along the northern boundary (MFT), where the Indian Plate is being subducted beneath Eurasia, the largest earthquakes in India have been recorded in the western region and to the east of the Himalayan Foreland Basin near the Shillong Plateau (Banerjee et al., 2008).

In a study completed by Martin and Szeglia (2010), 570 earthquakes were characterized, using 8,339 intensity observations occurring on the Indian subcontinent and surrounding plate boundaries. Figure 24 illustrates the locations of these earthquakes in relation to the Himalayan Foreland Basin. There is an observed data gap in the approximate location of the basin, with the southern margin being delineated by the earthquake data. This suggests that there is seismicity associated with the forebulge of the Himalayan Foreland Basin.

Convergence rates measured by Paul et al. (2001) suggest that the Indian Plate should not be expected to have frequent seismicity (Bilham, 2004). However, in a study completed by Bilham (2004), it is suggested that the formation of the forebulge is a source of intraplate seismicity. Normal faulting earthquakes were recorded along the northern margin of the forebulge with deep reverse faulting

occurring beneath the crest of the forebulge, and shallow reverse faulting occurring south of the forebulge where the Indian Plate is depressed. The location of the forebulge indicated by these earthquakes corresponds to the forebulge location predicted by the flexural models where the lithosphere has a rigidity between 8E24 and 1E25 Nm.

Figure 24: Earthquakes of India in relation to the Himalayan Foreland Basin System (taken from Martin and Szeglia, 2010).

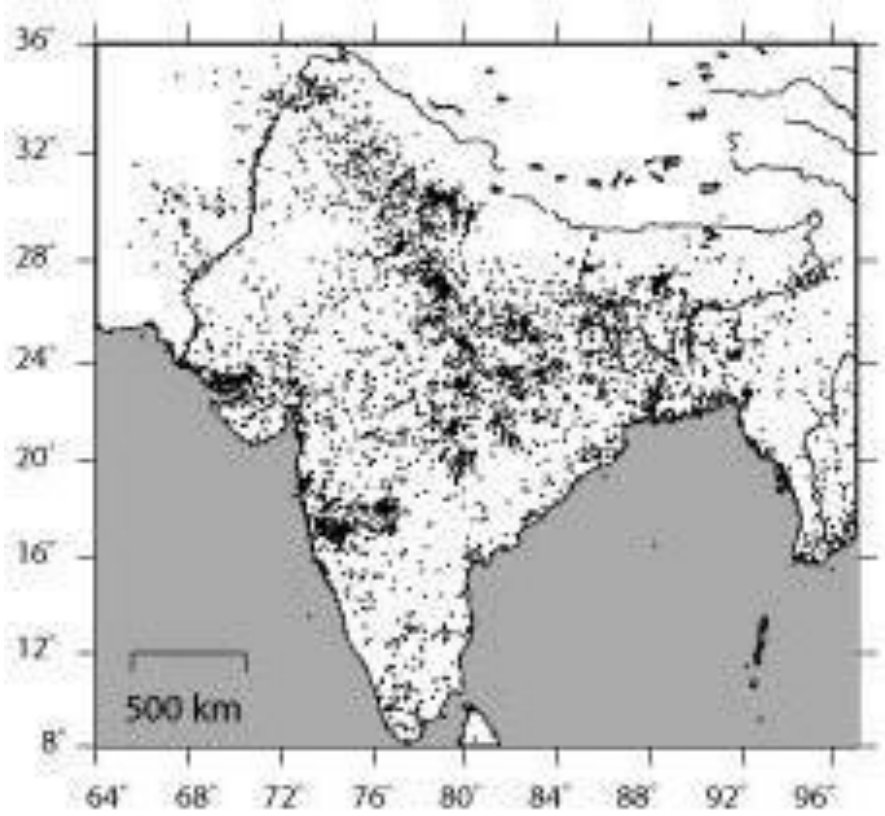

7. CONCLUSIONS

The Himalayan Foreland Basin is an elongate trough with an arcuate shape that mimics the shape of the Himalayan arc. The formation of the Himalayan Foreland Basin occurred during the Eocene following the continent-continent collision between the Indian and Eurasian Plates. The elastic Indian Plate flexed in response to loading of the Plate by the uplifting and thrusting Himalayan mountain range. The deepest part of the

foreland basin adjacent to the Himalayan Main Frontal Thrust is covered with about 4-6 km sediments.

This study finds that the Indian Plate has a flexural rigidity of 8E24 Nm – 1E25 Nm. Preferred models using realistic parameters predict that a low, broad forebulge developed on the Indian Plate approximately 400 km south of the MFT. The forebulge has an amplitude of about 30-50 m, and the lack of forebulge observed in the field and stratigraphic columns is probably the result of the small amplitude of the forebulge.

The basement of the Himalayan Foreland Basin is characterized by several basement ridges oriented perpendicular to the plate boundary. This study finds that the origin of these basement ridges is probably the result of compression of the Indian lithosphere, as the Indian Plate converges with and is subducted by Eurasia. As a result of compression, a buckling effect occurs creating a series of basement ridges. It is unlikely that a laterally varying load is responsible for the formation of the basement ridges; the ridges are probably the result of basin in-fill following the formation of the basement ridges.

The drainage pattern of the fluvial systems that traverse the Himalayan Foreland Basin is probably a reflection of the loading of the Indian Plate. The proposed flow reversal of the major fluvial system and the paleo-Ganges River in the Middle Miocene by DeCelles et al. (1998) is probably caused by the non-uniform subduction rates creating slab tilting as the Indian Plate is subducted beneath the Eurasian Plate, in addition to lateral variations in the load creating varying basin depths and subsequent sediment infill.

Some of the intraplate earthquakes described by Martin and Szeglia (2010) and Bilham (2004) on the Indian Plate are probably the result of lithospheric flexure of the Indian Plate in response to loading resulting in the formation of the forebulge. Normal faults are associated with the onset of the forebulge, and the location of the forebulge as predicted by the earthquakes corresponds with the location of the forebulge predicted by the flexural models.

8. REFERENCES

Banerjee, P., Burgmann, R., Nagarajan, B., Apel, E., 2008, Intraplate deformation of the Indian subcontinent: Geophysical Research Letters, v. 35, p. 1-5.

Bilham, R., 2004, Earthquakes in India and the Himalaya: tectonics, geodesy and history: Annals of Geophysics, v. 47, n. 2/3, p. 839-858.

Brookfield, M.E., 1998, The evolution of the great river systems of Southern Asia during the Cenozoic India-Asia collision: rivers draining southwards: Geomorphology, v. 22, p. 285-312.

Burbank, D.W., Beck, R.A., and Mulder, T., 1996, The Himalayan Foreland Basin: Geologic evolution of the Himalayan-Tibetan orogen: Annual Review Earth Planet Science, v. 28, p. 150-188.

Cattin, R., Martelet, G., Henry, P., Avouac, J.P., Diament, M., Shakya, T.R., 2001, Gravity anomalies, crustal structure and thermo-mechanical support of the Himalaya of Central Nepal: Geophysical Journal International, v. 147, p. 381-392.

Catuneanu, O., 2004, Retroarc foreland systems; evolution through time: Journal of African Earth Science and the Middle East, v. 38 (3), p. 225-242.

Cina, S.E., Yin, A., Grove, M., Dubey, C.S., Shukla, D.P., Lovera, O.M., Kelty, T.K., Gehrels, G.E., and Foster, D.A., 2009, Gangdese arc detritus within the eastern Himalayan Neogene Foreland basin: Implications for the Neogene evolution of the Yalu-Brahmaputra River System: Earth and Planetary Science Letters, v. 285, p. 150-162.

Crampton, S.L., and Allen, P.A., 1995, Recognition of forebulge unconformities associated with early stage foreland basin development: Example from the North Alpine Foreland Basin: American Association of Petroleum Geologists, Bulletin, v. 79, p. 1495-1514.

Clift, P.D., VanLaningham, S., 2010, A climatic trigger for a major Oligocene-Miocene unconformity in the Himalayan Foreland Basin: Tectonics, v.29, TC014, p. 1-18.

DeCelles, P.G., and Giles, K. A., 1996, Foreland basin systems: Basin Research, v. 8, p. 105-123.

DeCelles, P.G., Gehrels, G.E., Quade, J., and Ojha, T.P., 1998a, Eocene-early Miocene foreland basin development and the history of Himalayan thrusting, western and central Nepal: Tectonics, v. 17, no. 5, p. 741-765.

DeCelles, P.G., Gehrels, G.E., Quade, J., Ojha, T.P., Kapp, P.A., and Upreti, B.N., 1998b, Neogene foreland basin deposits, erosional unroofing, and the kinematic history of the Himalayan fold-thrust belt, western Nepal: GSA Bulletin, v. 110, no. 1, p. 2-21.

Duroy, Y., Farah, A., and Lillie, R.J., 1989, Subsurface densities and lithospheric flexure of the Himalayan foreland in Pakistan: Geological Society of America, Special Paper, v. 232, p. 217-236.

Flemings, P.B., and Jordan, T.E., 1989, A synthetic stratigraphic model of foreland basin development: Journal of Geophysical Research, v. 94, no. B4, p. 3851-3866.

Gahalaut, V.K., and Kundu, B., 2012, Possible influence of subducting ridges on the Himalayan arc and on the ruptures of great and major Himalayan earthquakes: Gondwana Research, v. 21, p. 1080-1088.

Gibling, M.R., Tandon, S.K., Sinha, R., and Jain, M., 2005, Discontinuity-bounded alluvial sequences of the southern gangetic plains, India: Aggradation and degradation in response to monsoonal strength: Journal of Sedimentary Research, v. 75, p. 369-385.

Hetenyi, G., Cattin, R., Vergne, J., Nabelek, J.L., 2006, The effective elastic thickness of the India Plate from receiver function imaging, gravity anomalies and thermomechanical modeling: Geophysical Journal International, v. 167, p. 1106-1118.

Jordan, T.A., and Watts, A.B., 2005, Gravity anomalies, flexure and the elastic thickness structure of the India-Eurasia collisional system: Earth and Planetary Science Letters, v. 236, p. 732-750.

Kumar, M.R., Mishra, D.C., Singh, B., Venkat Raju, D.C., Singh, M., 2013, Geodynamics of NW India: Subduction, lithospheric flexure, ridges and seismicity: Journal of Geological Society of India, v. 81, p.61-78.

Li, F., Dyt, C., and Griffiths, C., 2004, 3D modelling of flexural isostatic deformation: Computers & Geosciences, v. 30, p. 1105-1115.

Lyon-Caen, H., 1980, Deep Structure of the Himalaya and Tibet from Gravity and Seismological Data: PhD Dissertation, Massachusetts Institute of Technology, p. 1-153.

Lyon-Caen, H., and Molnar, P., 1983, Constraints on the structure of the Himalaya from an analysis of gravity anomalies and a flexural model of the lithosphere: Journal of Geophysical Research, v. 88, p. 8171-8191.

Lyon-Caen, H., and Molnar, P., 1985, Gravity anomalies, flexure of the Indian Plate, and the structure, support and evolution of the Himalaya and Ganga Basin: Tectonics, v. 4, no. 6, p. 513-538.

Mallick, K., Vasanthi, A., Sharma, K.K., 2012, Bouguer Gravity Regional and Residual Separation: Application to Geology and Environment: ISBN-10: 9400704054, p. 1-260.

Martin, S., and Szeliga, W., 2010, A catalog of Felt Intensity Data for 570 earthquakes in India from 1636 to 2009: Bulletin of the Seismological Society of America, v. 100, n. 2, p. 562-569.

Mishra, D.C., Laxman, G., Arora, K., 2004, Large-wavelength gravity anomalies over the Indian continent: indicators of lithospheric flexure and uplift and subsidence of Indian Peninsular Shield related to isostasy: Current Science, v. 86, p. 861-867.

Paracha, W., 2004, Kohat Plateau with reference to Himalayan tectonic general study: CSEG Recorder - Article, p. 47-52.

Paul, J., Burgmann, R., Gaur, V.K., Bilham, R., Larson, K.M., Ananda, M.B., Jade, S., Mukal, M., Anupama, T.S., Satyal, G., Kumar, D., 2001, The motion and active deformation of India: Geophysical Research Letters, v. 28 (4), p. 647-651.

Powers, P.M., Lillie, R.J., and Yeats, R.S., 1998, Structure and shortening of the Kangra and Dehra Dun reentrants, Sub-Himalaya, India: GSA Bulletin, v. 110, no. 8, p. 1010-1027.

Rao, M.B.R., 1973, The subsurface geology of the Indo-Gangetic plains: Journal of the Geological Society of India, v. 14, p. 217-242.

Royer, J.Y., Sandwell, D.T., 1989, Evolution of the eastern Indian Ocean since the Late Cretaceous: Constraints from Geosat altimetry: Journal of Geophysical Research: Solid Earth (1978-2012), v. 94, p. 13755-13782.

Sastri, V.V., Bhandari, L.L., Raju, A.T.R., Datta, A.K., 1971, Tectonics framework and subsurface stratigraphy of the Ganga basin: Journal of the Geological Society of India, v. 12, p. 232-233.

Seeber, L., and Gornitz, V., 1983, River profiles along the Himalayan Arc as Indicators of Active Tectonics: Tectonophysics, v. 92, p. 335-367.

Sella, G.F., Dixon, T.H., Mao, A., 2002, REVEL: a model for recent plate velocities from space geodesy: Journal of Geophysical Research, v. 107, p. 1-31.

Vogt, P.R., 1973, Subduction and aseismic ridges: Nature, v. 241, p. 189-191.

Watson, D.F., Philip, G.M., 1985, A refinement of inverse distance weighted interpolation: Geo-Processing, v. 2, p. 315-327.

Windley, B.F., 1988, Framework for the geology and tectonics of the Himalayas, Karakoram and Tibet, and problems of their evolution, in: R.M. Shackleton, J.F. Dewey, B.F. Windley (Eds.): Tectonic Evolution the Himalayas and Tibet, v. A326, p. 3-16.

Yin, A., 2006, Cenozoic tectonic evolution of the Himalayan orogen as constrained by along-strike variation of structural geometry, exhumation history, and foreland sedimentation: Earth-Science Reviews, v. 76, p. 1-131.

Yin, A., and Harrison, T. M., 2000, Geologic evolution of the Himalayan-Tibetan Orogen: Annual Review Earth Planet Science, v. 28, p. 211-280.

Zhou, H.W., Murphy, M.A., 2004, Tomographic evidence for wholesale underthrusting of India beneath the entire Tibetan plateau: Journal of Asian Earth Sciences, v. 25, p. 445-457.

INTERNET REFERENCES:

http://www.3ds.com/products/simulia/portfolio/abaqus/overview/

http://www.arcgis.com

http://www.geosci.usyd.edu/au/users/prey/Teaching/Geol-3101/Mountain02/structuregeocollision.htm

http://www.naturalearthdata.com/downloads/

http://www.shadedrelief.com/world_relief/home.html

http://www.simulia.com

9. APPENDICES

9.1 APPENDIX A: UNIFORM LOAD MODELS

Figure 25: Uniform Load Model D2.

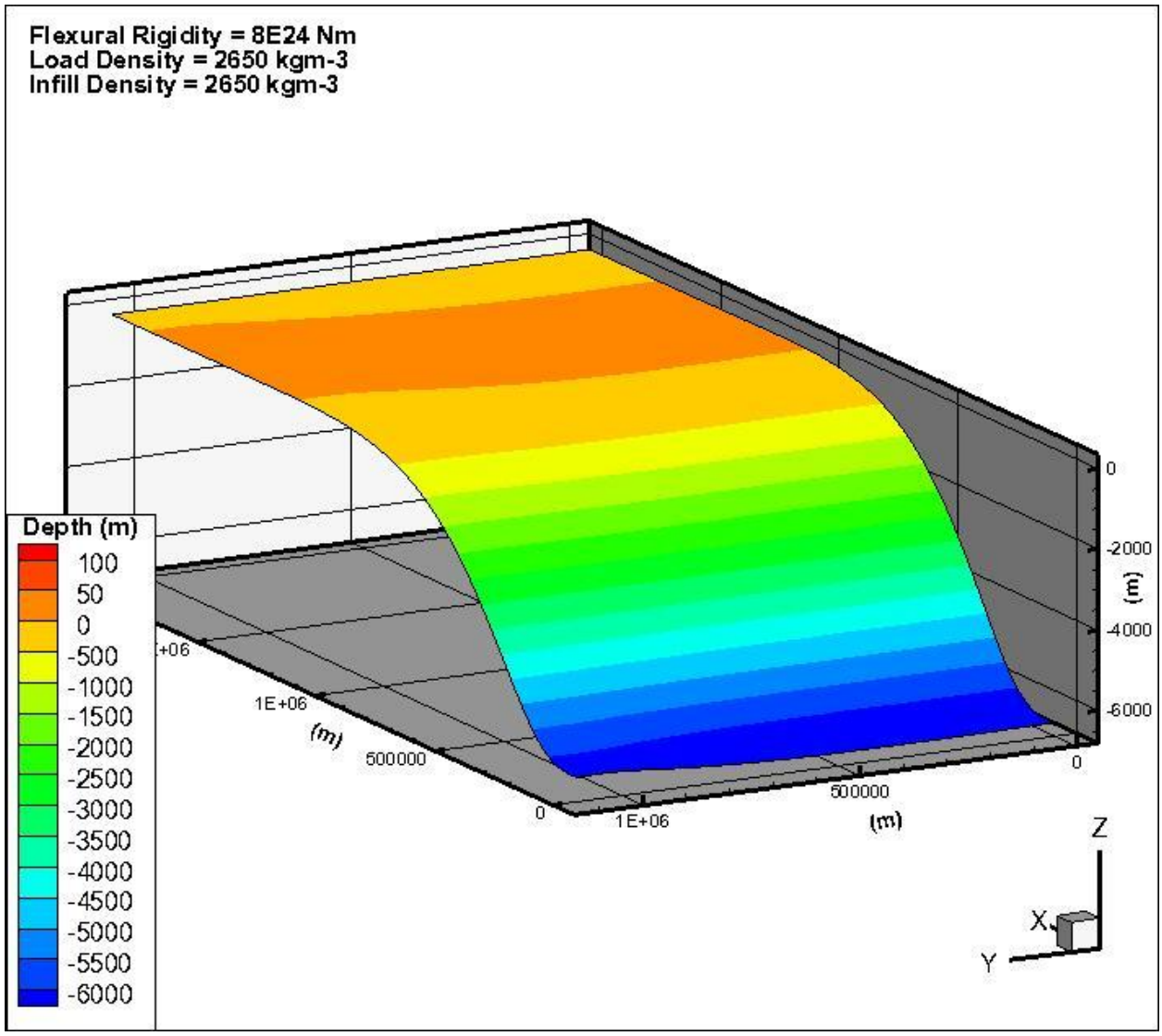

Figure 26: Uniform Load Model D4.

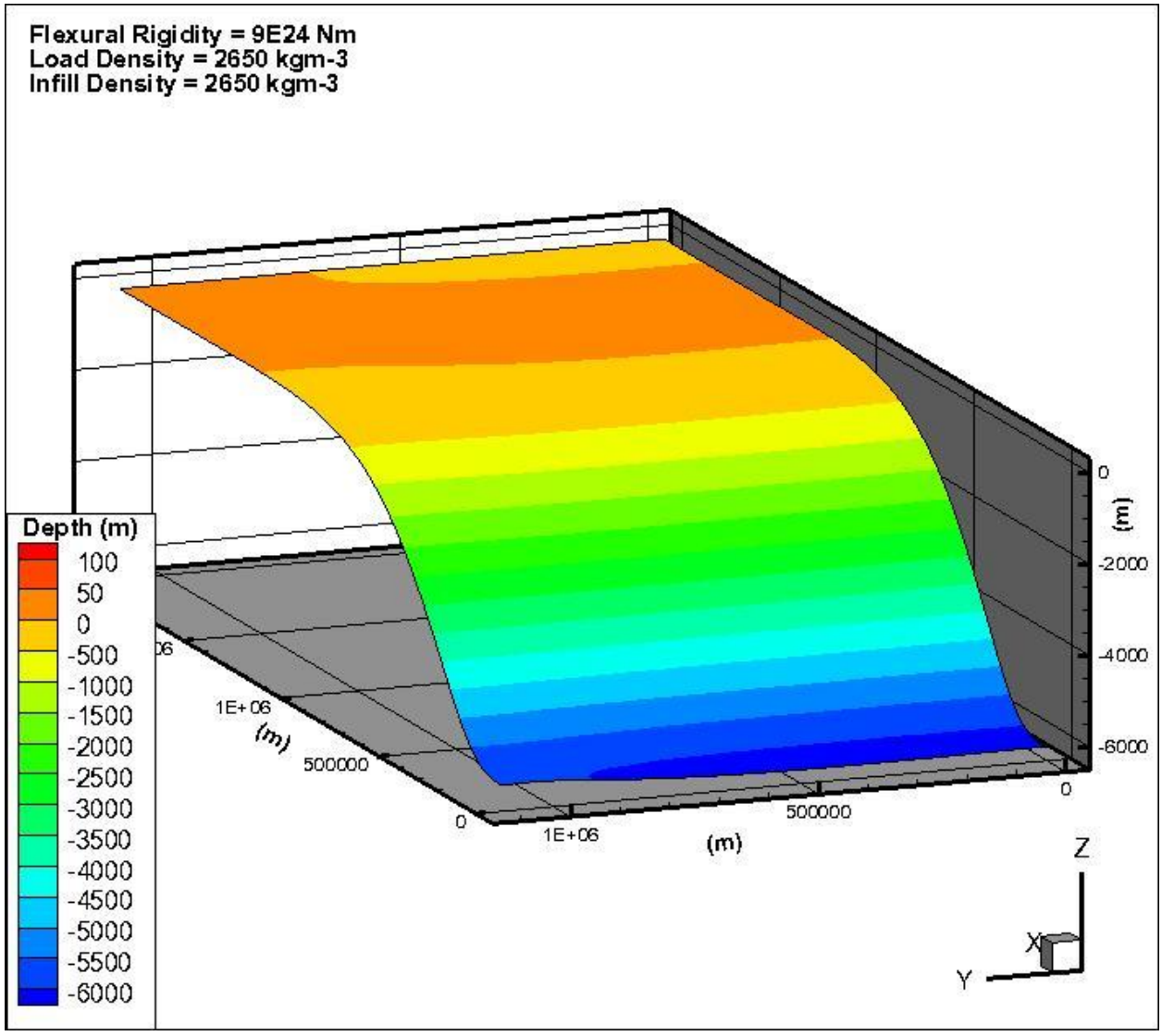

Figure 27: Uniform Load Model D5.

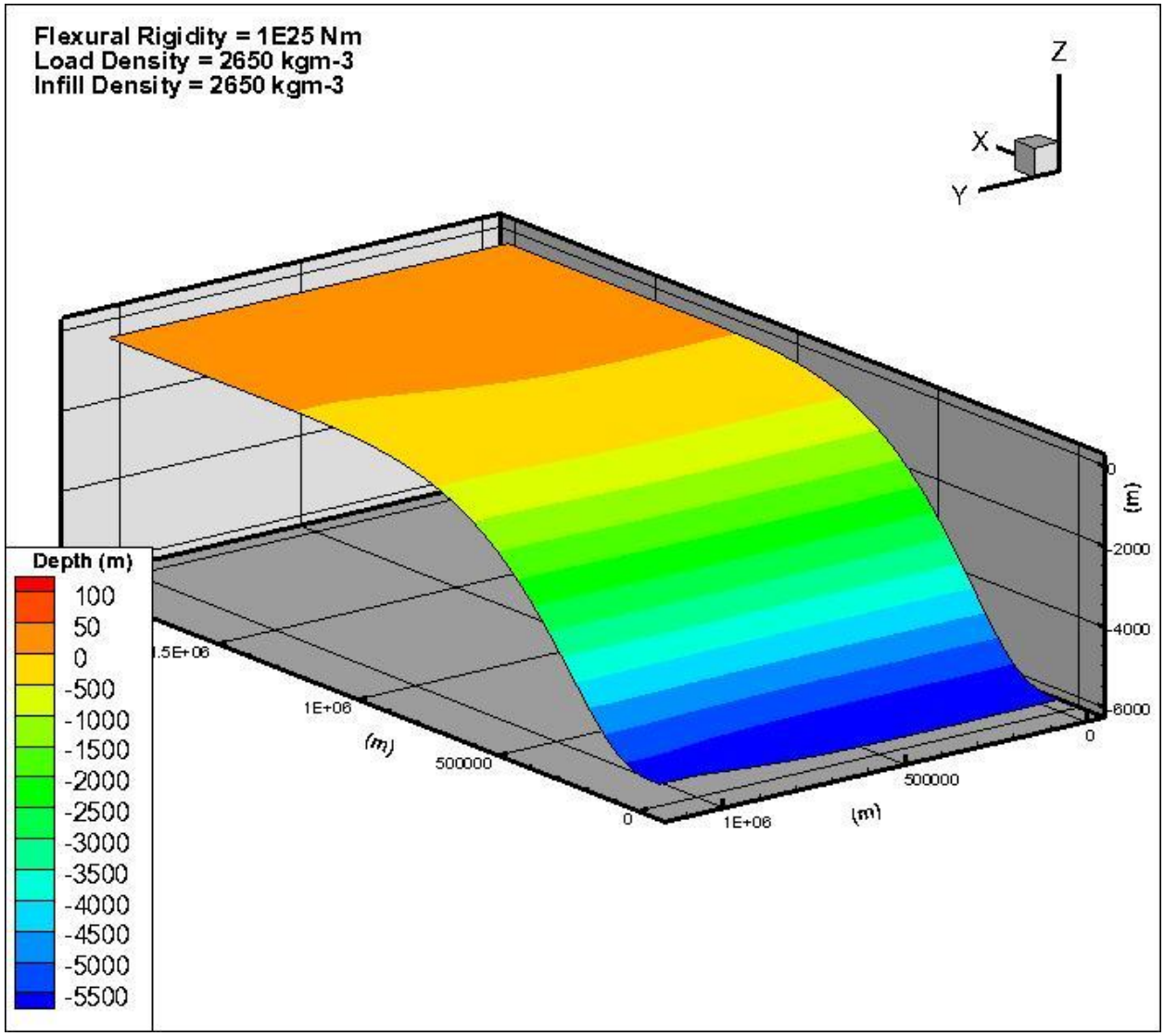

Figure 28: Uniform Load Model D9.

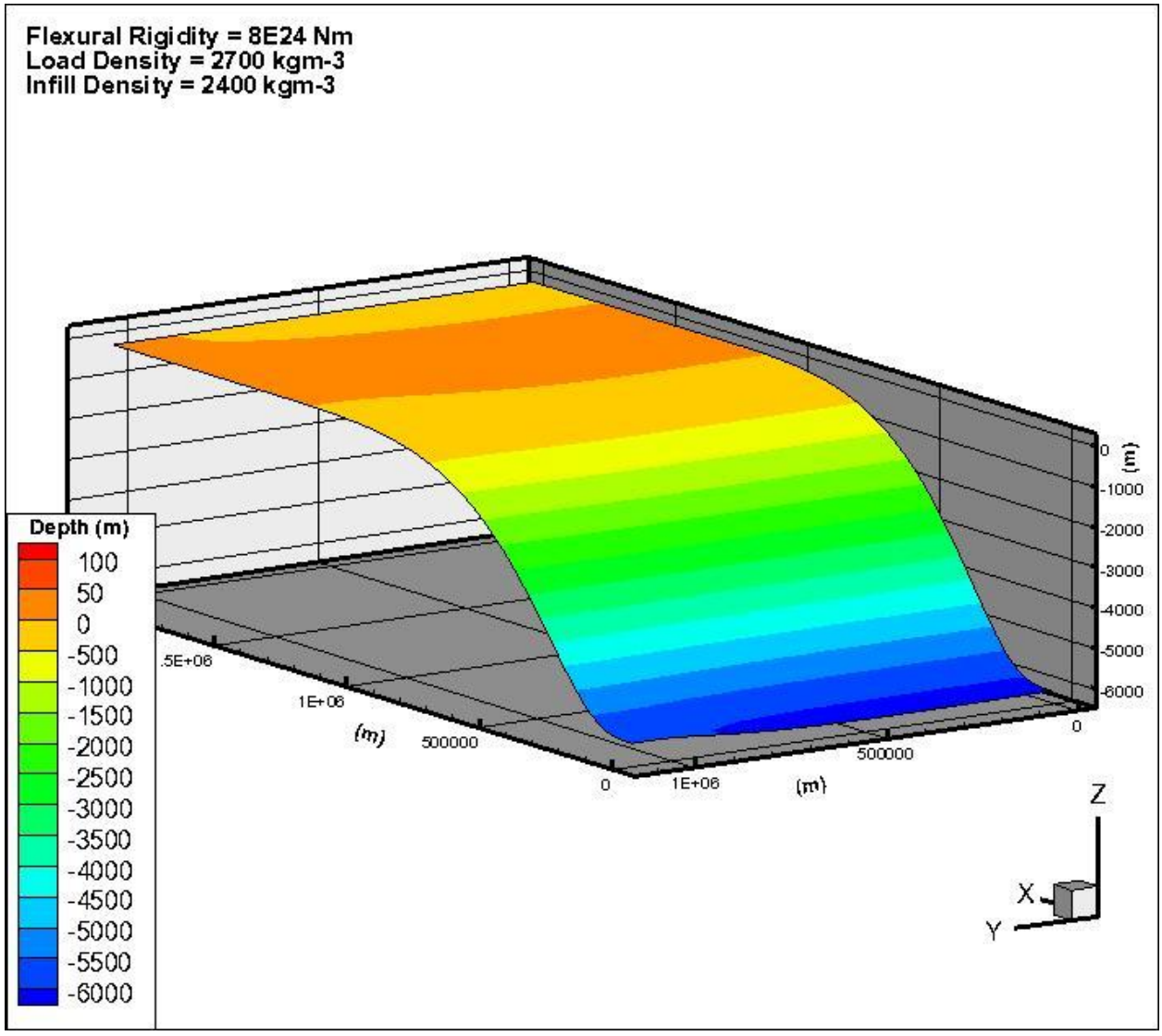

Figure 29: Uniform Load Model D10.

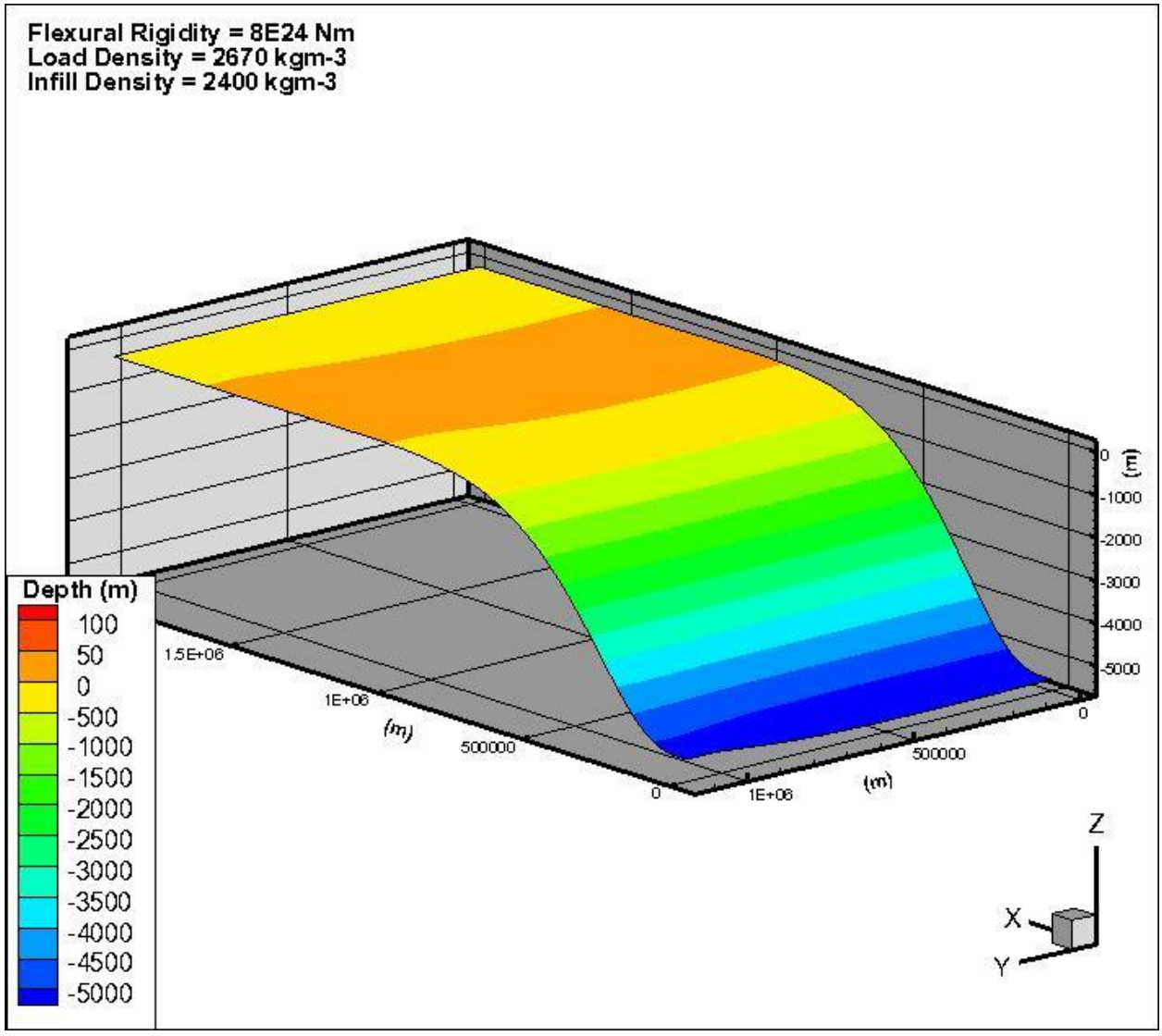

Figure 30: Uniform Load Model D11.

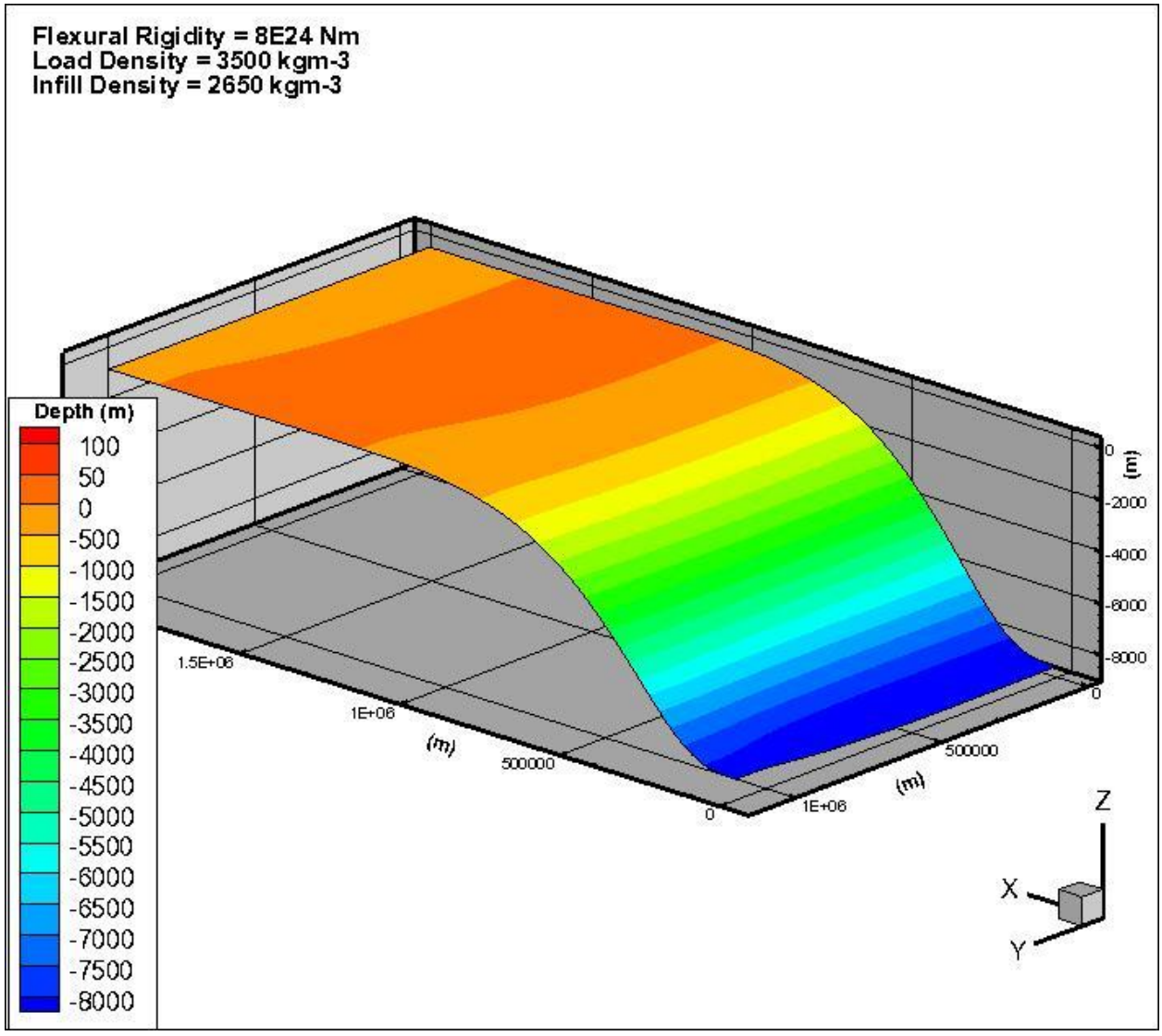

Figure 31: Uniform Load Model D12.

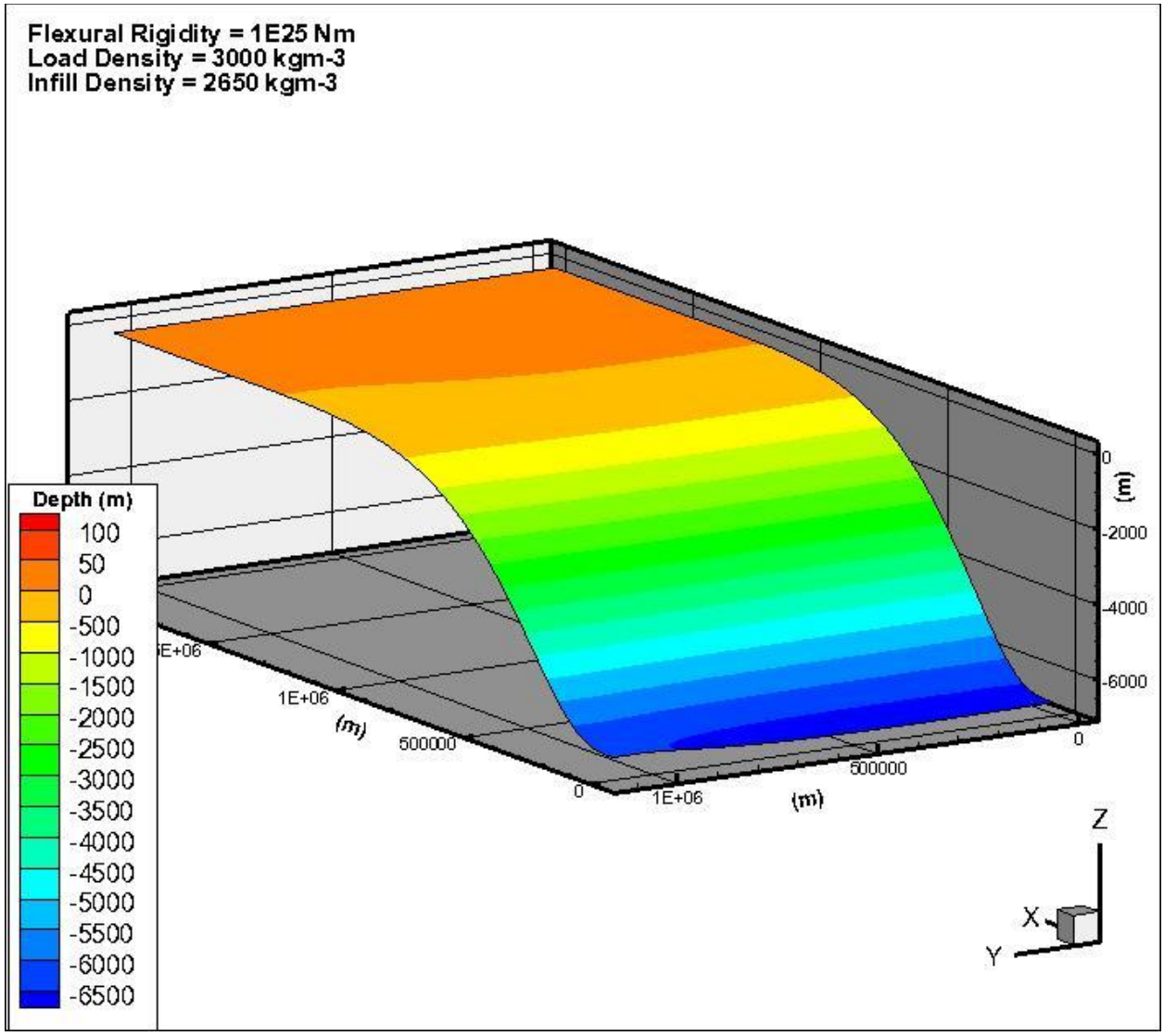

Figure 32: Uniform Load Model D13.

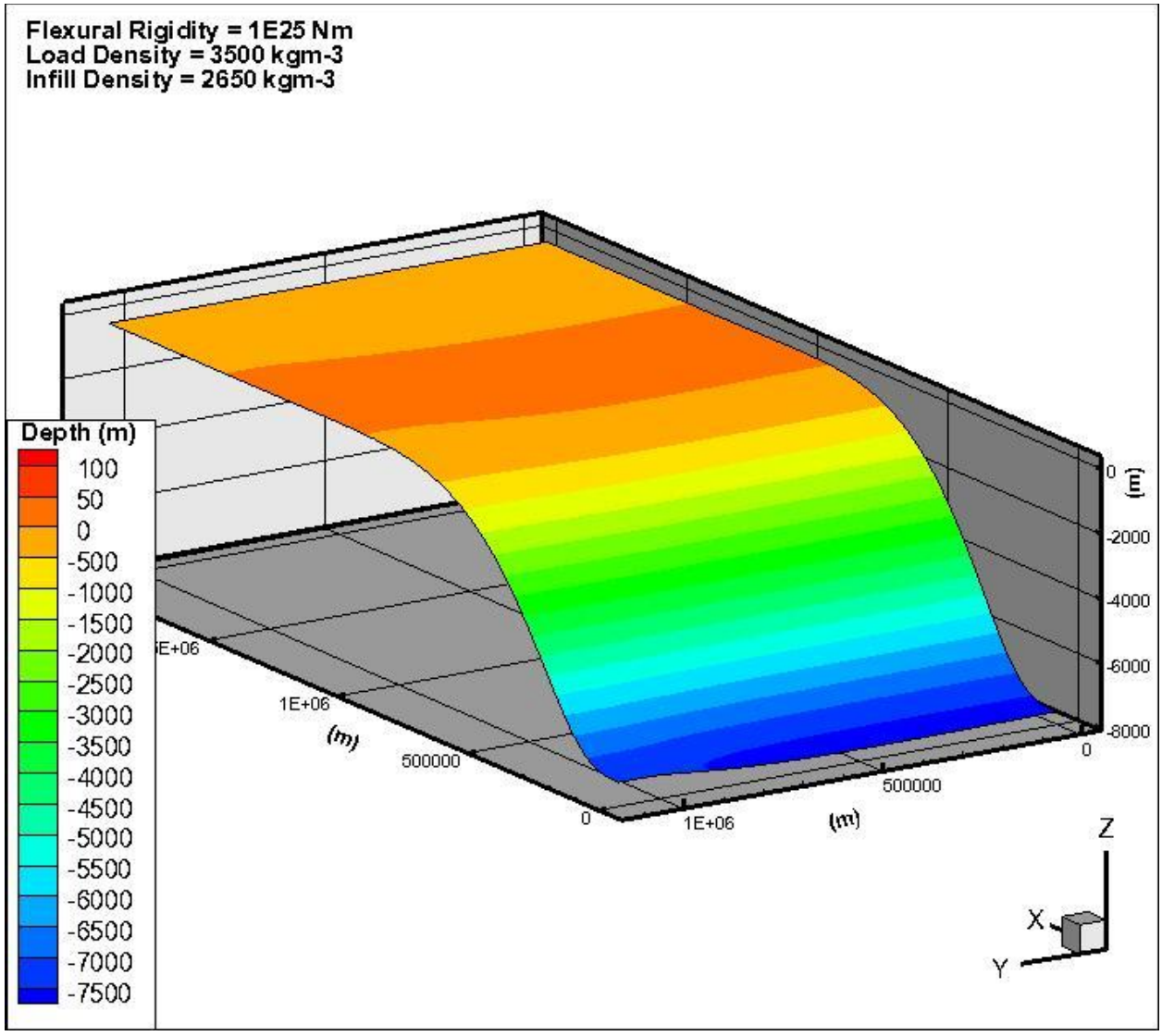

Figure 33: Uniform Load Model D16.

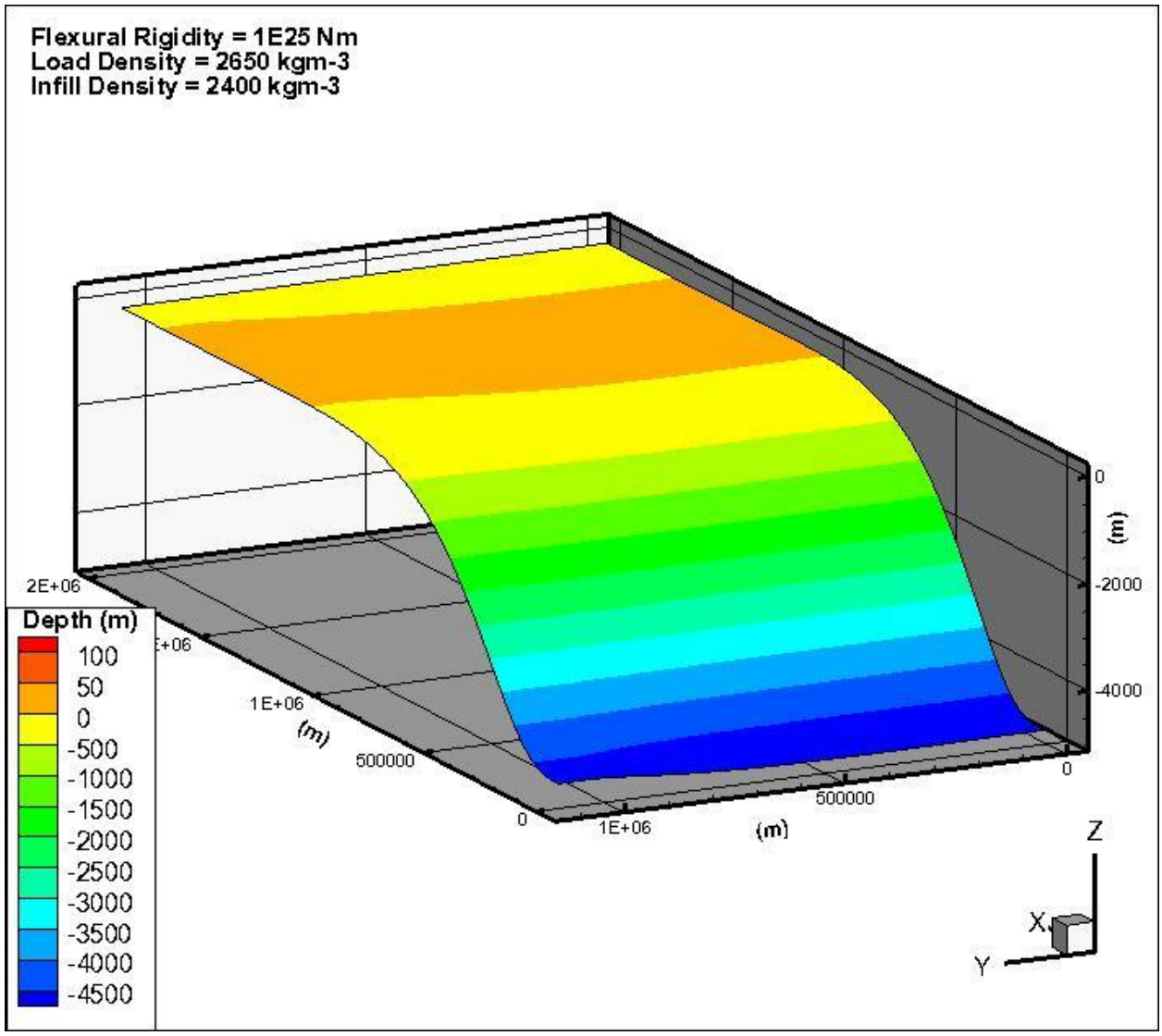

Figure 34: Uniform Load Model D17.

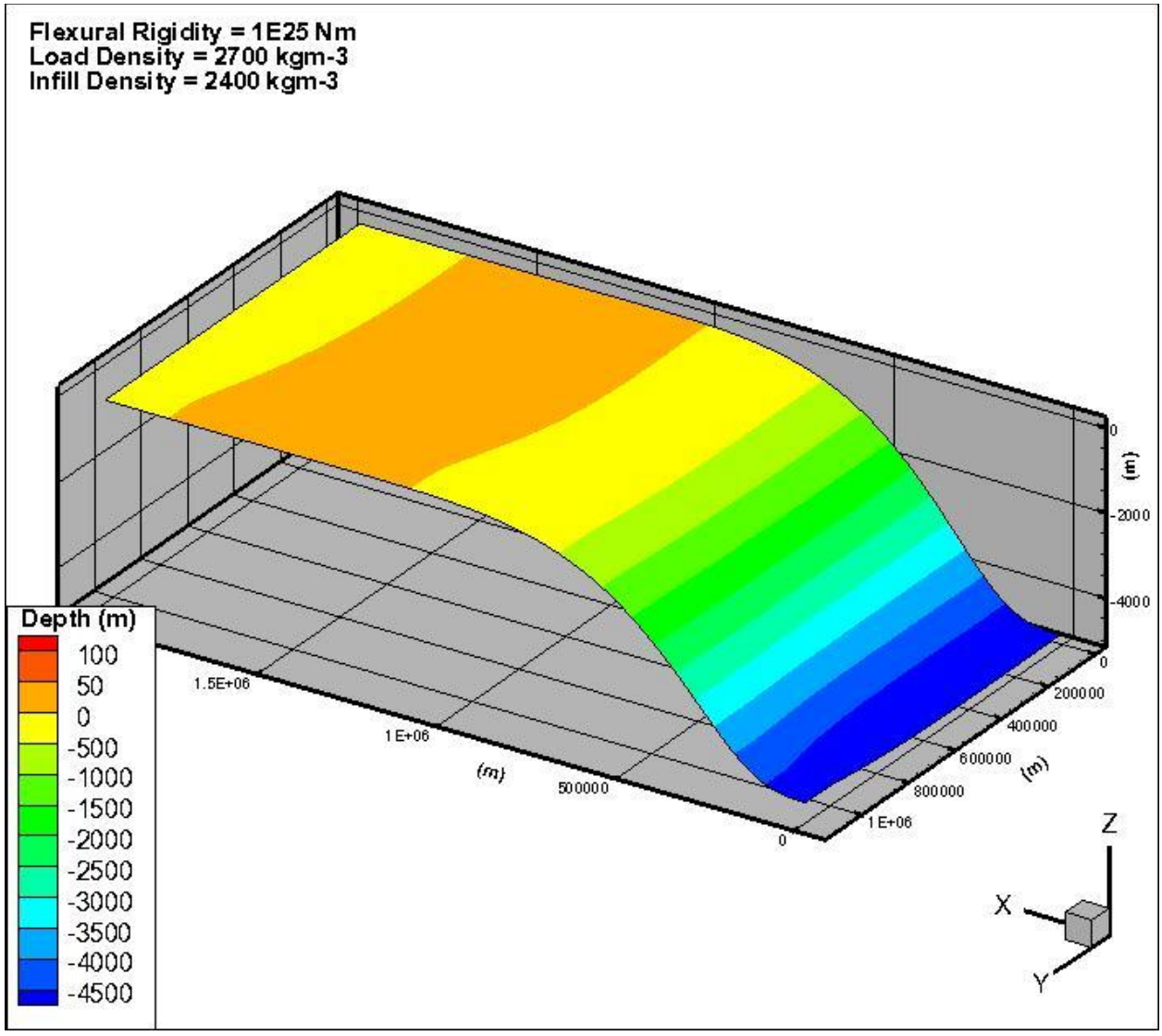

Figure 35: Uniform Load Model D1.

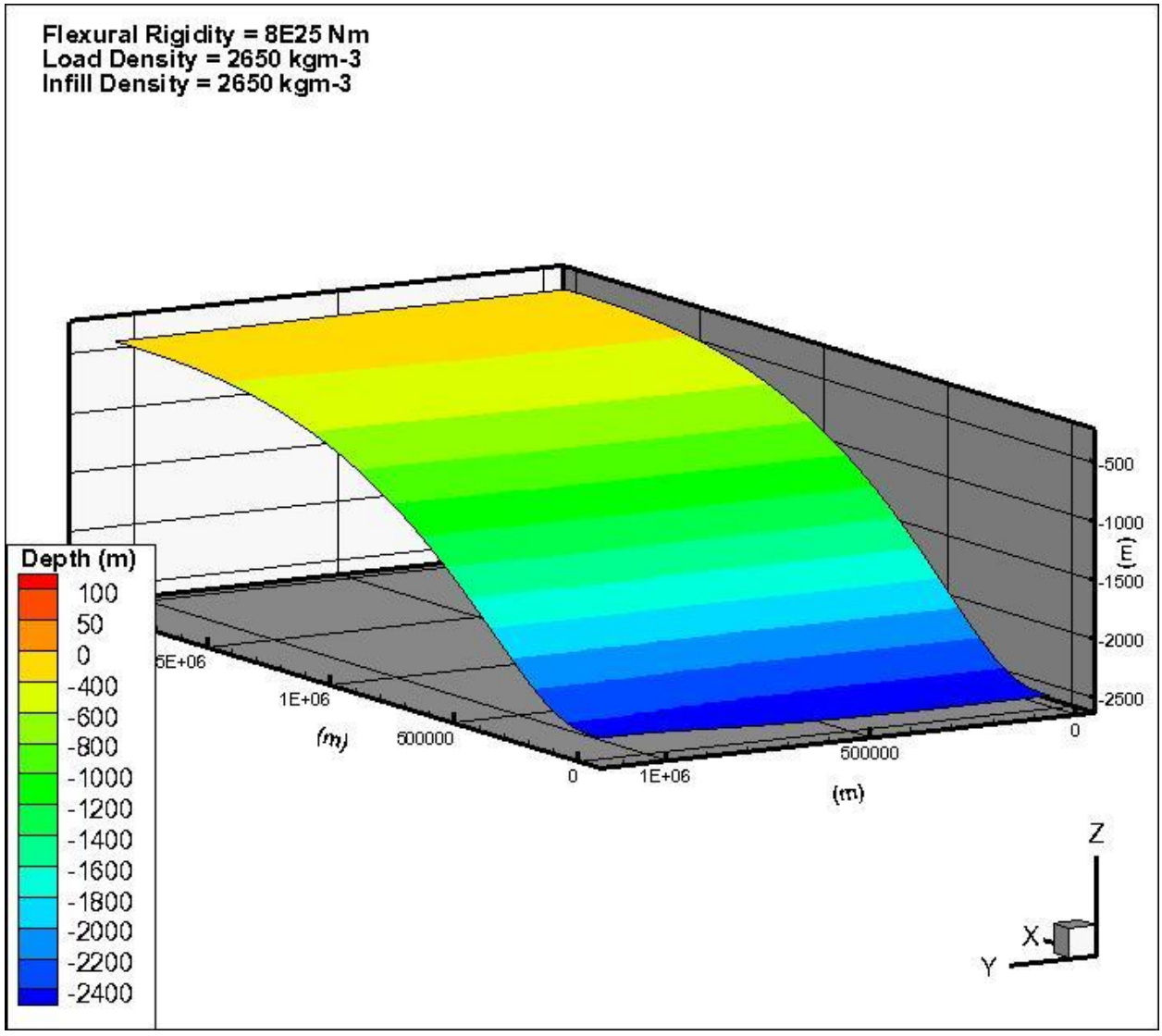

Figure 36: Uniform Load Model D3.

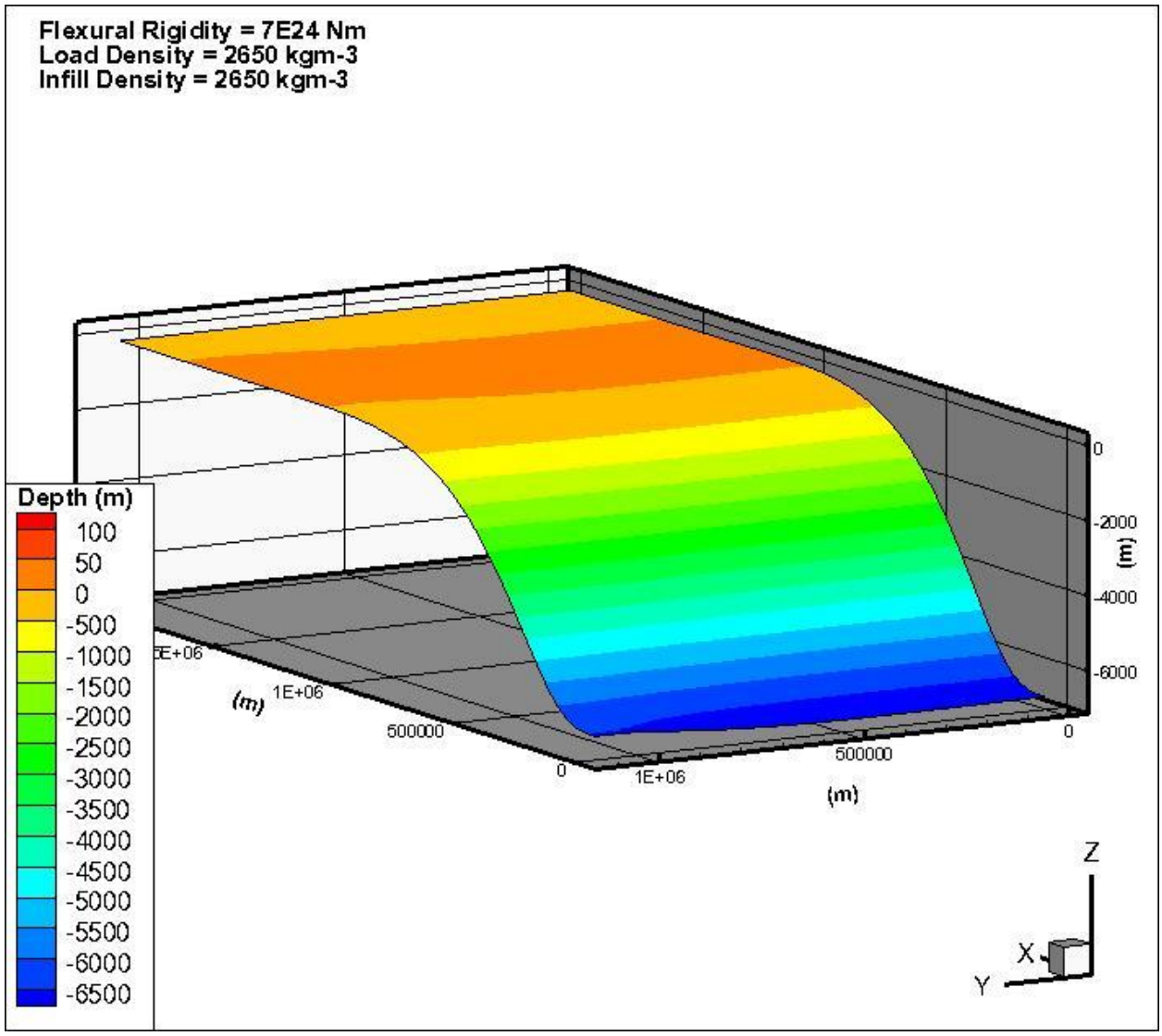

Figure 37: Uniform Load Model D6.

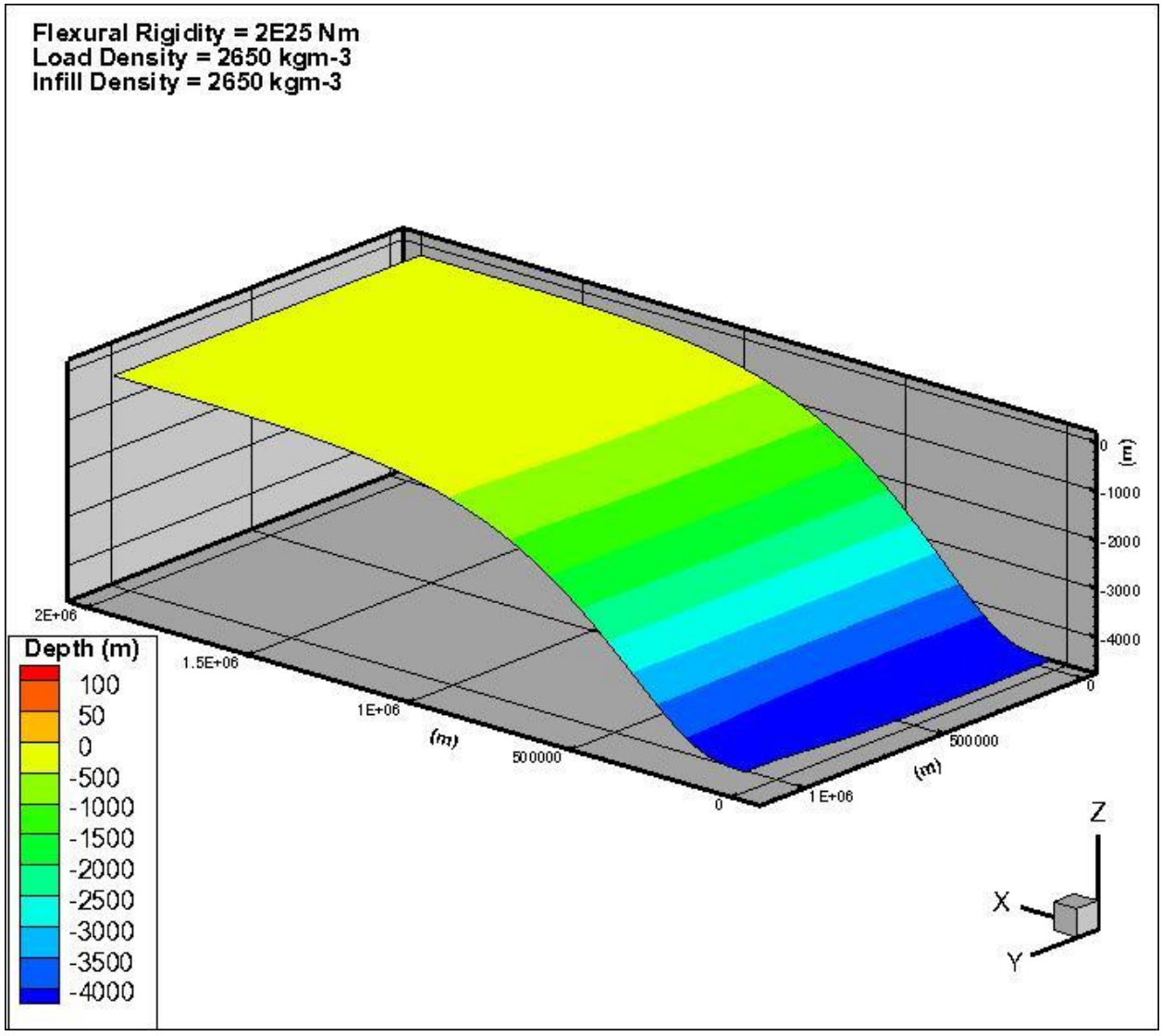

Figure 38: Uniform Load Model D7.

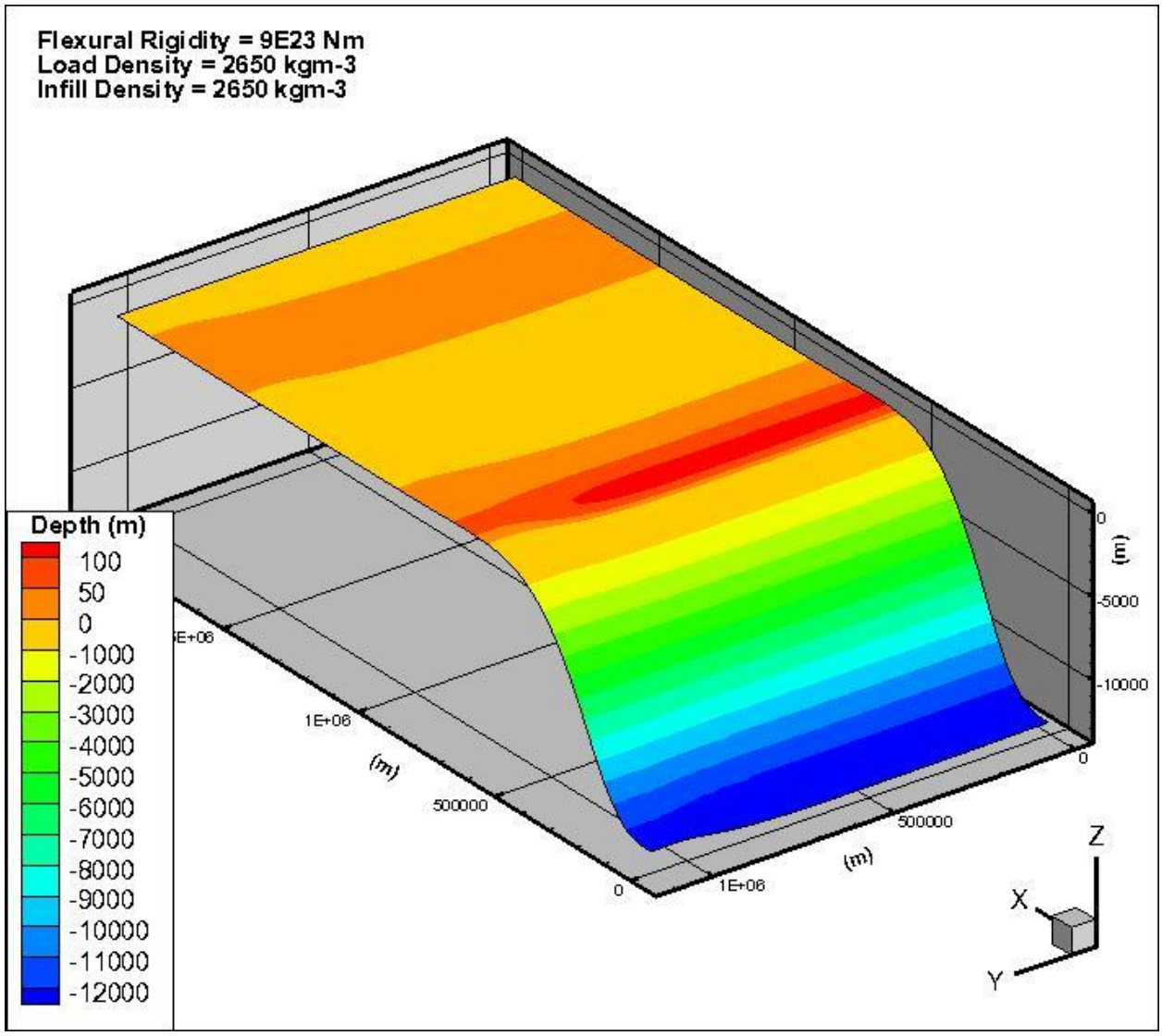

Figure 39: Uniform Load Model D8.

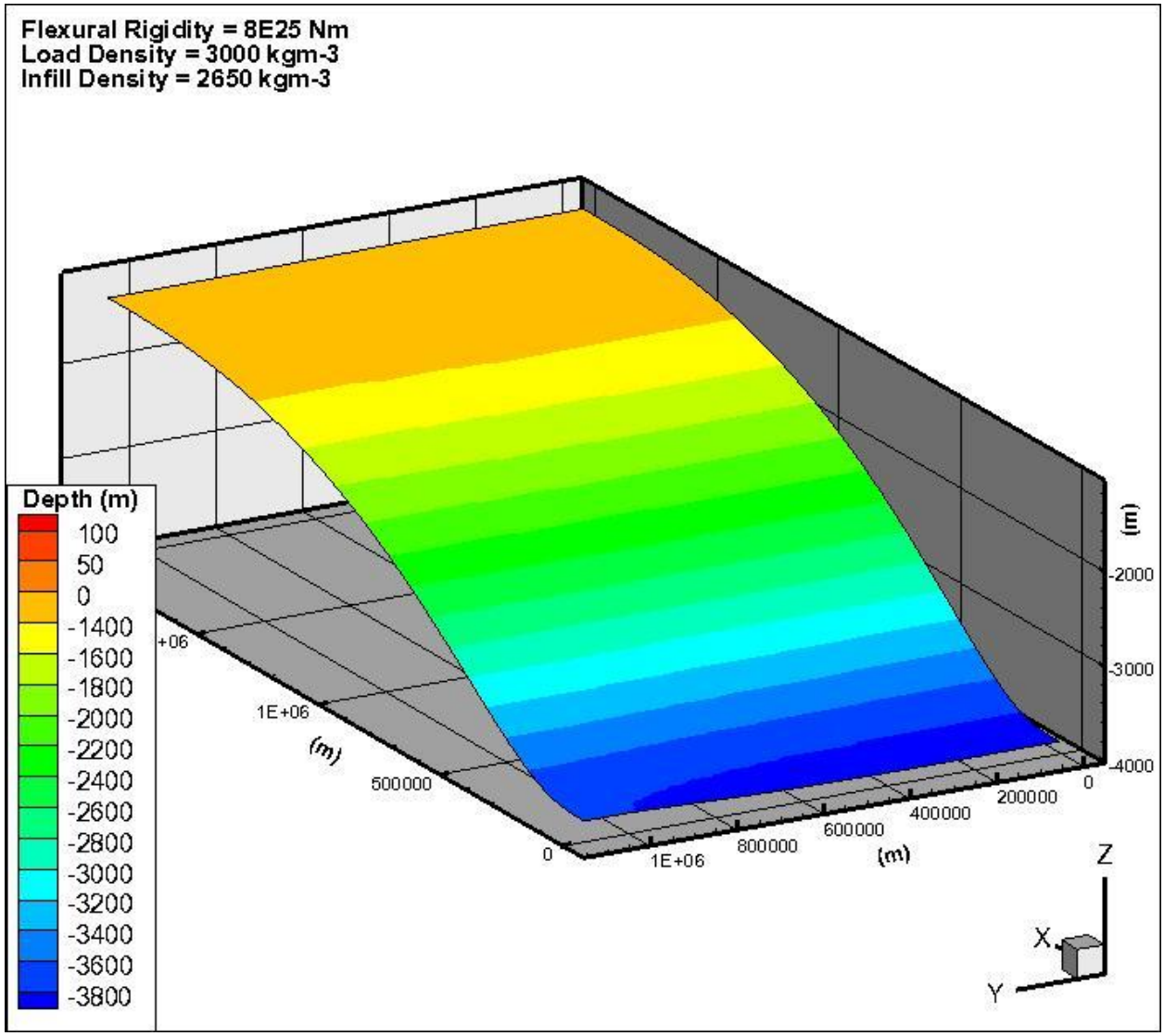

Figure 40: Uniform Load Model D14.

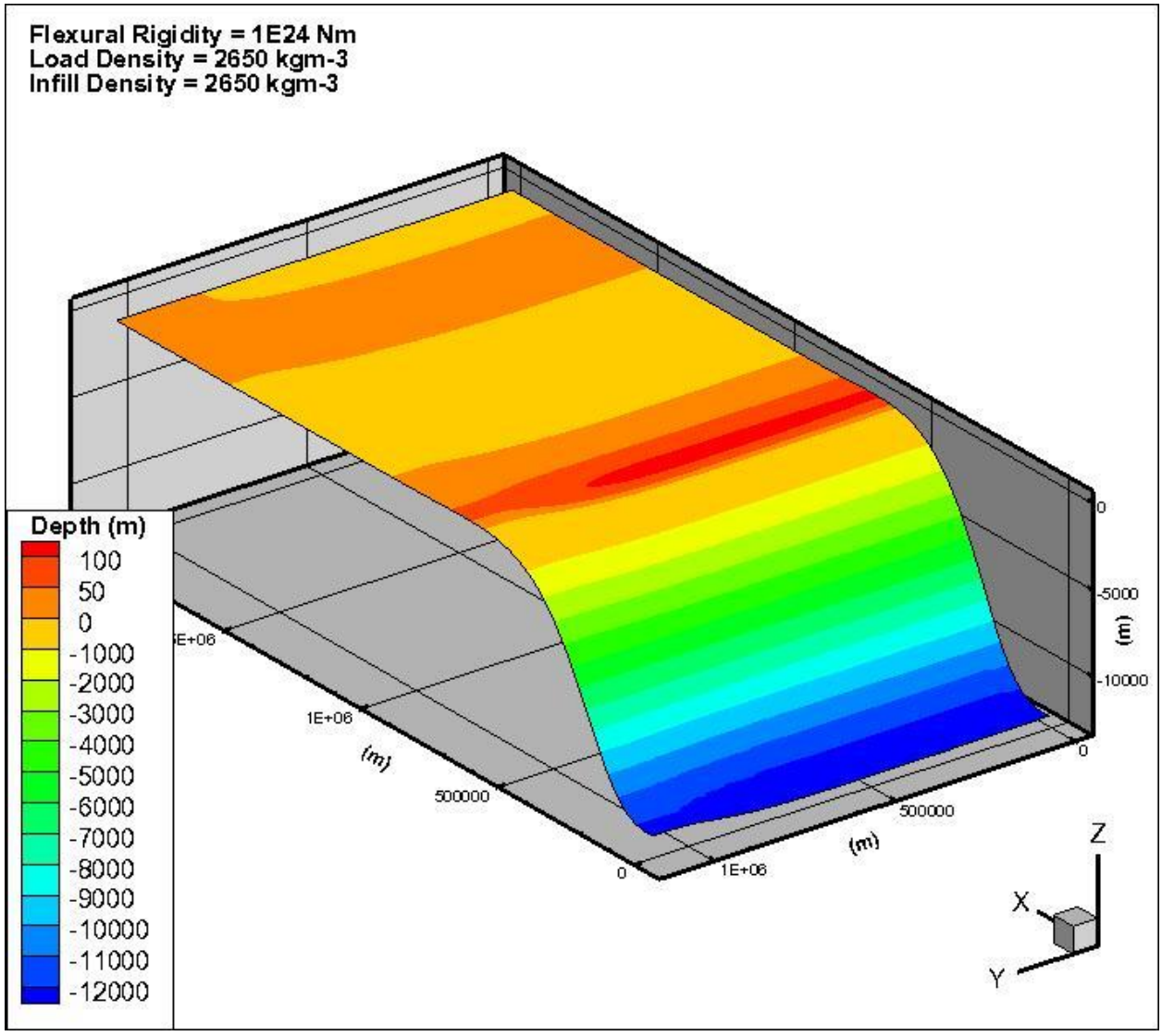

Figure 41: Uniform Load Model D15.

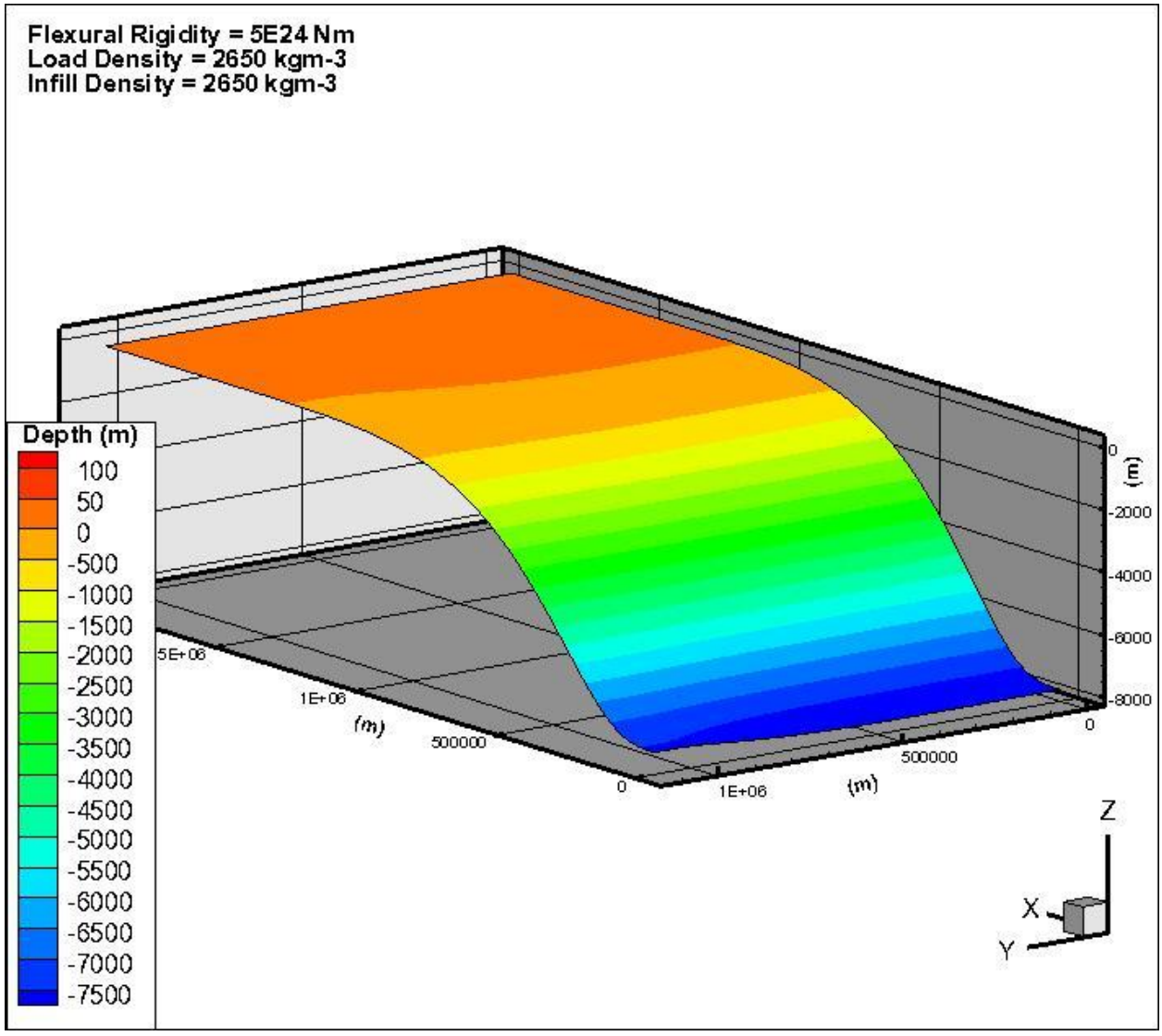

9.2 APPENDIX B: LATERALLY VARYING LOAD MODELS

Figure 42: Laterally Varying Load Model DLV1. Load of 7000 m placed on one-third (1/3) of model domain, 4000 m placed on remaining two-thirds (2/3) of model domain.

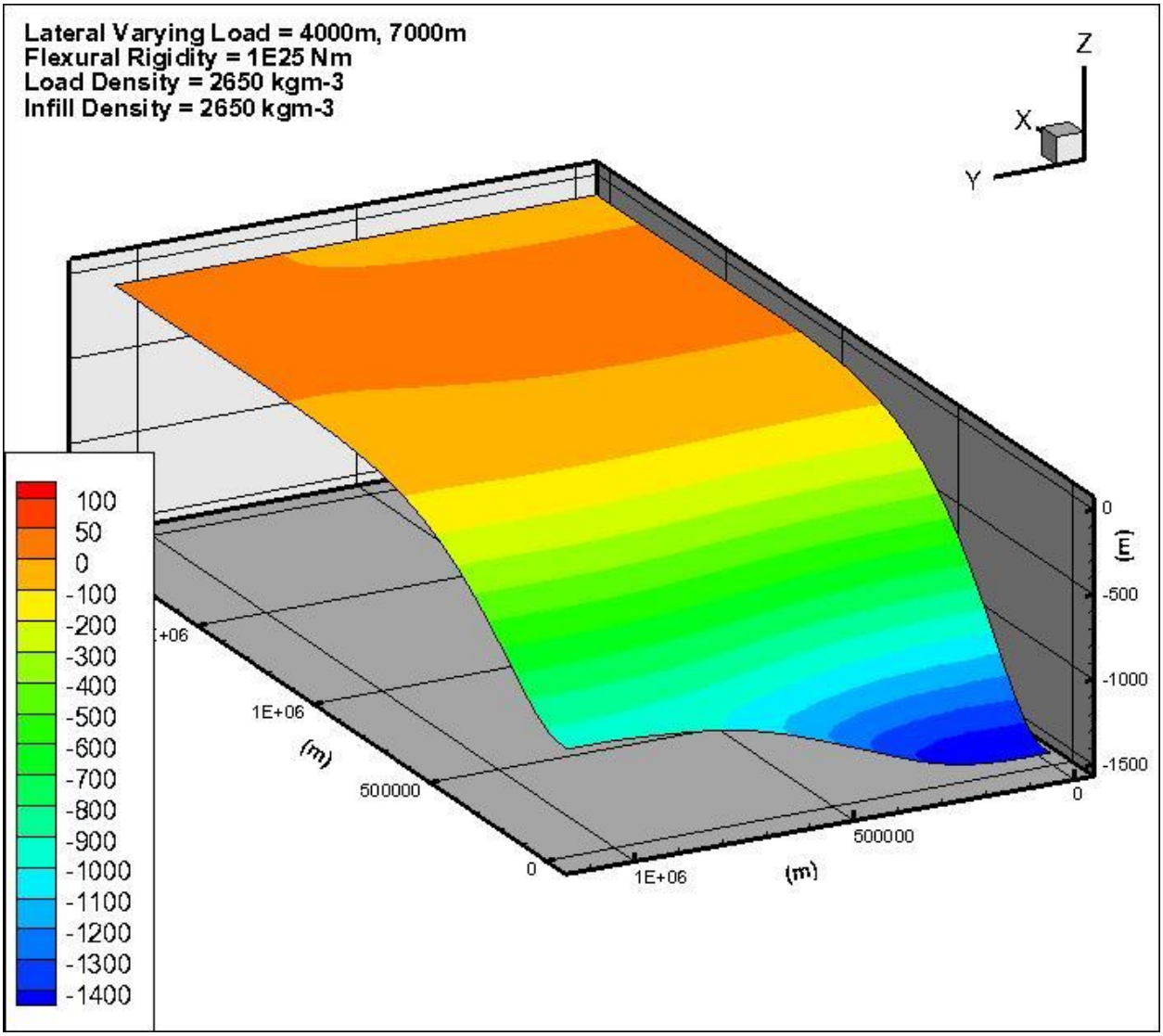

Figure 43: Laterally Varying Load Model DLV2. Load of 7000 m placed on one-half (1/2) of model domain, 4000 m placed on remaining one-half (1/2) of model domain.

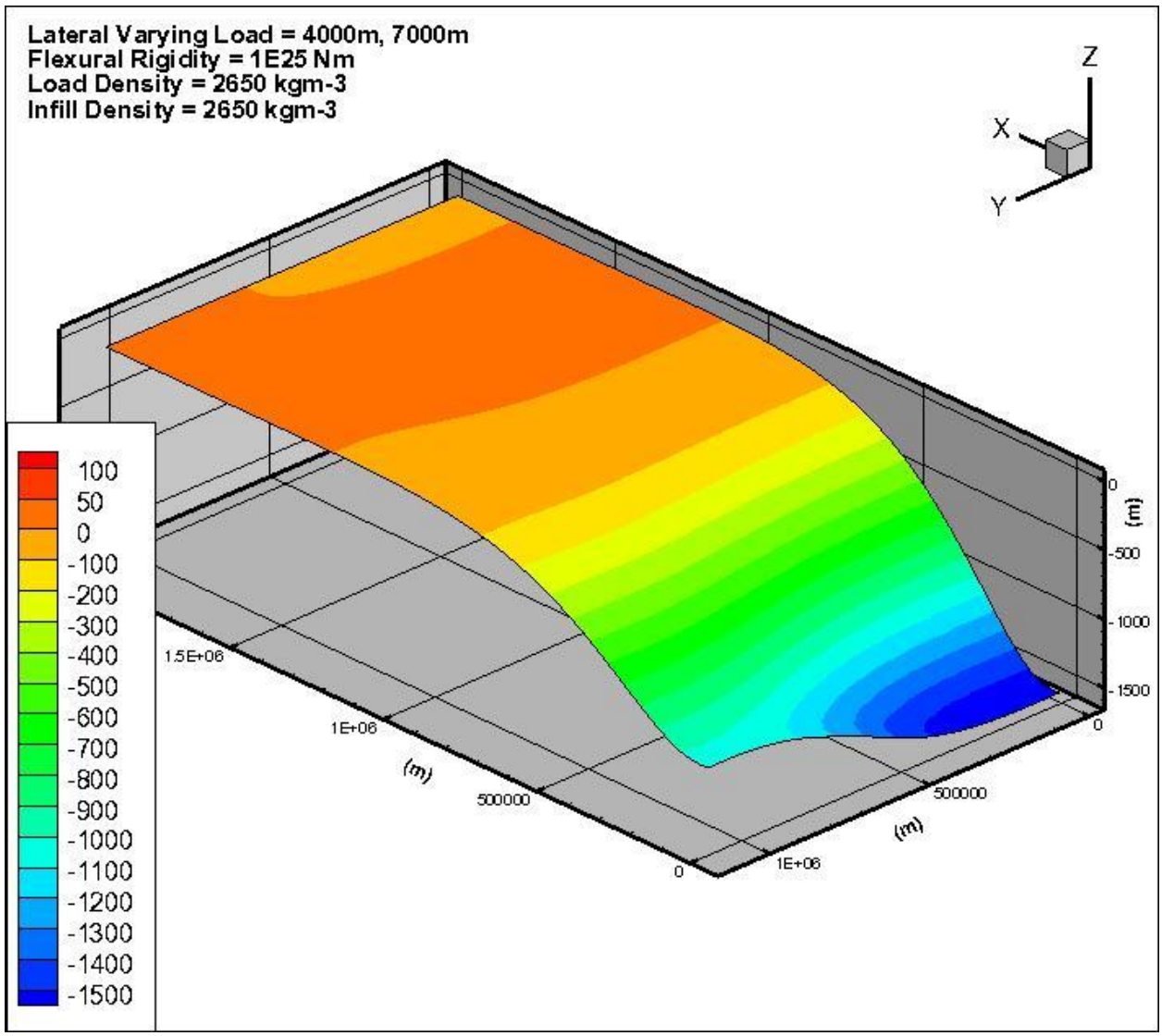

Figure 44: Laterally Varying Load Model DLV3. Load of 7000 m placed on one-third (1/3) of model domain, 4000 m placed on remaining two-thirds (2/3) of model domain.

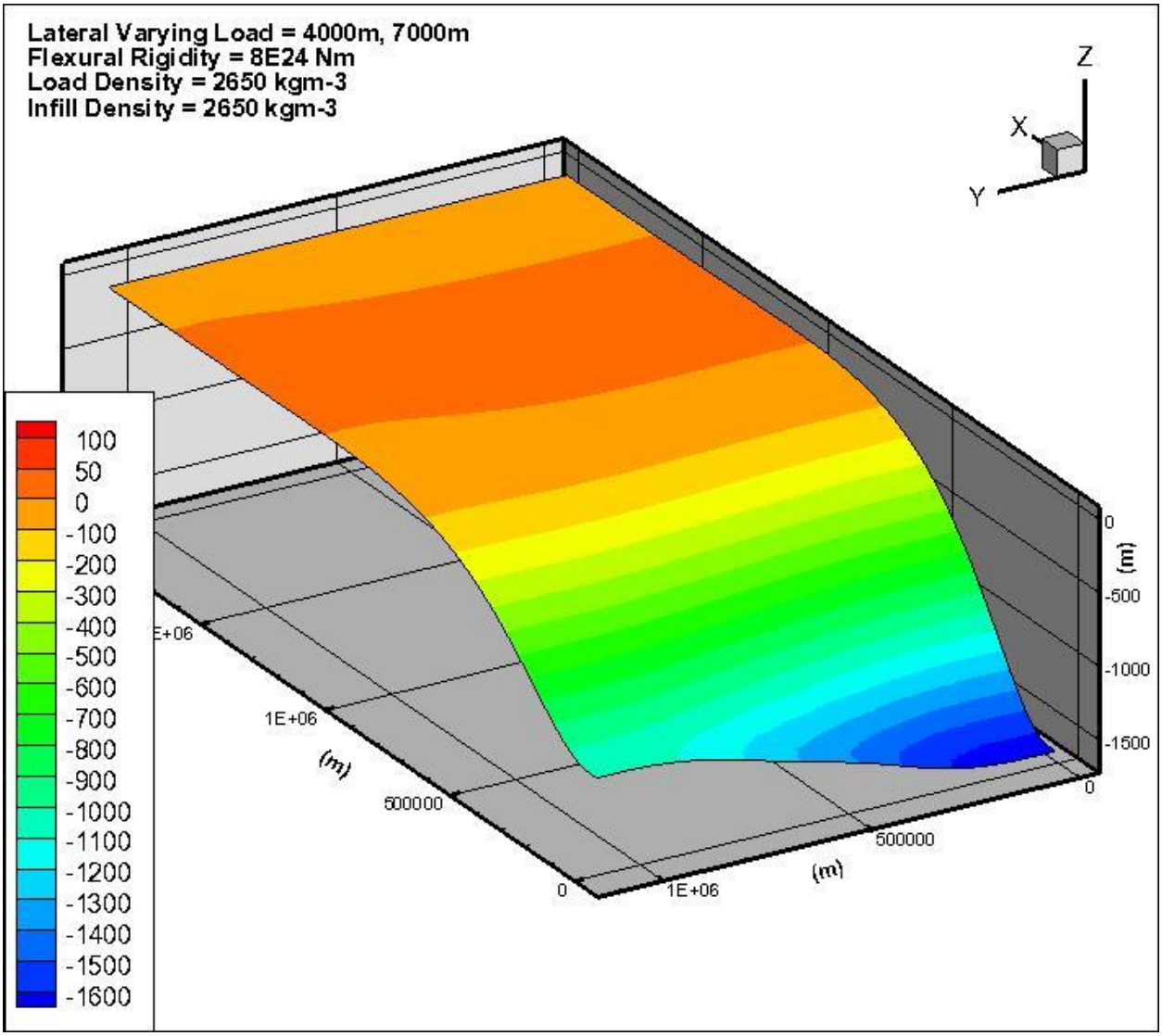

Figure 45: Laterally Varying Load Model DLV4. Load of 7000 m placed on one-half (1/2) of model domain, 4000 m placed on remaining one-half (1/2) of model domain.

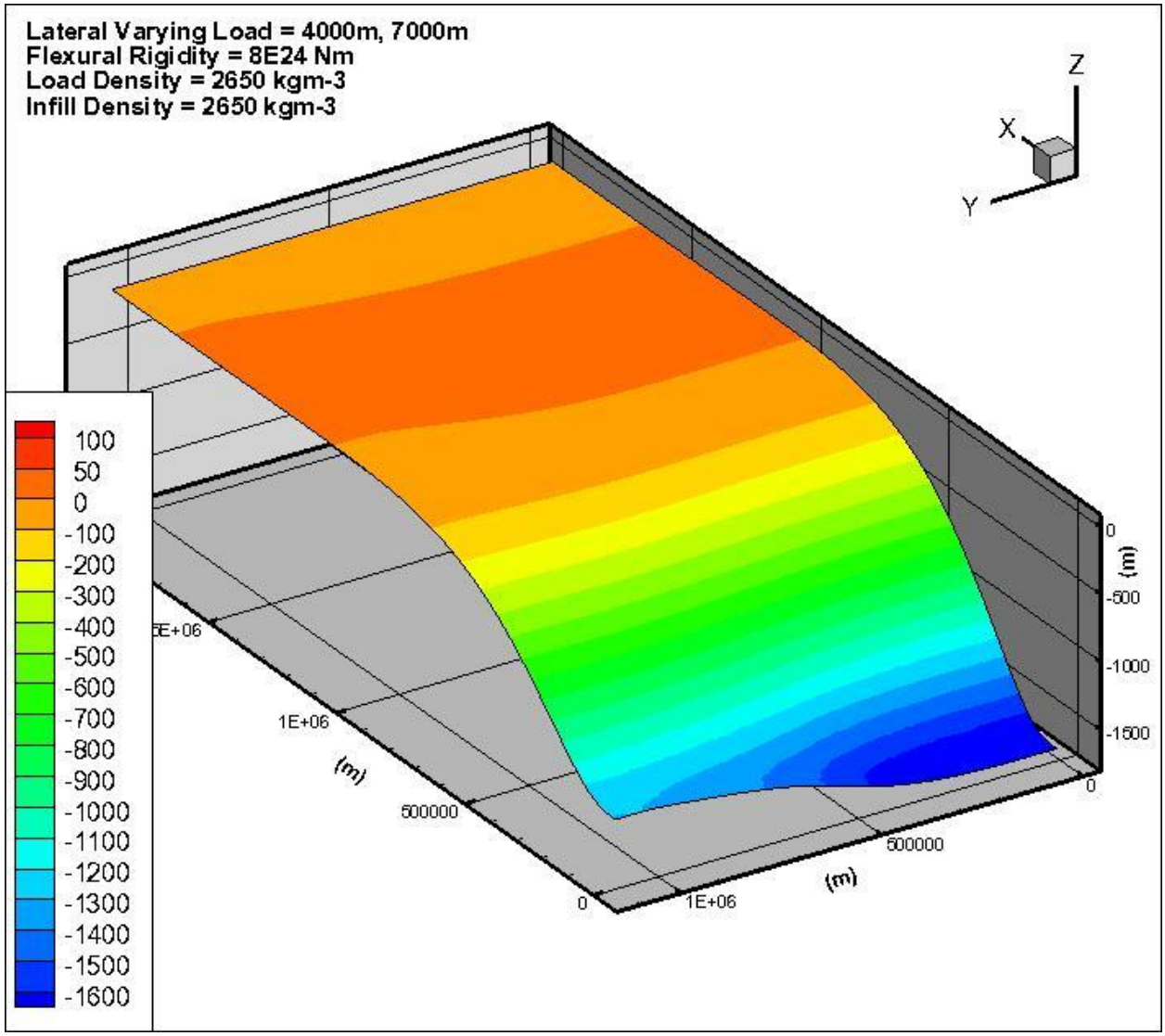

Figure 46: Laterally Varying Load Model DLV5. Load of 7000 m placed on one-third (1/3) of model domain, 5000 m placed on remaining two-thirds (2/3) of model domain.

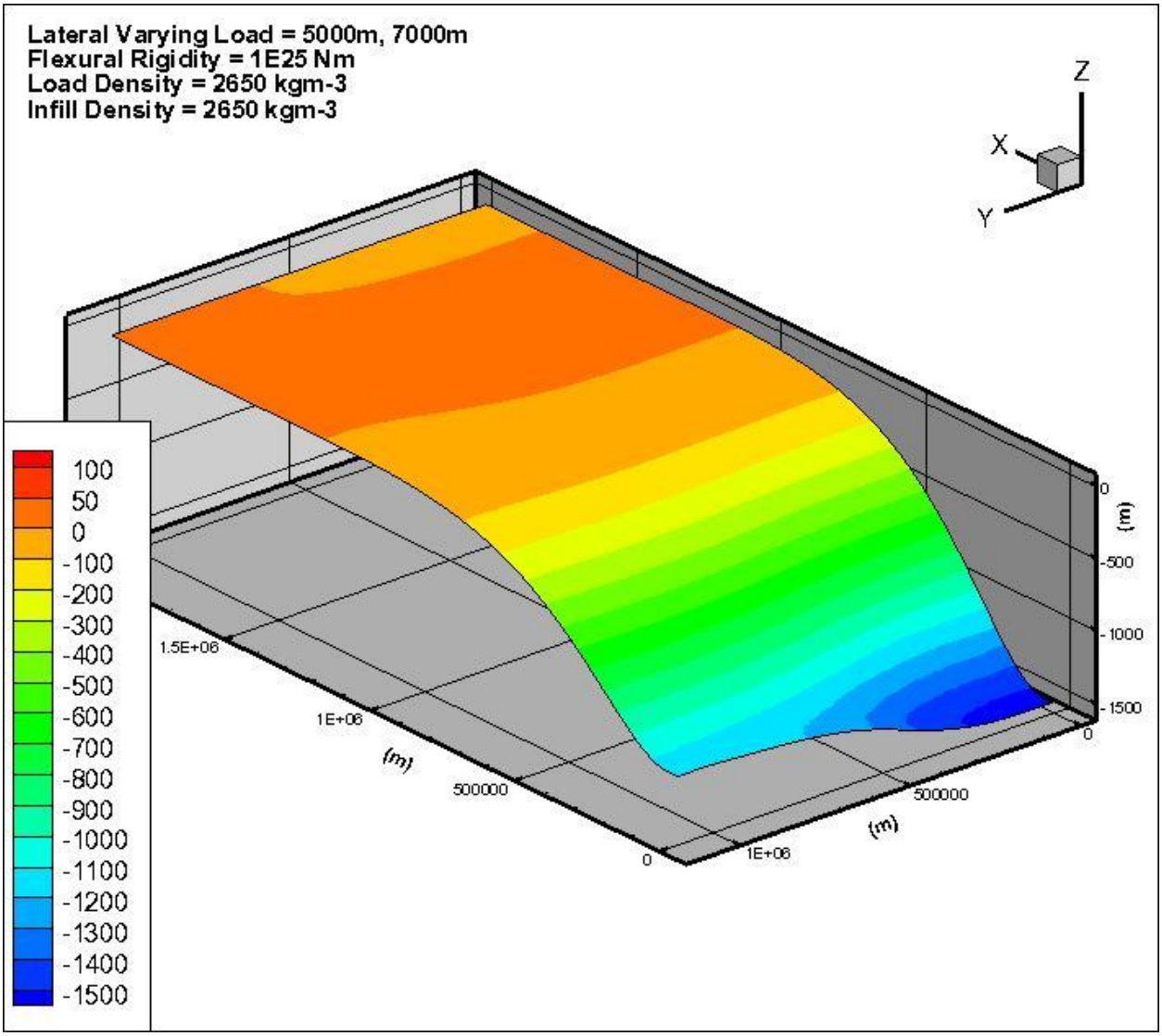

Figure 47: Laterally Varying Load Model DLV6. Load of 7000 m placed on one-half (1/2) of model domain, 5000 m placed on remaining one-half (1/2) of model domain.

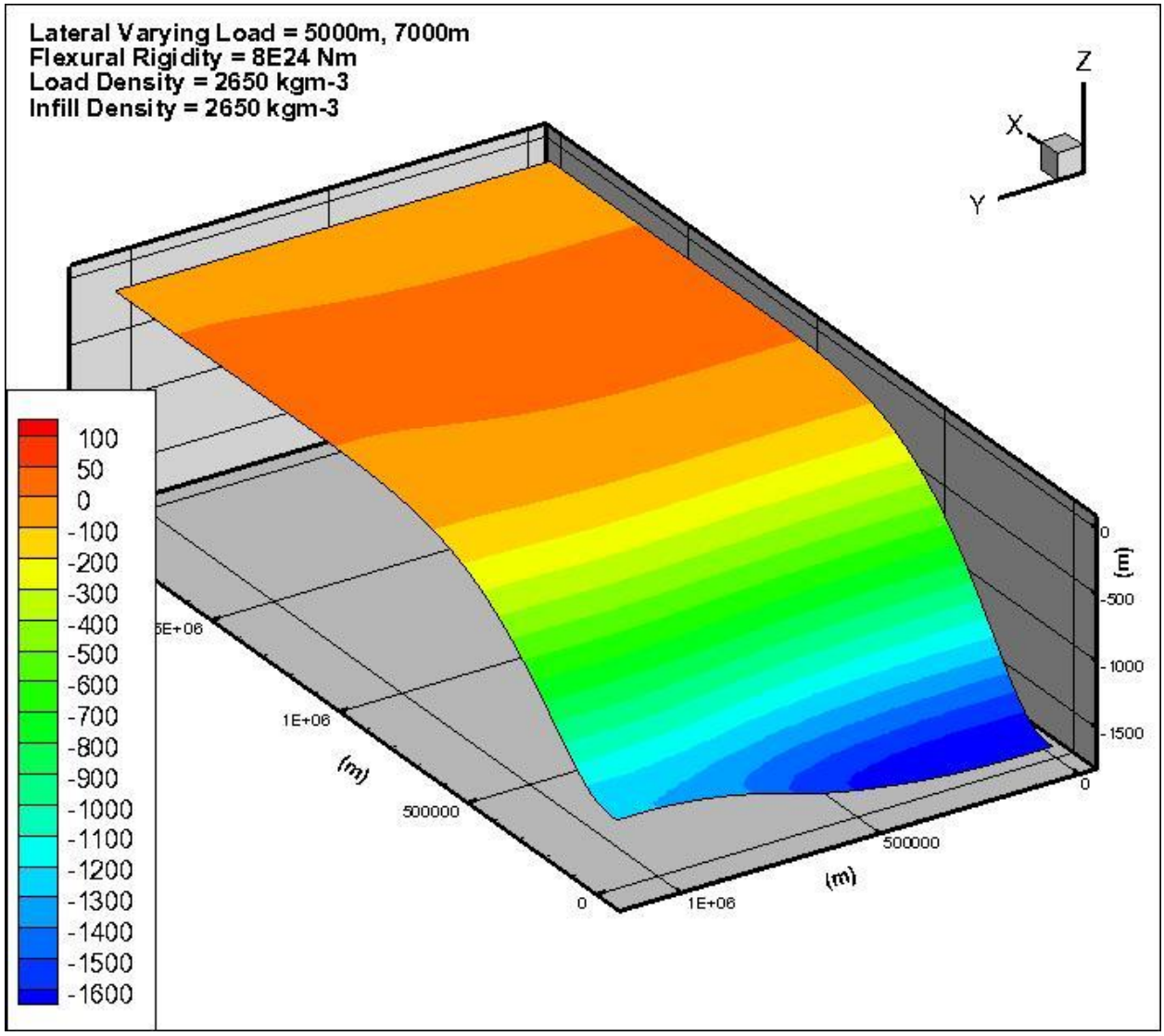

Figure 48: Laterally Varying Load Model DLV7. Load of 7000 m placed on one-third (1/3) of model domain, 4000 m placed on remaining two-thirds (2/3) of model domain.

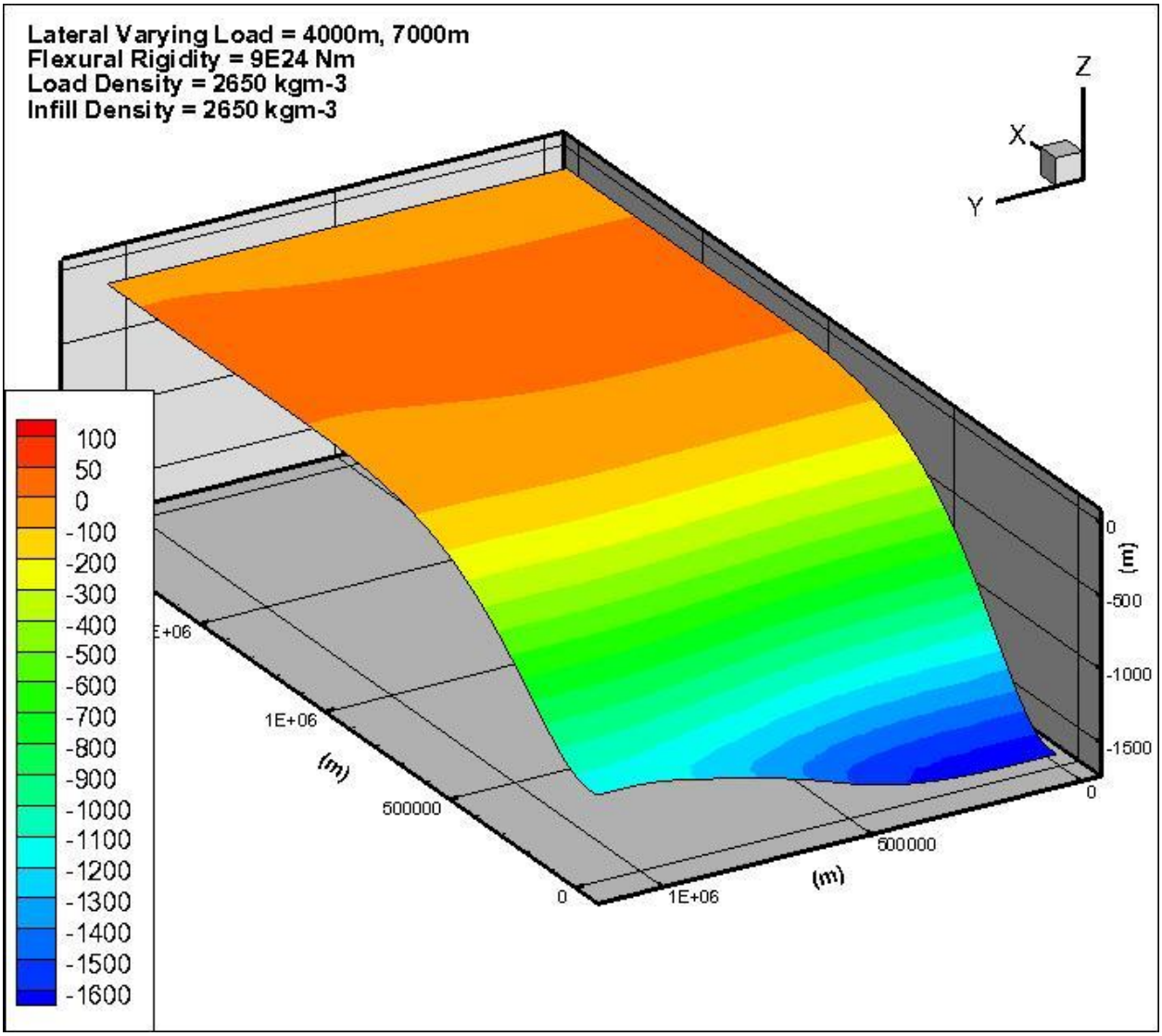

Figure 49: Laterally Varying Load Model DLV8. Load of 7000 m placed on one-third (1/3) of model domain, 5000 m placed on remaining two-thirds (2/3) of model domain.

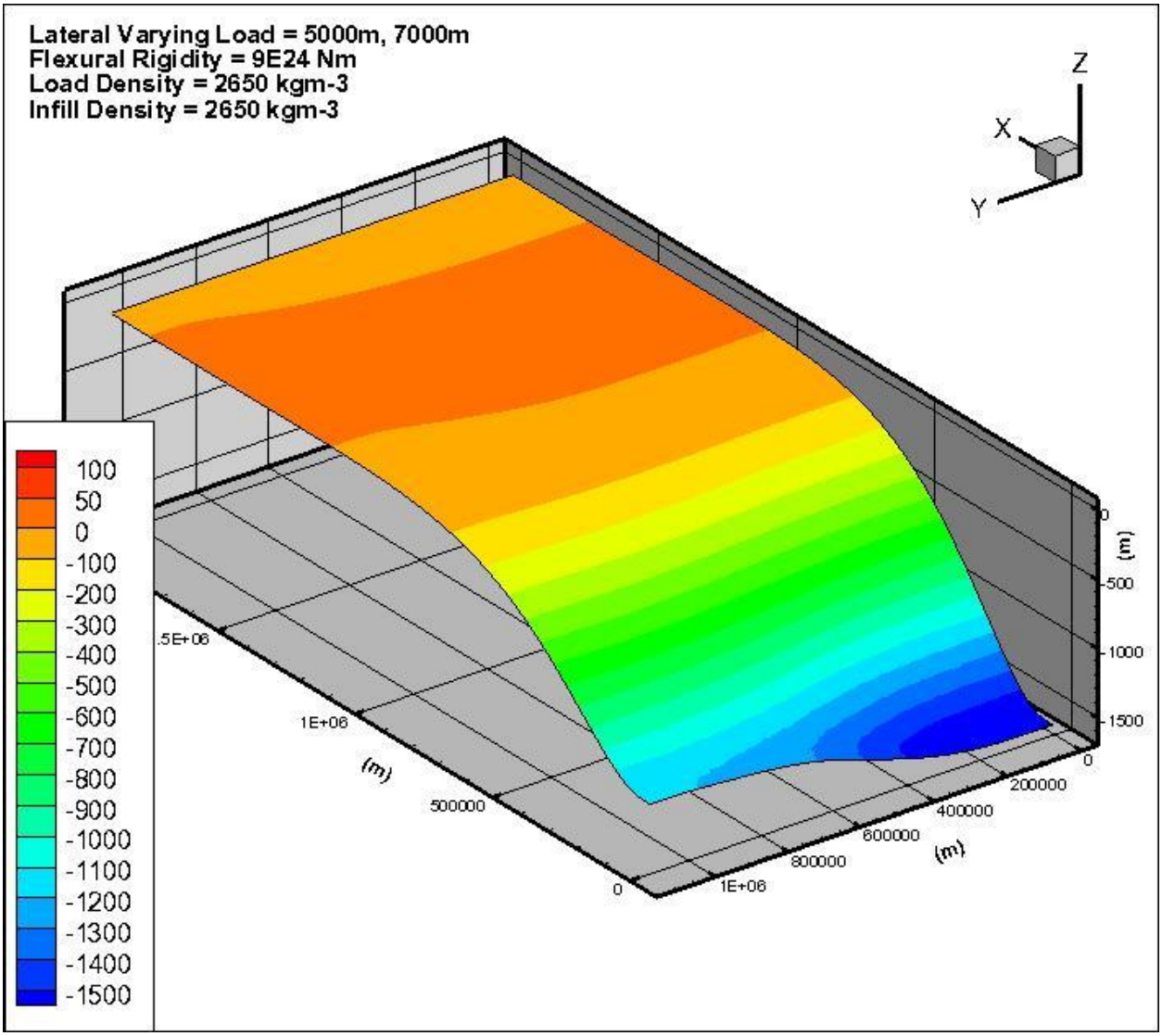

Figure 50: Laterally Varying Load Model DLV9. Load of 7000 m placed on one-third (1/3) of model domain, 3500 m placed on remaining two-thirds (2/3) of model domain.

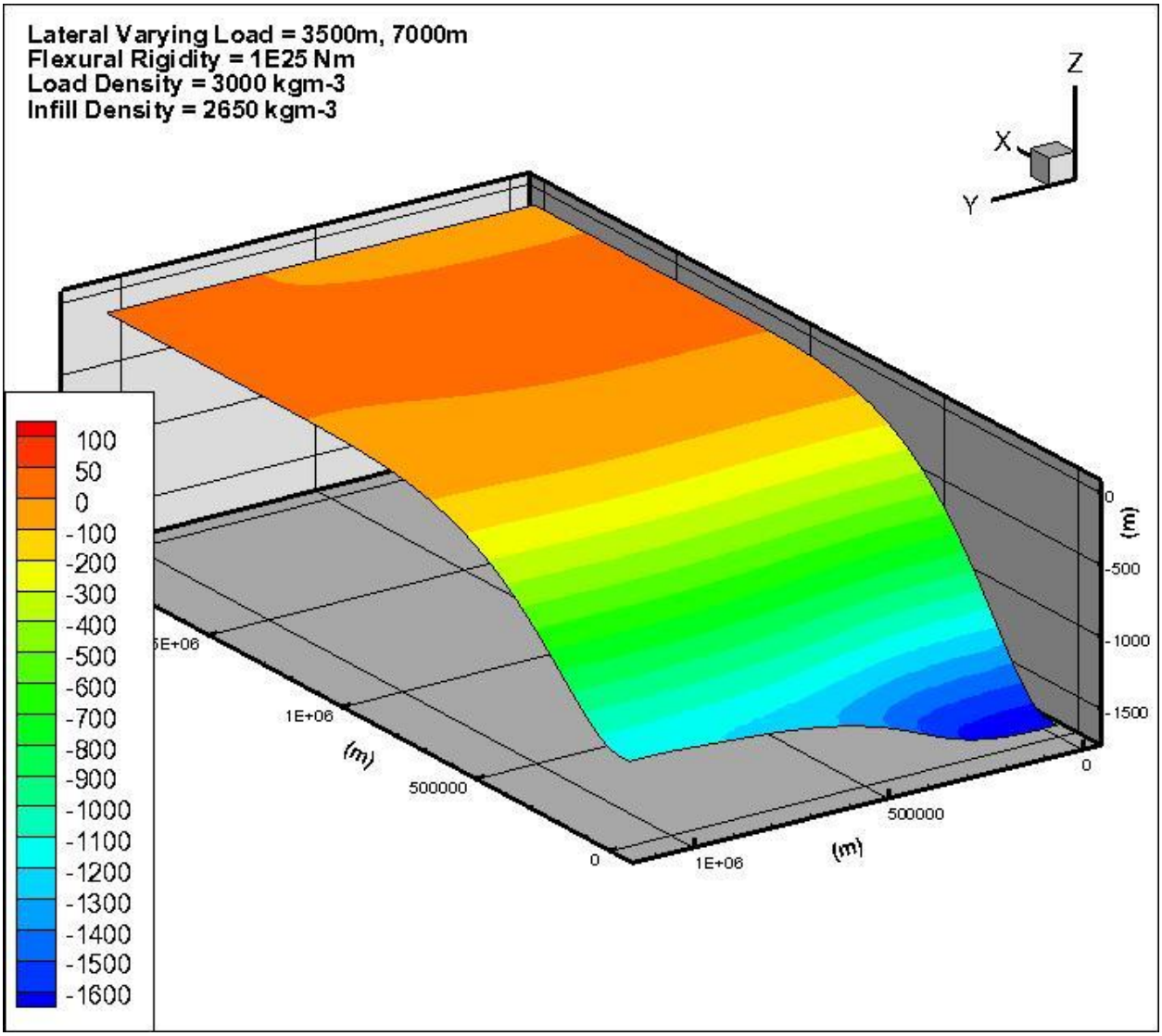

Figure 51: Laterally Varying Load Model DLV10. Load of 7000 m placed on one-third (1/3) of model domain, 3500 m placed on remaining two-thirds (2/3) of model domain.

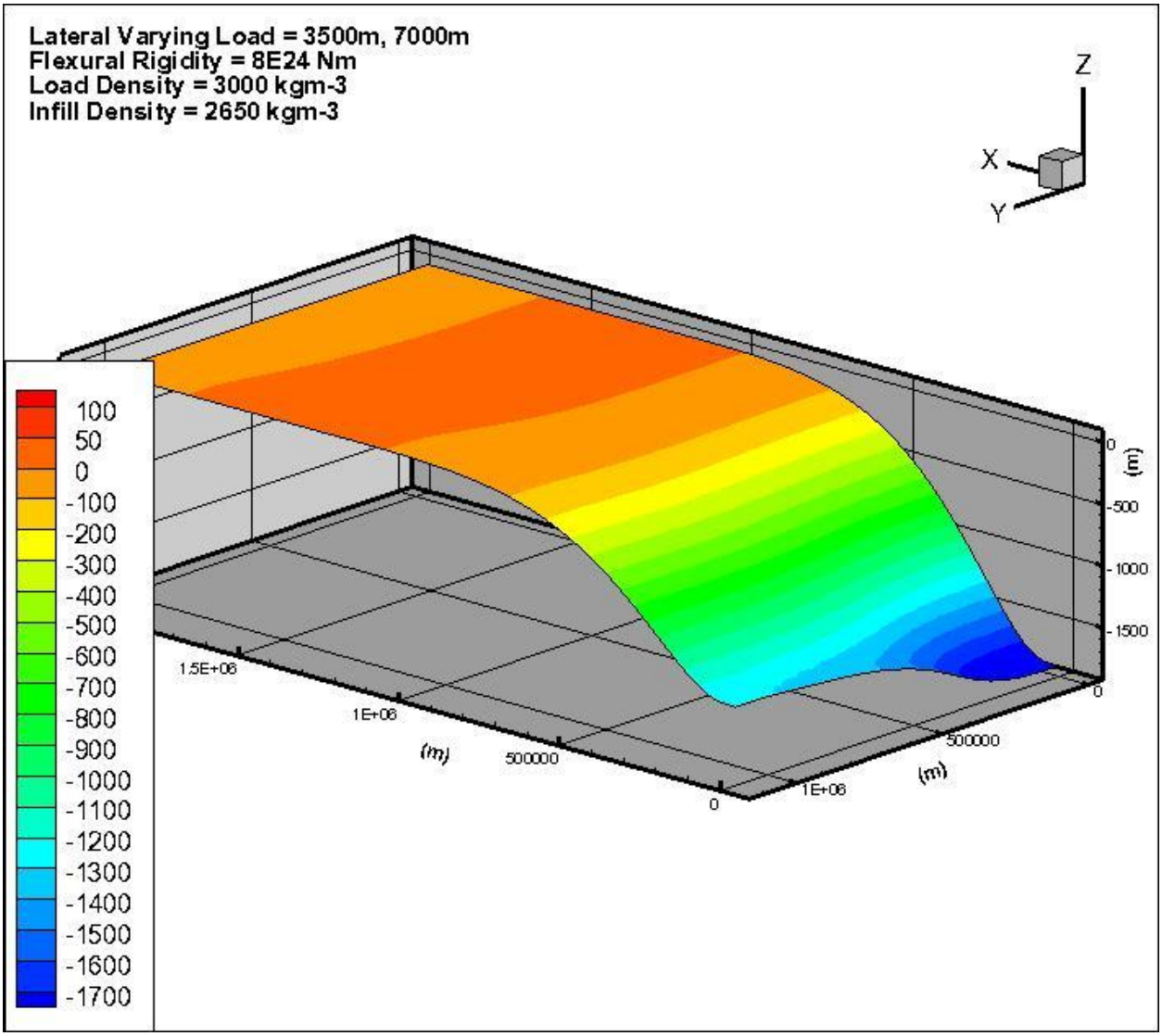

Figure 52: Laterally Varying Load Model DLV11. Load of 7000 m placed on one-third (1/3) of model domain, 3500 m placed on remaining two-thirds (2/3) of model domain.

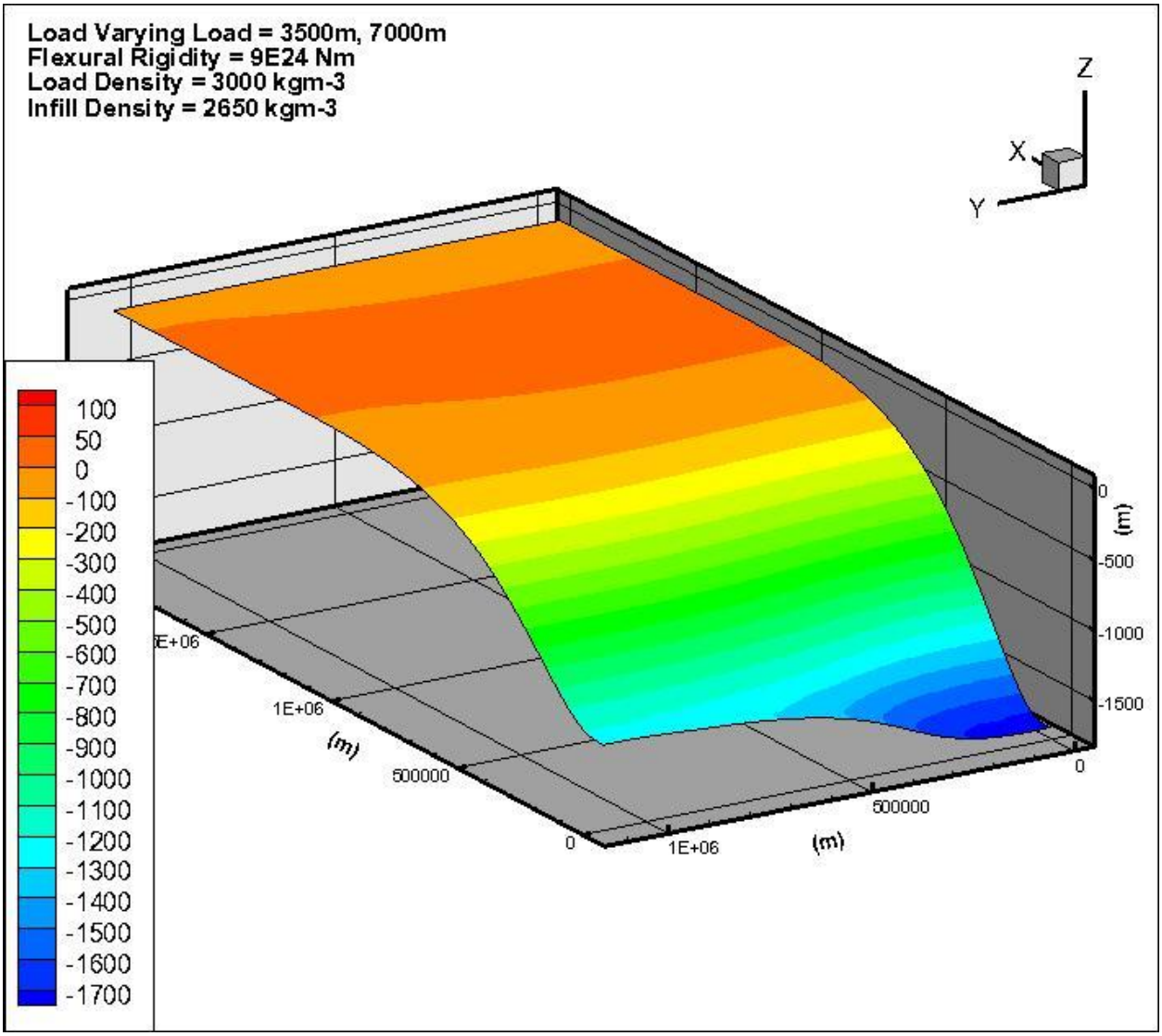

Figure 53: Laterally Varying Load Model DLVR1. Loads of 5000 m placed on edges of model domain.

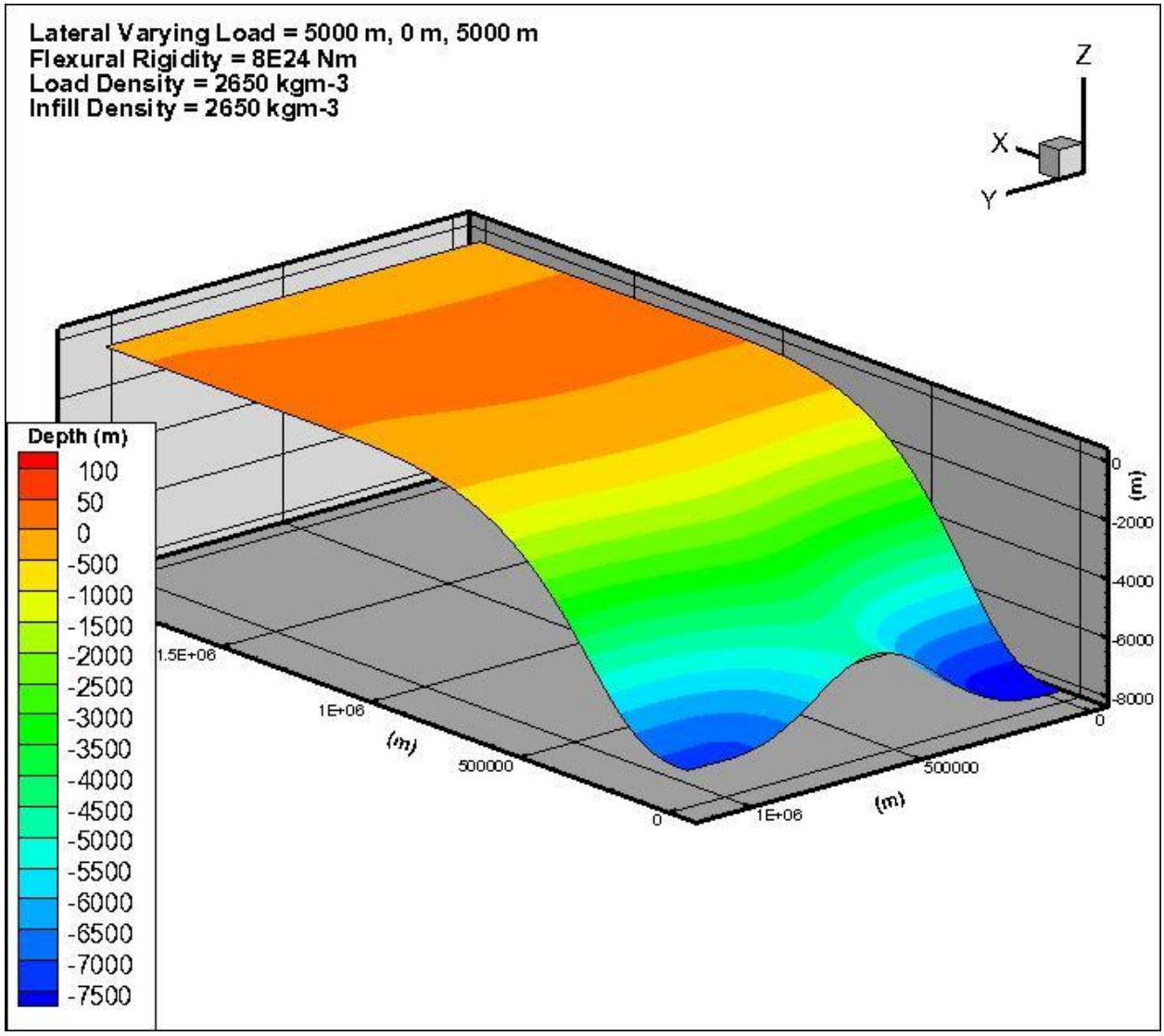

Figure 54: Laterally Varying Load Model DLVR2. Loads of 5000 m placed on edges of model domain.

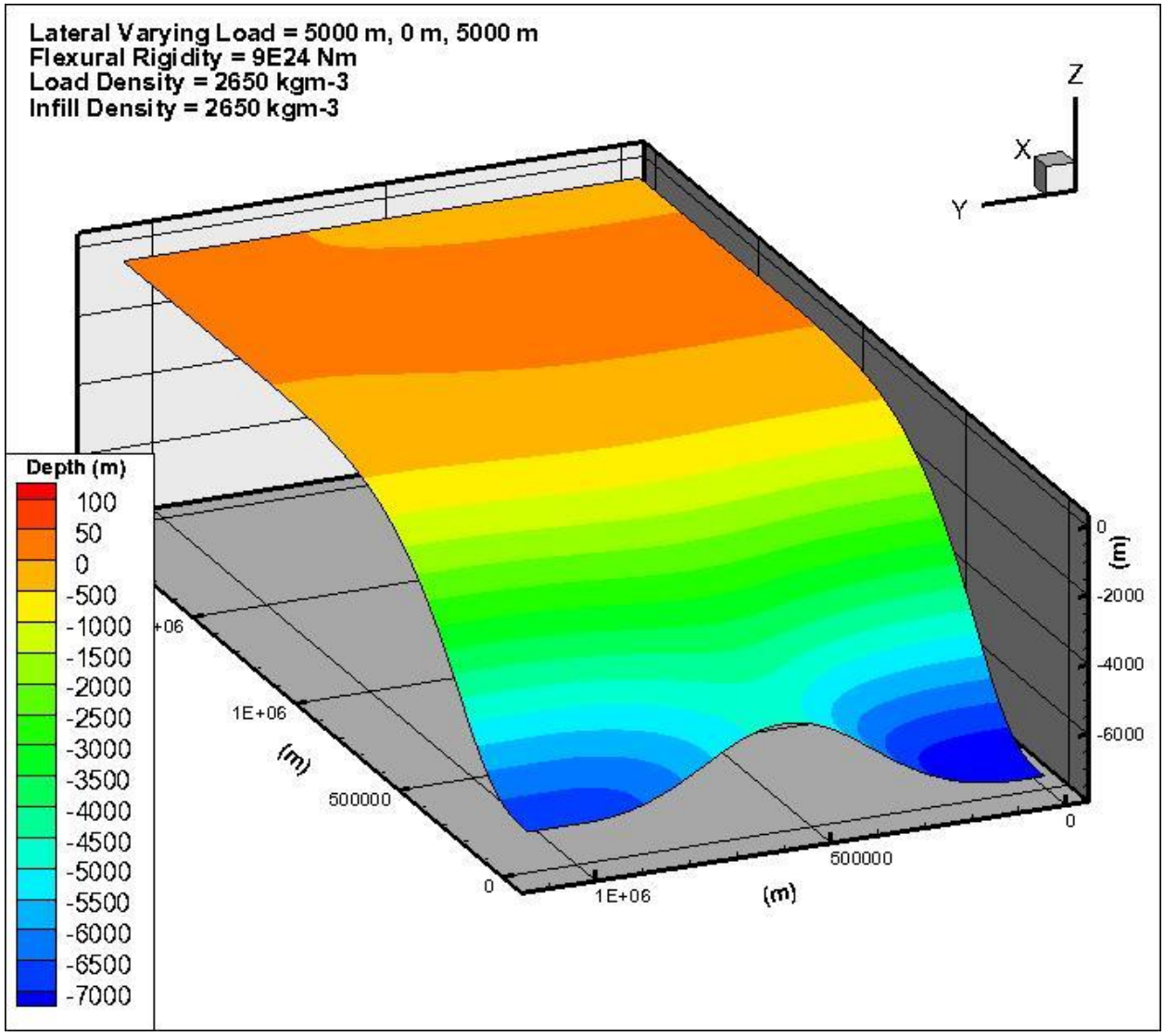

Figure 55: Laterally Varying Load Model DLVR3. Loads of 5000 m placed on edges of model domain.

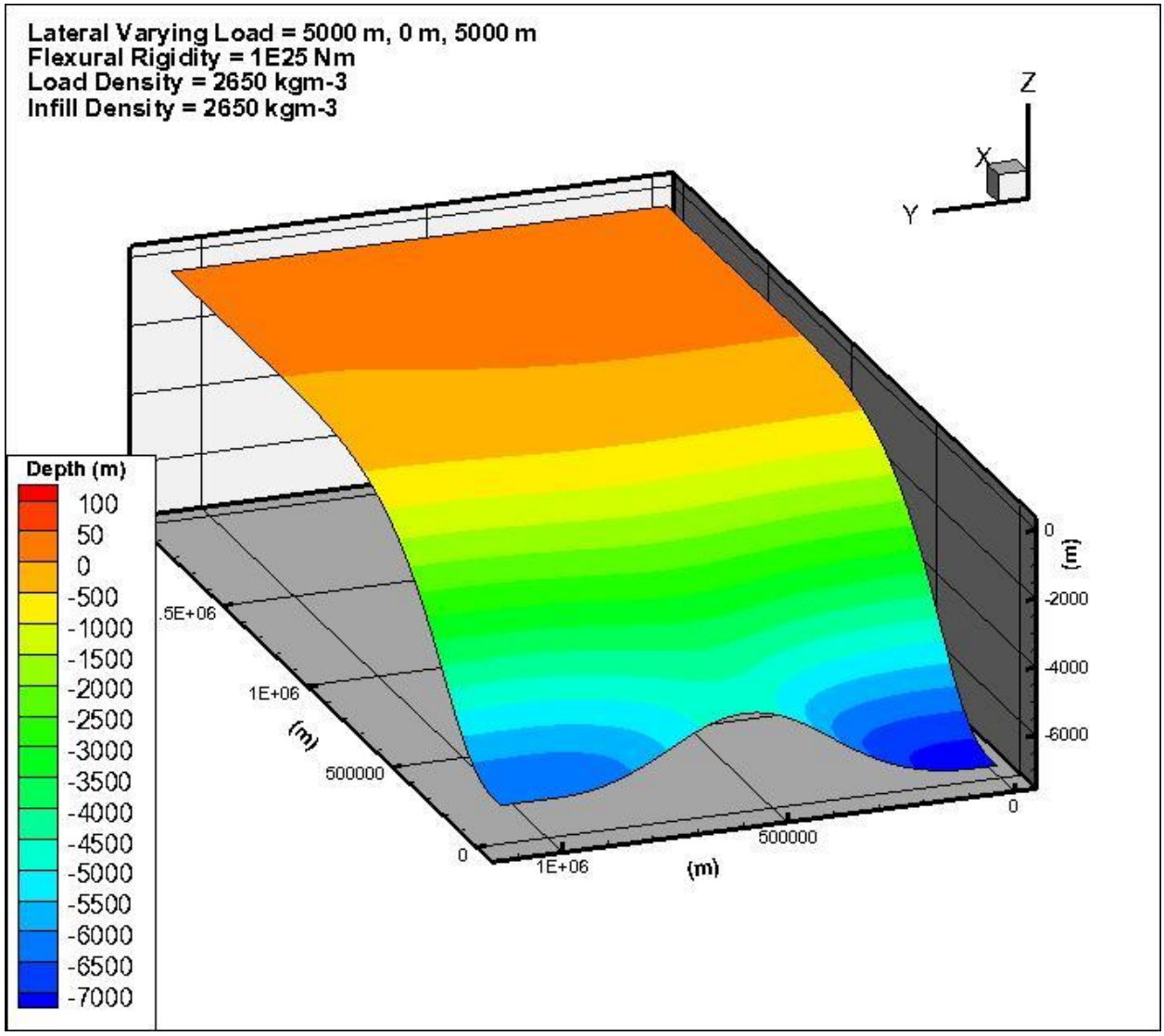

Figure 56: Laterally Varying Load Model DLVR4. Loads of 5000 m placed on edges and center of model domain.

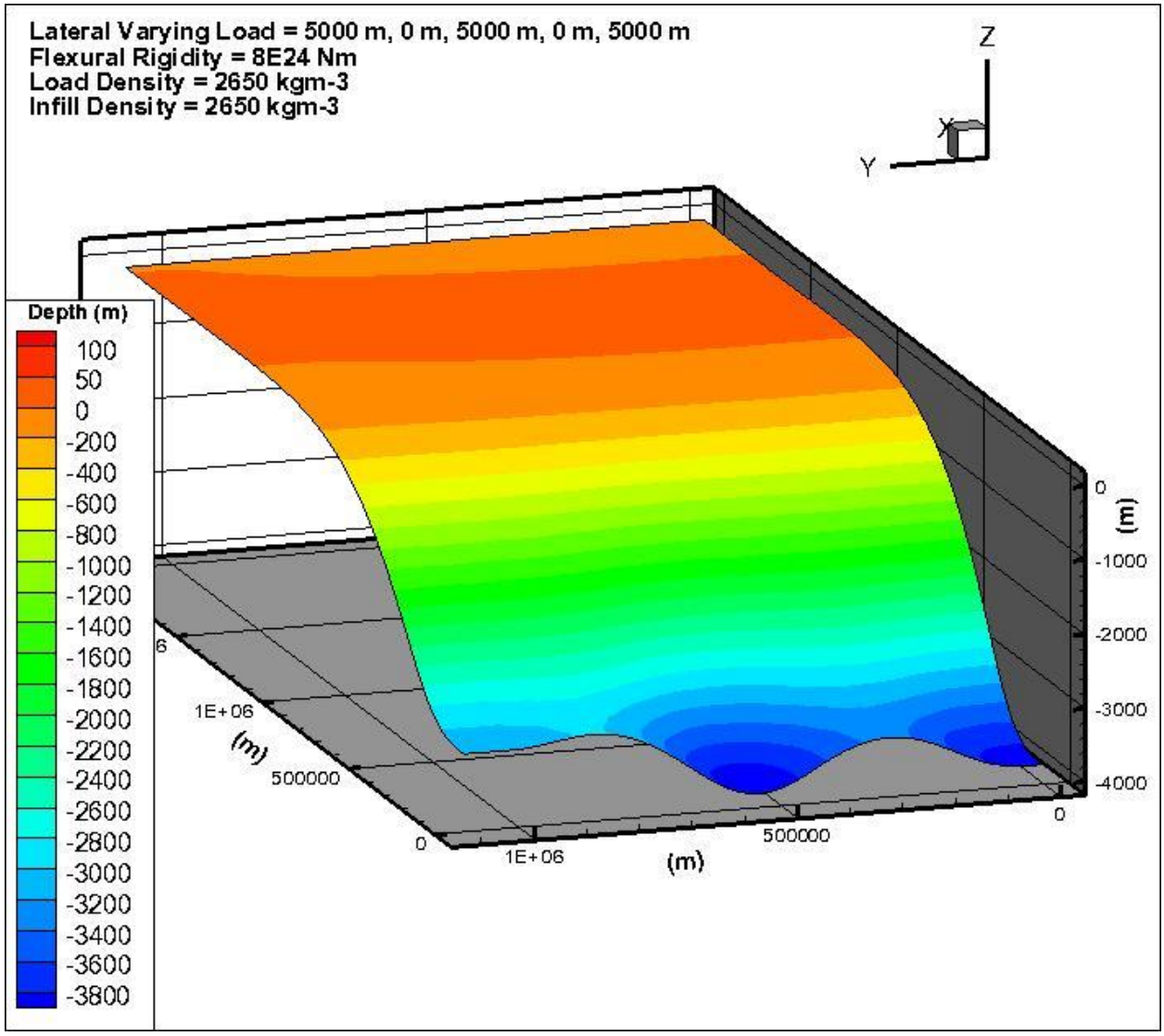

Figure 57: Laterally Varying Load Model DLVR5. Loads of 5000 m placed on edges and center of model domain.

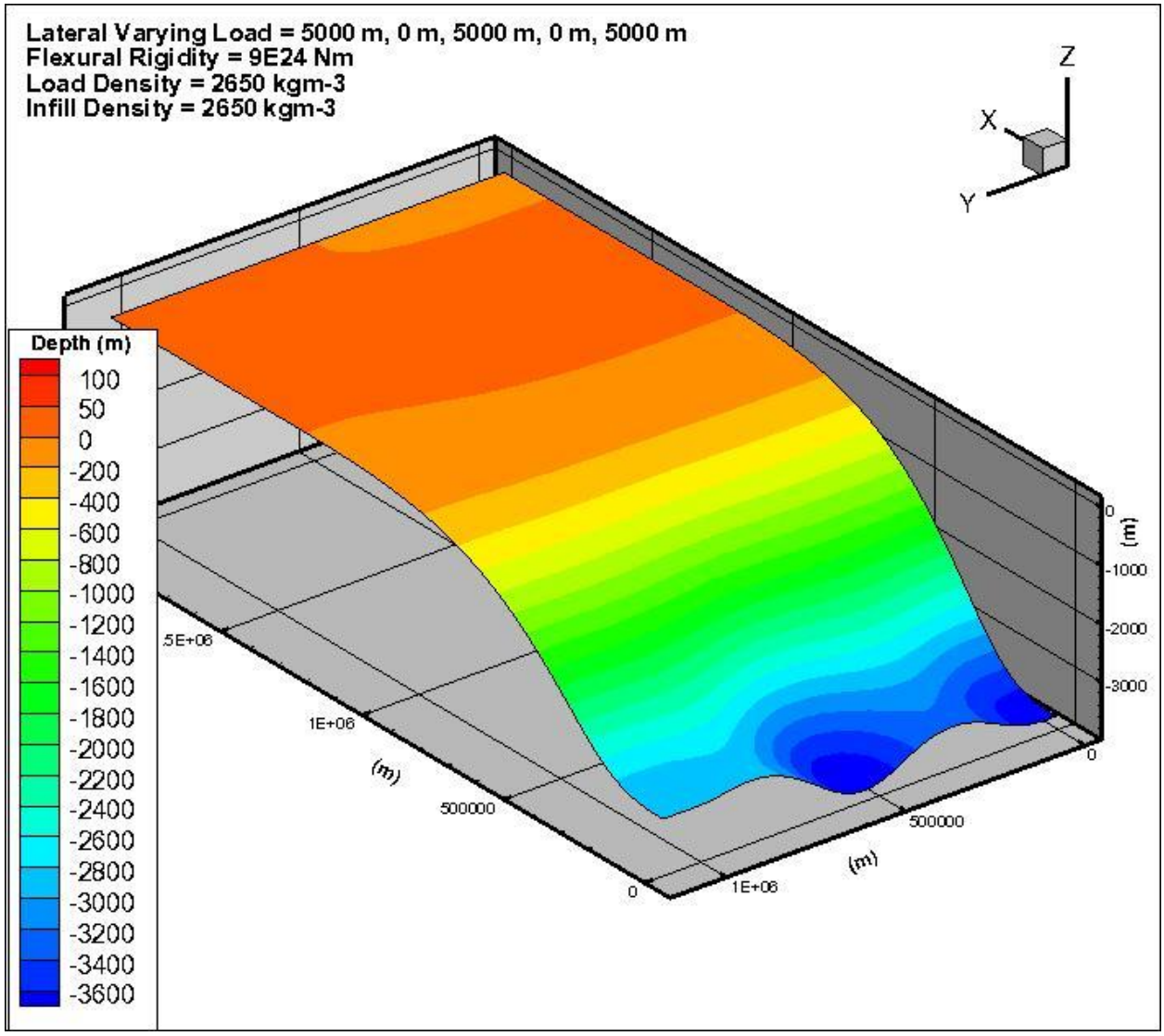

Figure 58: Laterally Varying Load Model DLVR6. Loads of 5000 m placed on edges and center of model domain.

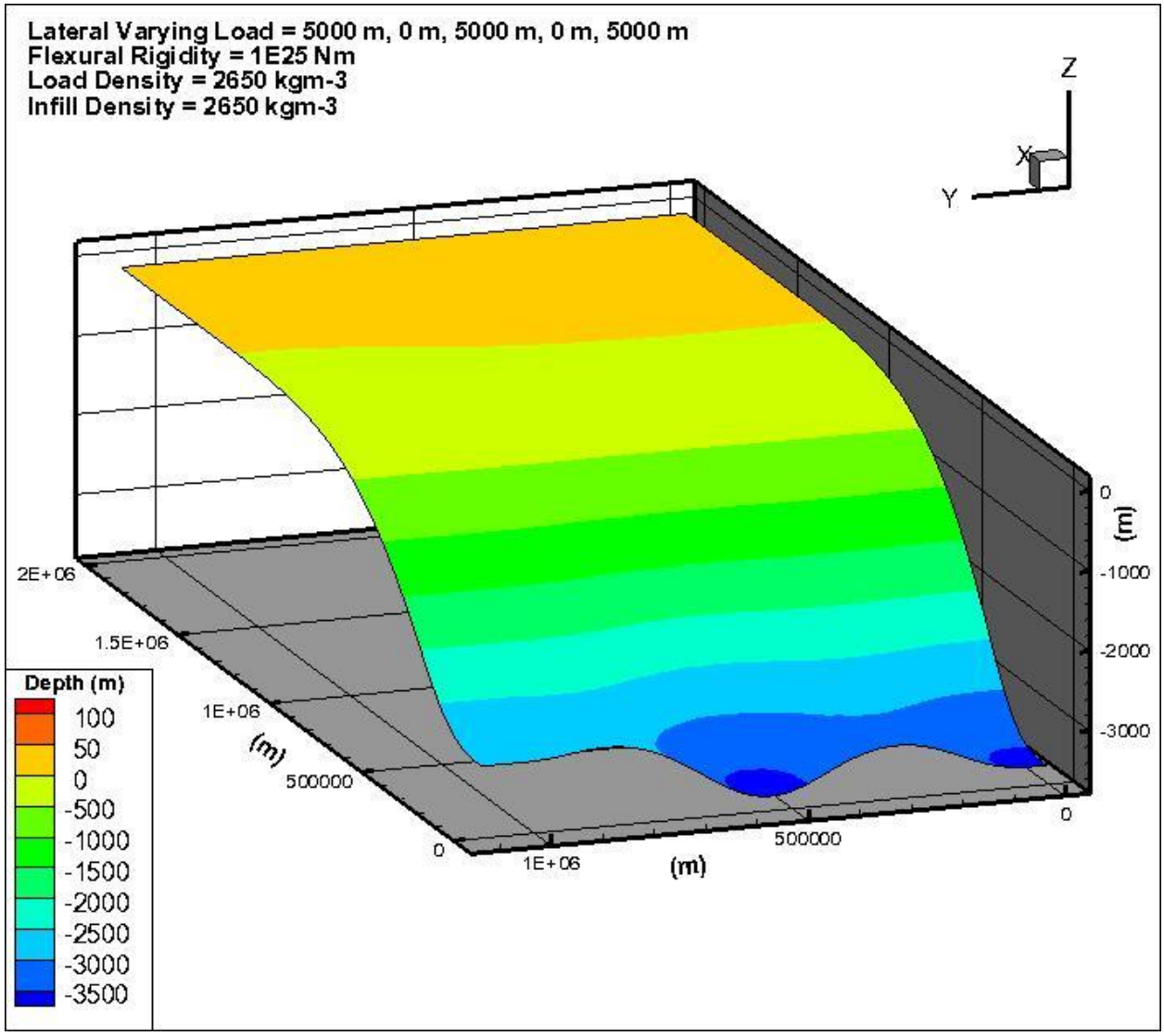

9.3 APPENDIX C: ADDITIONAL DEPTH TO BASEMENT MAPS

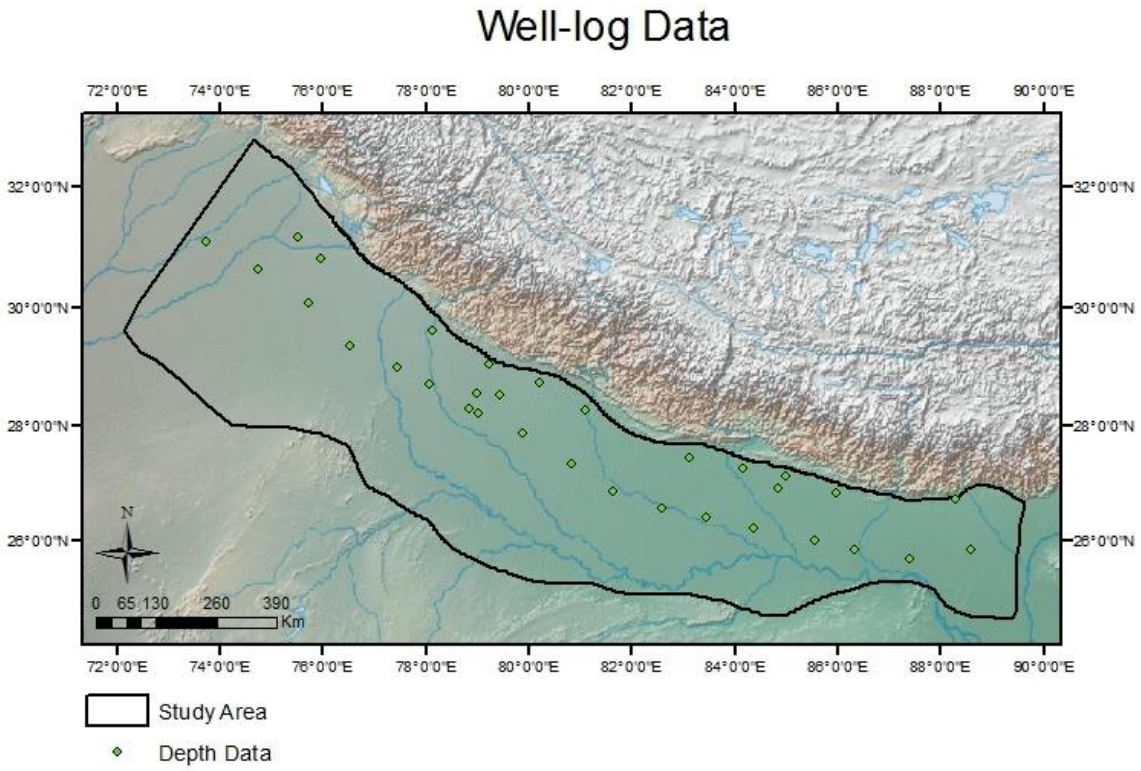

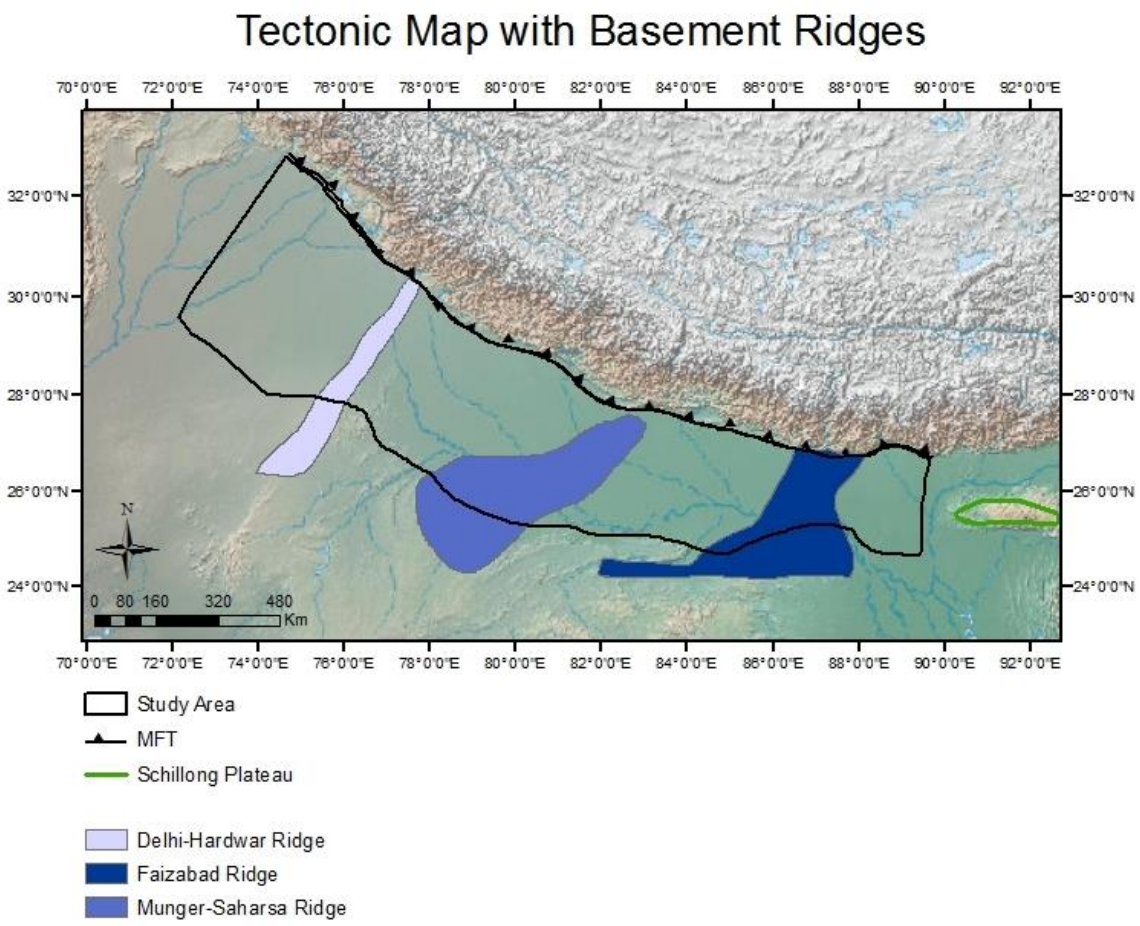
Tectonic Map with Basement Ridges
70°0'0"E
72°0'0"E
74°0'0"E
76°0'0"E
78°0'0"E
80°0'0"E
82°0'0"E
84°0'0"E
86°0'0"E
88°0'0"E
90°0'0"E
92°0'0"E
32°0'0"N
30°0'0"N
28°0'0"N
26°0'0"N
24°0'0"N
N
0 80 160 320 480
Km
Study Area
MFT
Schillong Plateau
Delhi-Hardwar Ridge
Faizabad Ridge
Munger-Saharsa Ridge

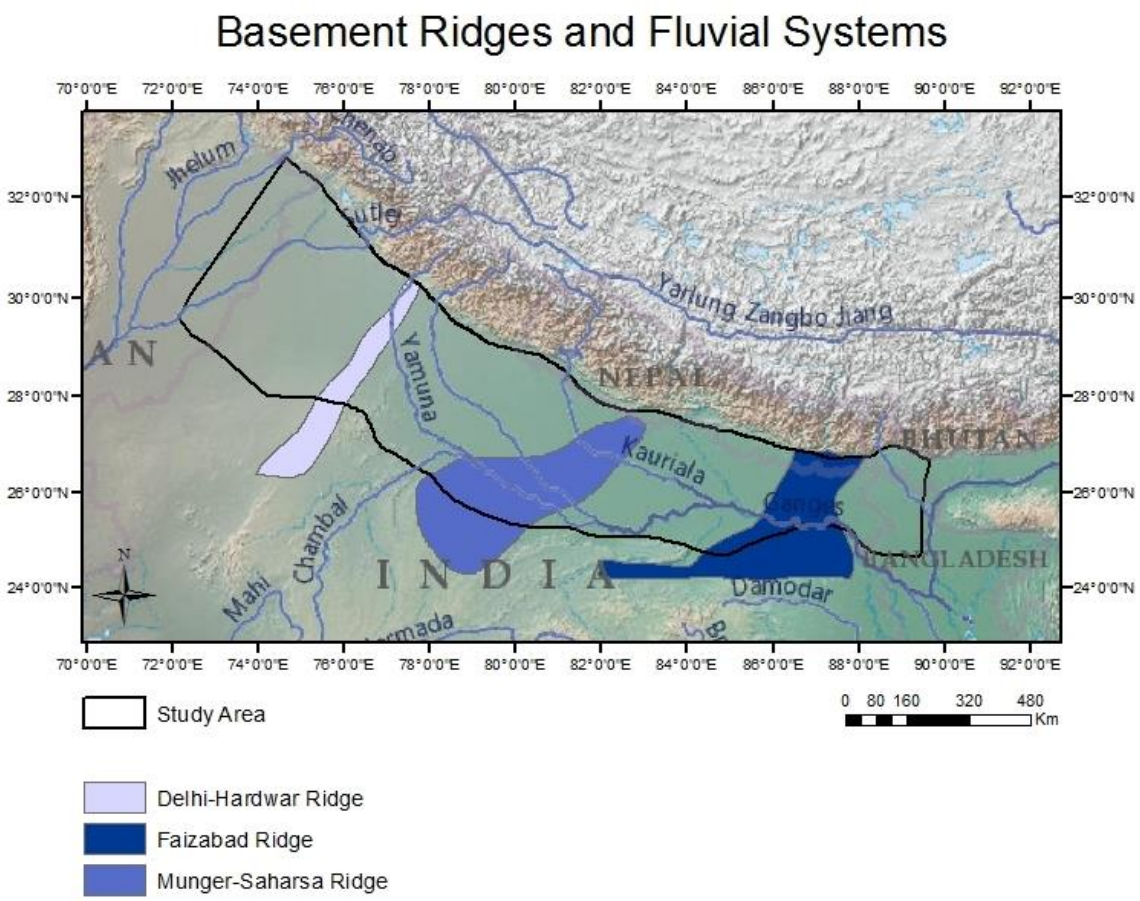
Basement Ridges and Fluvial Systems
70°0'0"E
72°0'0"E
74°0'0"E
76°0'0"E
78°0'0"E
80°0'0"E
82°0'0"E
84°0'0"E
86°0'0"E
88°0'0"E
90°0'0"E
92°0'0"E
32°0'0"N
30°0'0"N
28°0'0"N
26°0'0"N
24°0'0"N
Jhelum
Sutlej
Yarlung Zangbo Jiang
Yamuna
Kauriala
Damodar
Chambal
Mahi
NEPAL
BHUTAN
BANGLADESH
INDIA
N
Study Area
0 80 160 320 480
Km
Delhi-Hardwar Ridge
Faizabad Ridge
Munger-Saharsa Ridge

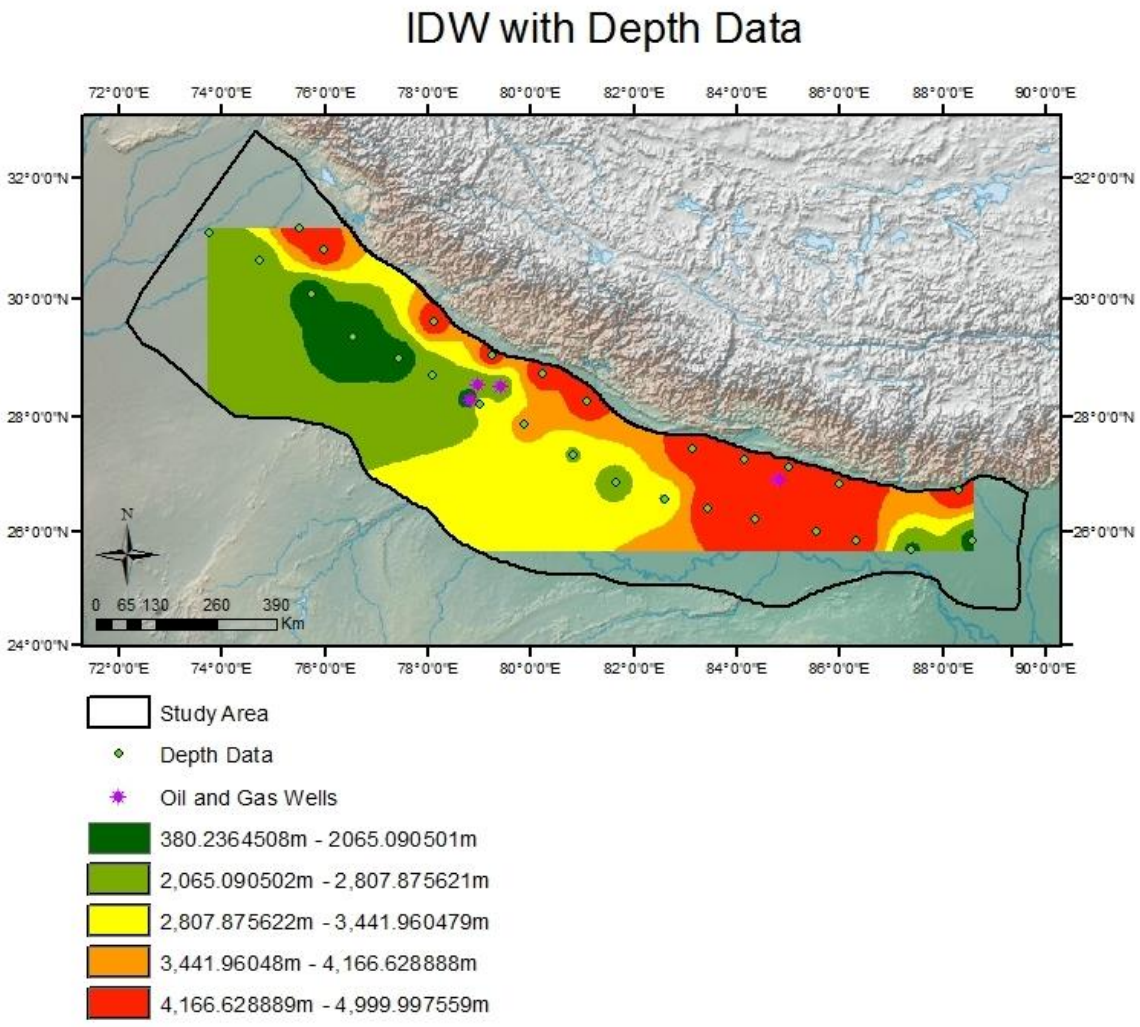
IDW with Depth Data
72°0'0"E
74°0'0"E
76°0'0"E
78°0'0"E
80°0'0"E
82°0'0"E
84°0'0"E
86°0'0"E
88°0'0"E
90°0'0"E
32°0'0"N
30°0'0"N
28°0'0"N
26°0'0"N
24°0'0"N
N
0 65 130 260 390
Km
Study Area
Depth Data
Oil and Gas Wells
380.2364508m - 2065.090501m
2,065.090502m - 2,807.875621m
2,807.875622m - 3,441.960479m
3,441.96048m - 4,166.628888m
4,166.628889m - 4,999.997559m

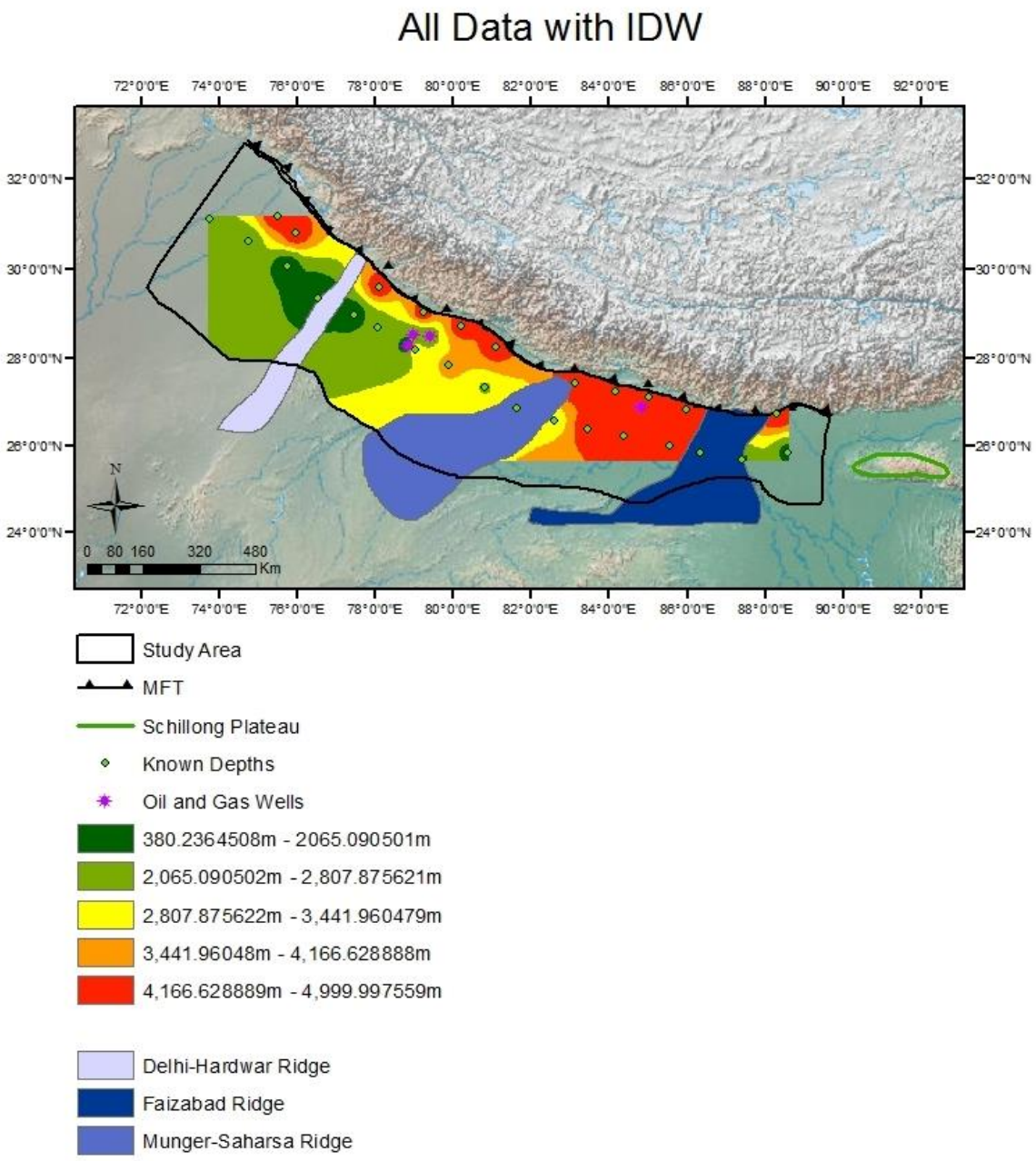
All Data with IDW
72°0'0"E
74°0'0"E
76°0'0"E
78°0'0"E
80°0'0"E
82°0'0"E
84°0'0"E
86°0'0"E
88°0'0"E
90°0'0"E
92°0'0"E
32°0'0"N
30°0'0"N
28°0'0"N
26°0'0"N
24°0'0"N
N
0 80 160 320 480
Km
Study Area
MFT
Schillong Plateau
Known Depths
Oil and Gas Wells
380.2364508m - 2065.090501m
2,065.090502m - 2,807.875621m
2,807.875622m - 3,441.960479m
3,441.96048m - 4,166.628888m
4,166.628889m - 4,999.997559m
Delhi-Hardwar Ridge
Faizabad Ridge
Munger-Saharsa Ridge